# University of Alberta

## A Physical Model for Broadband Ultrasonic Studies of Cancellous Bone

By

Qing Ji ©

A thesis submitted to the Faculty of Graduate Studies and Research in partial fulfillment of the requirement for the degree of Doctor of Philosophy

in

Medical Physics

Department of Physics

Edmonton, Alberta

Spring 1998

National Library of Canada
Acquisitions and Bibliographic Services
395 Wellington Street
Ottawa ON K1A 0N4
Canada

Bibliothèque nationale du Canada
Acquisitions et services bibliographiques
395, rue Wellington
Ottawa ON K1A 0N4
Canada

*Your file Votre référence*

*Our file Notre référence*

The author has granted a non-exclusive licence allowing the National Library of Canada to reproduce, loan, distribute or sell copies of this thesis in microform, paper or electronic formats.

The author retains ownership of the copyright in this thesis. Neither the thesis nor substantial extracts from it may be printed or otherwise reproduced without the author's permission.

L'auteur a accordé une licence non exclusive permettant à la Bibliothèque nationale du Canada de reproduire, prêter, distribuer ou vendre des copies de cette thèse sous la forme de microfiche/film, de reproduction sur papier ou sur format électronique.

L'auteur conserve la propriété du droit d'auteur qui protège cette thèse. Ni la thèse ni des extraits substantiels de celle-ci ne doivent être imprimés ou autrement reproduits sans son autorisation.

0-612-29052-2

Canada

## University of Alberta
## Faculty of Graduate Studies and Research

The undersigned certify that they read, and recommended to the Faculty of Graduate Studies and Research for acceptance, a thesis entitled **A Physical Model for Broadband Ultrasonic Studies of Cancellous Bone** submitted by Qing Ji in partial fulfillment of the requirements for the degree of Doctor of Philosophy in Medical Physics.

Dr. L. J. Filipow (Supervisor)

Dr. E. H. Pinnington (Co-Supervisor)

Dr. S. A. Jackson

Dr. J. R. Beamish

Dr. R. Hennig

Dr. J. Aldrich (External Examiner)

Dated: April 16th, 1998

# Abstract

A physical model to describe ultrasonic wave propagation in cancellous bone has been described in this thesis. The theoretical background for this model is based on Biot's theory. In order to prove the effectiveness and accuracy of this model, a broadband ultrasonic experimental system to study the ultrasonic properties of porous media was built as part of this project. The configuration details of this system as well as the fundamental techniques of measuring the attenuation and propagation velocities in a medium are presented in this thesis. The results of ultrasonic studies on water-saturated aluminum foams, which were used extensively as cancellous bone phantoms for studying basic mechanisms of wave propagation, and a detailed theoretical analysis of these experimental results are also presented. The experiments agree very well with the physical model established in this study. To extend this physical model to cancellous bone, several bovine bone samples and two types of cancellous bone phantoms were tested. The results of these experiments are also analyzed by the model.

# Acknowledgments

I would like to thank my supervisor, Dr. Larry Filipow for his support and supervision throughout this project. I have gained a lot of experience and confidence from his guidance and encouragement. My sincere thanks to my Co-supervisor Dr. E. H. Pinnington for his many valuable suggestions and support in frequent use of the Astrophysics Lab and providing an IEEE-488 GPIB interface. I would like to thank Dr. Stuart Jackson for his interest, help and contribution to this research project. A special thanks to Dr. Lawrence Le for his interest and collaboration during this research project. I would also like to thank Dr. John Beamish for many useful discussions and valuable suggestions. Finally, I would like to express my thanks to all my colleagues in the Department of Radiology and Diagnostic Imaging for helping me in various ways to the successful completion of this research.

Financial support provided by Department of Physics and Department of Radiology and Diagnostic Imaging of University of Alberta are gratefully acknowledged. Special thanks to the Faculty of Graduate Studies and Research and Capital Health Authority for supporting me to present part of this research in **UI'97.**

# Table of Contents


**Chapter One: Introduction** 1

1.1 Clinical Background 1

1.2 Ultrasonic Measurements of Bone 4

1.3 Objective of Thesis 9

1.4 Outline of Thesis 11

**Chapter Two: Broadband Ultrasonic Experimental System** 12

2.1 Apparatus 12

(1) Pulse Generator 14
(2) Detection of Ultrasonic Signals 16
(3) Transferring Data 16

2.2 The Measurement of the Propagation Velocity of an Ultrasonic Wave 18

2.3 Measurements of Attenuation 21

**Chapter Three: Propagation Velocity Measurement in The Frequency Domain** 28

3.1 The Difficulty in Determination of the Pulse Transit Time in Dissipative Material 28

3.2 The Phase spectral Analysis Method 32

3.3 An Example: The Phase Velocity Measurement for a Rubber Phantom 34

3.4 Discussion about Dispersion in the Dissipative Medium 37

3.5 Transmission Delay Time 38

**Chapter Four: The Theory of Ultrasonic Wave Propagation in Fluid Filled Porous Materials** 41

4.1 Biot's Theory 41

4.2 High Frequency Limit Solutions 45

4.3 Boundary Conditions 49

**Chapter Five: The Experimental Studies of the Ultrasonic Transport Properties of Water Saturated Aluminum Foams** 56

5.1 The Cellular aluminum Foam Sample 57

5.2 The Experimental Method and Procedure 58

5.3 Results 59

(a) Waveforms 59
(b) Measurements of the Propagation Velocities 60
(c) Amplitude Spectra 64
(d) BUA 64

5.4 Discussions 65

5.5 Experiments on the Gelatine-Water Mixture Filled aluminum Foams 70

(1) Ultrasonic Wave Propagation in Gelatine-Water Mixture 70
(2) The Ultrasonic Signal in Gelatine-Water Mixture Filled Aluminum Foams 72

**Chapter Six: Theoretical studies of the Ultrasonic Transport Properties of Water-Saturated Aluminum Foams** 75

6.1 The Mechanical Properties of Cellular Aluminum Foams 75

6.2 The Viscous Coupling in Water-Saturated Aluminum Foam 77

6.3 The inertial Coupling in Water-Saturated Aluminum Foams 78

6.4 The Propagation Velocities of an Ultrasonic Wave 80

6.5 Ultrasonic Transport Properties and r Values 82

(1) Transport Properties 82
(2) The relation Between the Motion of the Solid Frame and the Fluid 83

6.6 The Acoustic Scattering in the Water-Saturated Aluminum Foam 84

(1) The single Scattering Model 88
(2) The Scattering Attenuation Coefficient 90
(3) Implementation of the Single Scattering Model into Biot's theory 91
(a) The Dynamic Moduli of the medium 91
(b) The Dynamic Moduli of the Aluminum Foam 93
(c) Implementation of Scattering Model 94

6.7 The Numerical Simulations of the Transmission Signal 96
(1) Simulation Strategy 96
(2) Results 97

6.8 Discussions 101

**Chapter Seven: Ultrasonic studies of Other Cancellous Bone Phantoms** 102

7.1 Experiments of Bovine Bone Samples 103

7.2 Rubber Block Model 105

7.3 The Vancouver Phantom 108

7.4 Rubber Test Objects 110

7.5 Discussions 113

**Chapter Eight: Conclusion** 114

8.1 Further Works 114

8.2 Conclusion 116

**Appendix I: The Transmission Coefficients on An Open Cell Surface** 118

(1) Input Surface 118

(2) Output Surface 121

**Appendix II : Fast Fourier Transformation** 124

(1) Algorithm 124

(2) Applications 124

**Appendix III: The Waveforms in Various Solid Materials** 127

**Appendix IV: The Schematics of Pulse Generator (Main Circuit)** 130

**Appendix V: The Detailed Discussion about Numerical Simulation** 131

**References** 133

# List of Tables

Table 2.1 The propagation velocities of ultrasonic waves in different solid materials. 20

Table 3.1 The transmission time in a brass sample determined by leading edge and zero crossing points 29

Table3.2 The transmission time in rubber phantom determined by the leading edge and zero crossing points 30

Table 5.1 The velocities of fast and slow waves in the water-saturated aluminum foam sample 62

Table 5.2 The wave propagation velocities in gelatine mixture filled Al foams 74

Table 5.3 The wave propagation velocities in gelatine-water mixture 74

Table 6.1 The basic physical parameters of the water-saturated aluminum foams 81

Table 6.2 The velocities of fast and slow waves in the sample 81

Table 6.3 Calculated transmission coefficients 83

Table 6.4 Calculated r coefficients 84

Table 7.1 The measured parameters of bovine cancellous bone samples 105

Table 7.2 The physical parameters of the cancellous bone and water-saturated aluminum foams 105

Table 7.3 The comparison of BUA test results of Vancouver phantoms on different ultrasound systems. 112

Table 7.4 The test results of three rubber test objects 113

# List of Figures


Figure 1.1 The structure of bone 2

Figure 1.2 A typical structure of cancellous bone 3

Figure 1.3 Schematic diagram of the BUA measurement of bone 5

Figure 2.1 The experimental set-up for broadband ultrasonic measurements 13

Figure 2.2 The block diagram of the pulse generator 14

Figure 2.3 The high voltage electrical pulse generated by the pulse generator 15

Figure 2.4 A typical ultrasound pulse generated by the experimental system. (a) Signal, (b) Spectrum 18

Figure 2.5 The temperature calibrations of the propagation velocity in water 19

Figure 2.6 A typical "Leading Edge" of an ultrasonic pulse 21

Figure 2.7 The transmission signals of an ultrasound pulse through 5 rubber phantoms. (a) water pulse, (b) Thickness=0.876 cm, (c) Thickness= 1.092 cm, (d) Thickness=1.226 cm, (e) Thickness=1.407 cm, (f) Thickness=2.375 cm 26

Figure 2.8 The attenuation of ultrasound wave in rubber phantoms as a function of wave frequency 27

Figure 2.9 The ultrasonic attenuation in rubber is a linear function of thickness 27

Figure 3.1 The leading edge and zero crossing points of the water pulse and transmission pulse through a brass sample (2.54 cm) 29

Figure 3.2 The leading edge and zero crossing points of the water pulse and the transmission pulse through a rubber phantom (0.986 cm) 31

Figure 3.3 The phase difference spectrum. (a) before unwrap, (b) after unwrap 35

Figure 3.4 The phase difference spectrum in a rubber phantom. (a) before correction, (b) after correction 36

Figure 3.5 The phase velocity in a rubber phantom. Solid line: experiment, dashed line: K-K relation 39

Figure 4.1 Cross-section of an open cell surface 50

Figure 4.2 The waves generated on an open cell surface 51

Figure 4.3 The acoustic waves transmission through a finite sample 54

Figure 5.1 The cellular aluminum foam sample (40PPI) 58

Figure 5.2 The waveforms of the transmission pulses through (a) 95% porosity sample, (b) 93% porosity sample, (c) 90% porosity sample, (d) 88% porosity sample. In each waveform, top: water pulse, bottom: (1) slow wave, (2) fast wave, (3) unknown third wave 61

Figure 5.3 The phase velocities obtained from transmission pulses.(a) 95% porosity sample, (b) 93% porosity sample, (c) 90% porosity sample, (d) 88% porosity sample. 63

Figure 5.4 The amplitude spectra for the transmission pulse through (a) 95% porosity sample, (b) 93% porosity sample, (c) 90% porosity sample, (d) 88% porosity sample 66

Figure 5.5 The BUA in (a) 95% porosity sample, (b) 93% porosity sample (c) 90% porosity sample, (d) 88% porosity sample 68

Figure 5.6 The experiment system designed for gelatine-water mixture filled aluminum foams 71

Figure 5.7 The ultrasonic signals in Gelatine-water mixture. Top: in Fluid phase Bottom: in gelatiniate phase 72

Figure 5.8 The transmission waveforms in Gelatine-water mixture filled cellular aluminum foam (90% porosity sample). Top: The mixture in fluid phase, bottom: the mixture in gelatinate phase 73

Figure 6.1 The relation of stress and strain in a cellular metal foam 76

Figure 6.2 The scattering wave measured in 90% porosity sample (rotating the receiver 90 degrees with the propagation direction 86

Figure 6.3 The amplitude spectrum of the scattering wave in 90% porosity sample 87

Figure 6.4 Illustration of the scattering of a wave by a single scatterer 88

Figure 6.5 The strategy for the numerical simulation. The input pulse is a water pulse. 97

Figure 6.6 The simulated tansmission pulses for the 88% porosity sample without considering scattering attenuation. Top: experiment, Bottom: theory 99

Figure 6.7(a) The simulation of the transmission pulses in the 88% porosity sample. Top: Experiment, Bottom: Theory 99

Figure 6.7(b) The simulation of the transmission pulses in the 90% porosity sample. Top: Experiment, Bottom: Theory 100

Figure 6.7(c) The simulation of the transmission pulses in the 83% porosity sample. Top: Experiment, Bottom: Theory 100

Figure 7.1 The ultrasonic transmission signals in cancellous bone samples 104

Figure 7.2 A diagrammatic representation of the rubber block model phantoms in this study 106

Figure 7.3 The transmission pulse in phantom #1 (2 mm hole diameter) 107

Figure 7.4 The transmission pulse in phantom#2 (1 mm hole diameter) 108

Figure 7.5 The transmission signals in Vancouver phantoms, the water pulse is shown on the top 111

Figure 7.6 The attenuation in the Vancouver phantom as a function of wave frequency. 111

Figure 7.7 The attenuation in rubber test objects 112

Figure A1.1 The input surface of an open cell sample 118

Figure A1.2 The output surface of an open cell sample 121

Figure A2.1 The ultrasonic signal measured in time domain (1024 data points, time interval between two adjacent points is 0.1 μs) 125

Figure A2.2 The amplitude distribution after FFT, only first 512 data points are meaningful 126

# Chapter One : Introduction

## 1.1 Clinical Background

Osteoporosis is a common disease among the aged population and is becoming a growing health problem because of the growing number of elderly persons in our society. The clinical syndrome of osteoporosis consists of a reduced amount of bone tissue per unit volume of anatomic bone and can result in fractures of the vertebrae, femoral neck, or the distal forearm after trauma [17]. In clinical diagnosis, osteoporosis is defined as bone mass below 2.5% of standard.

Although a number of factors can contribute to osteoporosis, in many cases the exact cause of this disorder is not known. Long-term calcium deficiency can lead to osteoporosis, owing to the mobilization of bone mineral to maintain normal calcium concentrations in blood. Most commonly, osteoporosis is associated with advancing age in both men and women. At menopause (about age 50), women begin to lose bone mass more rapidly than men as the result of decreasing estrogen levels.

To diagnose osteoporosis and monitor the process of treatment, it is essential to develop non-invasive and accurate equipment for bone quality measurement. Bone consists of a collagen rich organic matrix upon which a crystalline mineral phase (primarily calcium and phosphate) is deposited. The mineral phase deposited within the organic matrix contains 99% of the body's calcium, 80% to 85% of the body's phosphate, and most of the magnesium. There are two major forms of bone: compact (or cortical) bone

and cancellous (or trabecular ) bone. As shown in Figure 1.1, cortical bone forms the external envelopes of the skeleton; cancellous bone forms plates that transverse the

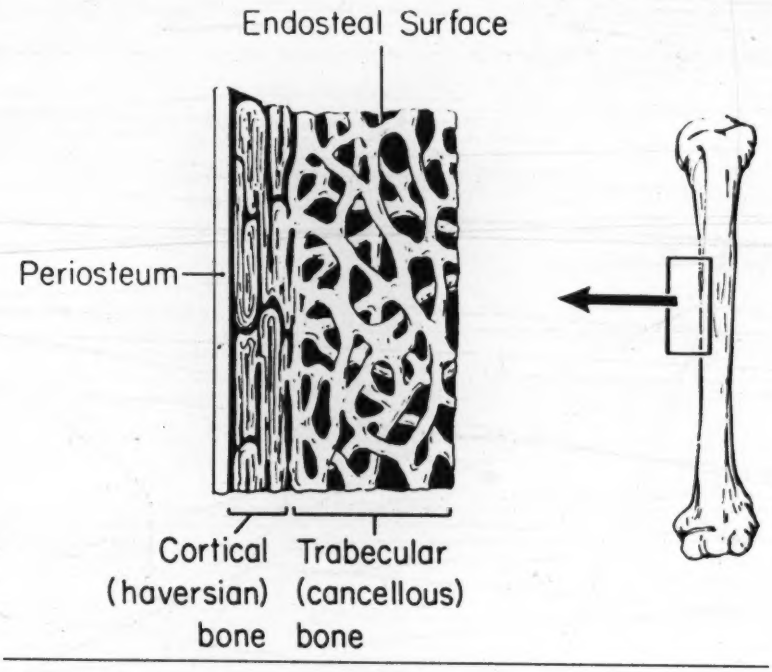


Figure 1.1 The Structure of Bone

internal cavities of the skeleton. The proportions of cancellous and cortical bone vary from one site to another in the skeleton. Vertebral bodies of the spine contain principally cancellous bone, and the peripheral skeleton (arms and legs) contains predominately cortical bone. The cancellous bone is distinguished from the cortical bone by its lighter density and higher porosity (volume percentage of voids). In cancellous bone, the solid bone material forms a complex solid frame with fatty bone marrow filling among the voids. Figure 1.2 shows a typical cancellous bone structure.

Figure 1.2 A Typical Structure of Cancellous Bone

Bone is a living tissue and is continuously remodeling throughout life. Osteoclasts reasorb bone in microcopic cavities within the bones, whereas osteoblasts rebuild the bone surfaces and refill the cavities. The remodeling process is influenced by mechanical and electrical forces, hormones, and other factors. Osteoporosis is the result of loss of balance between the resorption and rebuilding processes. Although the reduction of bone mass in osteoporosis produces equal losses of both bone mineral and organic matrix (the ratio of the amount of mineral ralative to the amount of matrix in the bone does not change), the bone structure (especially for cancellous bone) will suffer deformation due to the body weight and other mechanical influences.

The measurement of bone quality has been the subject of intensive research over many years. The development of appropriate techniques has been hindered by the complexities associated with the bone structures. Current techniques for bone quality

measurements include radiogrammetry[14,21,29,63], radiographic photodensitometry[29], single-photon absorptiometry (SPA)[29], dual-photon absorptiometry (DPA)[29], dual-x-ray absorptiometry (DXA)[29], and quantitative computed tomography (QCT)[29]. All of those methods are based on the application of ionizing radiation and the physical quantity measured by these techniques is the bone density or bone mineral content (BMC). Although the density or BMC is a major determinant of bone quality (the strength or the fragility), it has been noted that the "structure factors" of bone, especially cancellous bone are important and prevent complete correlation of bone quality with only bone mass (density).

The requirements for a good diagnostic procedure for bone quality measurement should include: (1) high precision or reproducibility for longitudinal studies, (2) low cost, (3) low radiation dose, (4) minimal inconvenience for the patient. It is these requirements which lead to the development of a new technique, because even though high precision and accuracy measurements of bone density or BMC can be achieved by some of the radiological techniques (such as DPA and QCT), but they are only available in some major medical centers. The cost are high for those techniques.

### 1.2 Ultrasonic Measurements of Bone

Ultrasound is a mechanical disturbance propagating as a wave at a supra-audible frequency. A propagation medium, which must have inertia and elasticity, is required for ultrasound. When an ultrasonic wave propagates in the medium, the characteristics of the ultrasonic field will be affected in a manner that depends upon the acoustic properties of

the medium. These changes in the field may produce a unique signature of the medium. Because it is non-ionizing radiation, ultrasound has been widely used for non-invasive detection of defects and investigation of the mechanical properties of engineering materials. In diagnostic medical applications, ultrasound image plays an important role such as in the case of obstetrical applications where risk to the patient must be minimized.

The first application of ultrasonic techniques in the characterization of bone tissue can be traced back to 1949. At that time Tesismann and Pfander[60] first reported the ultrasonic attenuation coefficients and propagation speed in the skull. More recently in 1976 Yoon and Katz[36, 64] reported their experimental results of the elastic constants of human femur specimens (cortical bone ) using an ultrasonic method. According to Yoon

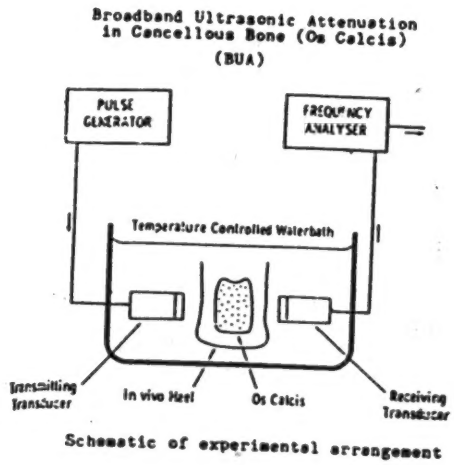


Figure 1.3 Schematic Diagram of the BUA Measurement of Bone

and Katz, the cortical bone has an approximately cylindrical symmetry along the weight bearing direction, and therefore can be tested by ultrasound in three perpendicular directions. The elastic constants of cortical bone can be determined by measuring the propagation velocities in these three directions.

In 1987 and 1988, Ashman reported the results of elastic properties of cancellous bone measured by an ultrasonic technique[3,4]. Because cancellous bone does not have the same symmetry as cortical bone does[25,65], Ashman tested the propagation velocity along the weight bearing axis using both contact pulse transmission and continuous wave techniques. From the propagation velocities, the Young's modulus along that direction can be calculated. The results of ultrasound tests were correlated very well with the results of mechanical tests.

The application of ultrasonic technique in clinical diagnosis of osteoporosis was first suggested by Langton in 1984[37]. The method proposed by Langton is called broadband ultrasonic attenuation (BUA), in which two broadband ultrasonic transducers (1MHz center frequency) are set in a water bath (Figure 1.3), one serving as transmitter and the other as receiver. The heel (predominately cancellous bone) is placed in the water bath between the transducers and the attenuation of the beam through the heel bone is measured relative to water alone. The attenuation of the ultrasonic wave in the heel bone is plotted as a function of the ultrasound frequency. According to Langton, there is approximate linearity from 0.2 to 0.6 MHz in the curve of attenuation against frequency. The slope is defined as the BUA value. The biggest achievement of Langton's work is that he found the BUA value of a young healthy female is significantly higher than the

BUA value for an osteoporostic female with hip fracture; therefore BUA value is thought to be a potential diagnostic index of bone quality. Using BUA as a diagnostic index of osteoporosis has following advantages: (1) no ionizing radiation dose to the patient, (2) the equipment is easy to operate and convenient for the patient. (3) the cost is low and (4) BUA has the potential to obtain more information about bone quality. The problem of using BUA as a diagnostic index lies in the correlation of the measured BUA value and the physical parameters of bone tissue. Since the cancellous bone is a very complex two phase porous medium, the correlation depends not only on bone density but also on the microstructure of the cancellous bone. As pointed out by Langton, the physical meaning of BUA still remains unclear.

Following Langton's work, ultrasonic studies of cancellous bone have been focused on three major directions: (1) direct comparison studies[18,23,35,45,55], (2) in-vitro comparison studies[41,42,43,53,58,59] (3) phantom studies[13,27,59]. The purpose of the studies is to find the relation between the ultrasonic parameters (BUA and speed of sound (SOS)) and the physical quantities of bone (porosity, elasticity). The goal is to develop a "diagnostic index". A diagnostic index need not be a physical quantity in nature, the only requirement is that it can provide a sensitive measure to discriminate a diseased individual or population from the healthy population. However, it is desirable that a measured quantity be a physical quantity or at least correlate with a physical quantity, which may be measured, calculated or calibrated with the true value so that a diagnostic index can be used to quantitatively evaluate the changes of the bone quality.

Direct comparison studies attempt to find the correlation between BUA and BMC using the regular ionizing radiation techniques. The advantage of this approach is it can provide first hand clinical data. But since the study has to be in-vivo, and the physical quantities of the bone are very difficult to control, the results of the study can not give a quantitative description of the behavior of ultrasound through bone. With the accumulation of clinical data through comparison studies, it has been found that the correlations between BUA and bone parameters are not very consistent. For instance, the linear regression between BUA and bone density ranges between 0.55 to 0.82, and depends on the test objects and test machine.

In-vitro tests of cancellous bone specimens can give more accurate and reliable information about the physical quantities of the bone and, in a limited range, allow control of the physical quantities of the bone specimen. Since the study is in-vitro, it is possible to compare the BUA or SOS with all the physical quantities of the sample. The in-vitro comparison studies of BUA and SOS with anisotropy, elasticity, thickness and density (porosity) have been performed by many researchers. The studies show that the BUA and SOS are influenced by all these physical quantities and the linear correlations are actually very poor. For some physical quantities such as thickness and density, their relations with the BUA and SOS are not linear .Since cancellous bone is a very complicated two phase system, the descriptions of some physical quantities is very difficult. For instance, cancellous bone is an anisotropic material, but there is not any symmetry found in cancellous bone specimen, therefore it is very difficult to quantitatively describe the anisotropic behavior of this type of bone. Furthermore, all the physical quantities in

cancellous bone are dependent on others, therefore to isolate one single physical quantity and investigate its influence on BUA or SOS is almost impossible. In order to do the comparisons, some assumptions have to be made. This is where phantom studies show promise.

Cancellous bone is a natural biological material, its physical quantities are difficult to control and describe, and its acoustic properties are usually not stable. Phantom study is the attempt to develop a cancellous bone mimic (phantom) with controllable physical quantities to study the behavior of ultrasound through the porous material. An ideal phantom should be (1) a material with ultrasonic properties that approach those of cancellous bone; (2) it should be durable and stable and allow controlled variations in at least some of the physical qualities. Cancellous bone is both heterogeneous and anistropic. This makes it very difficult to design an ideal cancellous bone phantom. In practice, the bone phantom or phantoms can be designed to mimic some of the material properties of cancellous bone tissue, with particular reference to the physical quantity of interest.

From a physics point of view, BUA and SOS are the results of the interactions of an ultrasonic wave with the medium. The way the ultrasonic wave propagates in the medium determines the BUA and SOS. In spite of all the previous studies that have been done to date the physical model of ultrasonic wave propagation in cancellous bone is still not fully understood.

### 1.3 Objective of Thesis

The primary objective of this research is to develop and establish a model for the description of the ultrasonic wave propagation in the cancellous bone. The ultrasonic wave propagation in fluid-filled porous media, such as cancellous bone, is a very complicated physical problem. To understand the acoustic properties of a medium, it is essential to know how particles move in this medium corresponding to wave propagation. In a fluid-filled porous material, the particles of the fluid and the particles of the solid will interact with each other, and as a result, very complicated motion modes will be formed in the medium. Ultrasonic wave propagation in fluid-filled porous material should be different from that in a single component material. To fully study this problem, a set of phantoms with a structured solid frame filled with fluid are needed. Since the interactions of the structure (solid frame) with the fluid are the major interests of this study, these phantoms need not to mimic all the properties of cancellous bone. After investigations of the many possible materials, it was found that water-saturated cellular aluminum foams are appropriate phantoms. The cellular aluminum foams are newly developed engineering materials with high strength and low densities. The aluminum foams have an open cell structure and their cell sizes and porosities can each be designed in a certain variable range independently. Compared with cancellous bone, the cell structure of the aluminum foam is simple and uniform. When an aluminum foam is saturated with water, it is a typical fluid-filled porous solid material. To test the ultrasonic properties of the water-saturated aluminum foams, a broadband ultrasonic experimental system was designed and built for this project. This system had to be able to measure all the ultrasonic parameters of the phantoms. The fundamental theory used to understand acoustic wave propagation in

fluid-filled porous materials is Biot's theory. The Biot's theory was the major theoretical tool used to analyze the experimental results, and ultimately develop a model.

### 1.4 Outline of Thesis

This thesis will present the experimental results of broadband ultrasonic studies of water-saturated aluminum foams and the numerical simulations based on Biot's theory. Following the introduction, Chapter 2 describes the broadband ultrasonic experimental system built for this research and the basic principles of pulse transmission techniques for measuring the propagation velocity and attenuation of the acoustic waves. In Chapter 3, dispersion and phase velocity measurements in dissipative materials will be discussed. Chapter 4 introduces Biot's theory and discusses mode conversion on open cell surfaces. In Chapter 5, the experimental results of broadband ultrasonic studies of the water-saturated and the gelatine-water mixture filled cellular aluminum foams are presented. Chapter 6 presents a simple physical model for description of the ultrasonic transport properties of water-saturated aluminum foams. The model is based on Biot's theory and single scattering theory. The results of numerical simulation using this model are also presented. In Chapter 7, the broadband ultrasonic experimental results on cancellous bone samples and two cancellous bone phantoms will be presented. A discussion of the results as well as possible future research using the physical model to study cancellous bone is presented in Chapter 8.

# Chapter Two: Broadband Ultrasonic Experimental System

In this chapter, the major specifications of the broadband ultrasonic experimental system built for this project will be described. This system was designed to measure the propagation velocity and the attenuation of ultrasonic wave in the test sample.

The pulse transmission technique (PTT) is one of the most fundamental and useful methods in broadband ultrasonic measurements. The basic idea of PTT is to place an ultrasonic transmitter probe on one side of the test object, a receiver probe on the other. A very short acoustic pulse, which is generated by the transmitter, travels through the test object and is then detected by the receiver. From the detected transmission signal, the attenuation of the pulse in the object and the time of the pulse traveling through the object can be obtained, which then allows the acoustic properties of the test object to be determined. Because the acoustic pulse usually contains a specific range of frequencies, the acoustic properties of the test object as a function of acoustic wave frequency can also be obtained by doing Fast Fourier Transformation (FFT) on the transmission signal. Based on the principle of PTT, a broadband ultrasonic experimental system was designed and built for this purpose.

## 2.1 Apparatus

The apparatus of the experimental system is shown in Figure 2.1. The system, which is immersed in water in a big water tank, consists of two identical broadband P wave

ultrasonic transducers (centered at 1 MHz frequency), and a sample and transducer holder which ensure the alignment between the probes and the sample. The broadband ultrasound

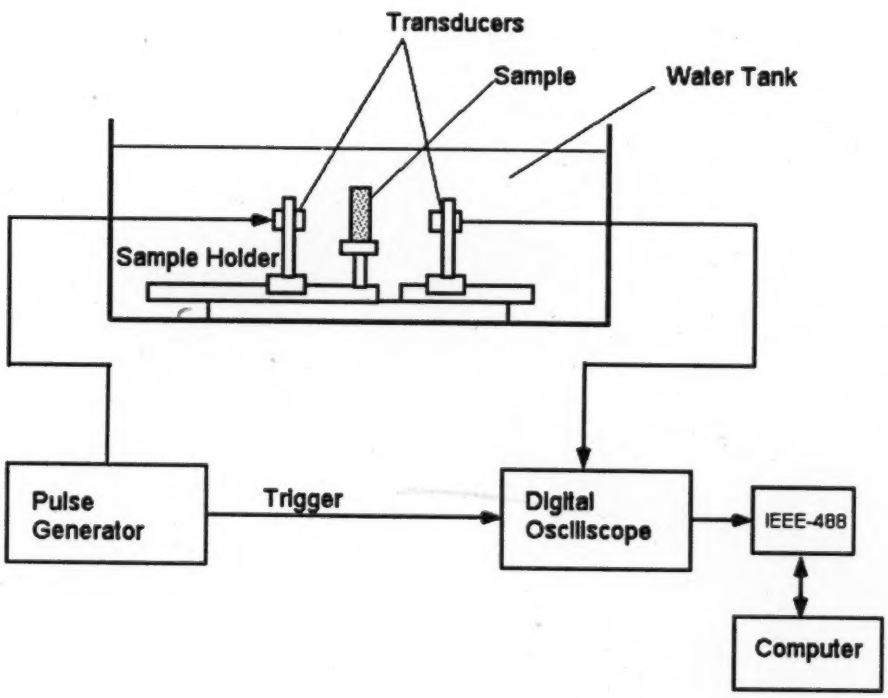


Figure 2.1 The Experimental Set-Up For Broadband Ultrasonic Measurements

transducers are water immersible, which will permits good acoustic coupling between the probes and water. One of the transducers serves as transmitter and the other as receiver. The transmitter probe is pulsed by a pulse generator. The transmitted signal is received by the receiver probe and digitized by a digital oscilloscope (LeCroy 400). The digitized

signal can be displayed on the screen of the oscilloscope or transferred to a personal computer through an IEEE-488 interface for data analysis.

(1) Pulse Generator

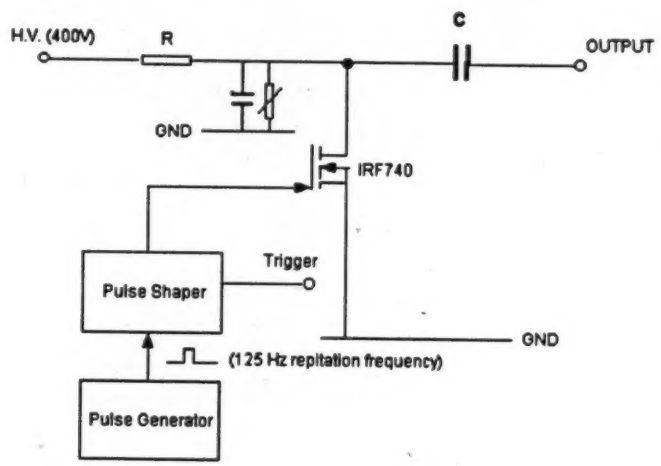


Figure 2.2 The Block Diagram of the Pulse Generator

The transmitter is pulsed by a high voltage electrical pulse (usually 125V to 400 V negative pulse). To effectively excite the transducer, the width of the electrical pulse must be much shorter than the width of the ultrasound pulse[57]. The bandwidth of the transducer is about 0.5 MHz (centered at 1MHz frequency). Corresponding to this bandwidth, the width of the ultrasound pulse is estimated at about 2μs. Therefore, the width of the electrical excitation pulse must be 400 ns(1/5 of the ultrasound pulse) or shorter. Ideally, the shape of the electrical pulse should be as short as possible to a δ function.

Figure 2.2 shows the block diagram of the pulse generator built for this research. The working principle of this pulse generator is based on charge and discharge of the capacitor C through a fast field effect transistor IRF750. The field effect transistor (FET) works like a switch, when it is off, the capacitor is charged through a high voltage power supply, when it is on, the capacitor is discharged through the FET and generating at the output end a high voltage negative electrical pulse. The FET is controlled by a pulse applied to its base. The shape and width of the output pulse depend on the control pulse. The control pulse is generated from a square wave pulse generator circuit, and then regulated and shaped into a δ function spike by a shape circuit. The pulse width of the control pulse is about 200 ns. The final output pulse has a pulse width of about 300 ns as shown in Figure 2.3.

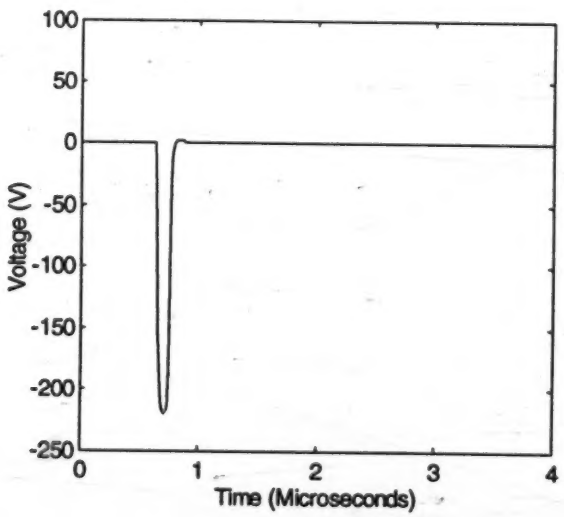


Figure 2.3 The High Voltage Pulse Generated by The Pulse Generator

(2) Detection of Ultrasound Signals

The ultrasound pulse generated by the transmitter travels through the coupling medium (water) and the test sample before arriving at the receiver, which is an identical transducer to the transmitter. The received waveform is sent to a Lecroy 9400 digital oscilloscope. The Lecroy 9400 digital oscilloscope has a fast 8 bit vertical resolution A/D converter with a sampling rate of 100MS/s. which digitizes the ultrasound pulse. In order to improve the signal-to-noise ratio, the recorded waveform is stored in a 32 KB memory and processed by a built-in function called "continuous average". Continuous average consists of repeated addition, with unequal weight, of recurrences of the source waveform. Each newly acquired waveform is added to the accumulated average according to the formula:

$$S(i, new) = \frac{(N-1)}{N} \times S(i, old) + \frac{1}{N} \times W(i) \qquad (2.1)$$

until the random noise in the screen has reached acceptable minimum. The whole process usually takes about several seconds to several minutes which depends on the intensity of the signal. Because the repetition frequency of pulse generator is 125 Hz, the waveform obtained is therefore the average of several hundred to several thousand waveforms. Here $i$ is the index over all data points of the waveform, $W(i)$ is newly acquired waveform, $S(i, old)$ and $S(i, new)$ are the old and new accumulated averages and $N$ is the weighting factor and may be set as 2, 4, 8, ..., 256. In this experimental system, $N$ is set as 256.

(3) Transferring Data

The operation and the memory of the oscilloscope can be accessed by a PC through a IEEE-488 GPIB bus. The manufacturer of the oscilloscope provided all the operation codes for remote control through an IEEE-488 bus. The IEEE-488 bus that was used is NI-488 (1989) (National Instruments). The manufacturer of IEEE-488 bus provided a C programming language interface, allowing the remote operations of the oscilloscope and the data transfer between the oscilloscope and the PC to be easily done by simply programming the procedures.

A C-software was developed for data acquisition and the operation control of the oscilloscope. The major function of this software includes: (1) initialization of the IEEE-488 bus, (2) control of the operation states of the IEEE-488 bus, (3) setting operation and data acquisition modes for the digital oscilloscope, (4) setting ASCII data file format and (5) transferring the data file from the memory of the oscilloscope to the PC. The waveform stored in the memory has 32,000 data points and the time interval between two adjacent data points is 10 ns (100MS/s Sampling rate). In practice, a 32,000 data point file is too big and not necessary for data processing. For convenience, only 1024 data points, which cover the major time window (from trigger to main pulse) of the oscilloscope were chosen. The time interval between two adjacent data points was thus 100ns. Figure 2.4 shows a typical ultrasound pulse and its spectrum detected by this system. It has to be noted that the ultrasound pulse in Fig 2.4 (a) also includes the sensitivity and frequency response of the receiver transducer. Since the transmitter and receiver are identical, the

real amplitude spectrum emitted from transmitter should be the square root of the received spectrum profile multiplied by a constant.

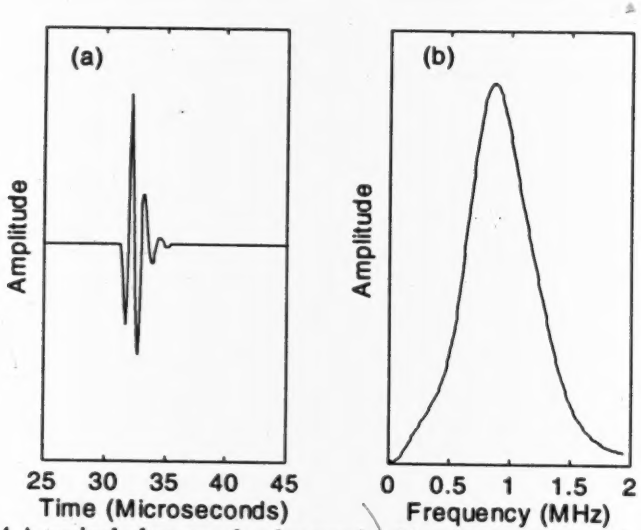


Figure 2.4 A typical ultrasound pulse received by the experimental system. (a) Signal, (2) Spectrum . The distance between the two transducers is 5.5 cm.

## 2.2 The Measurement of the Propagation Velocity of Ultrasonic Wave

The propagation velocity of an ultrasonic wave in a test sample can be measured by this experimental system. Two waveforms need to be recorded in the procedure. For the measurement, the distance between the transmitter and receiver is fixed as *L*. The waveform of the ultrasound pulse traveling directly through water is recorded as the reference, namely the water pulse. Then the test sample is inserted between two transducers, and the waveform of the ultrasound signal traveling through the test sample is

recorded as the sample pulse. The propagation velocity of the ultrasonic wave in the test sample can then be obtained by[58]:

$$V = \frac{V_w d}{d - V_w \Delta t} \qquad (2.2)$$

where $V_w$ is the propagation velocity of ultrasound wave in water, $\Delta t$ is the time difference between the sample pulse and the water pulse and $d$ is the thickness of the sample.

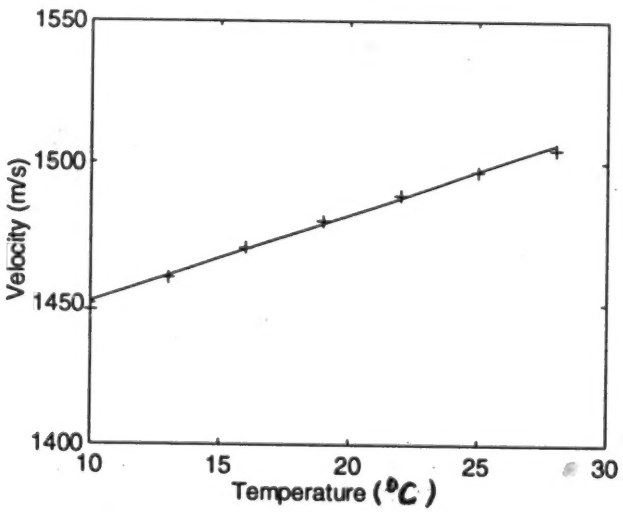


Figure 2.5 Temperature Calibrations of the Ultrasonic Velocity in Water

The propagation velocity of the ultrasound wave in water is an important parameter in this experiment. Because it is temperature dependent, $V_w$ as a function of temperature must be measured as the calibration curve. The propagation velocity of ultrasonic wave in water was measured first in this experiment. Figure 2.5 shows a

temperature calibration curve of the propagation velocity of an ultrasonic wave in water. The temperature range measured in Figure 2.5 is between 10 to 30 $C^{o}$. The calibration curve measured in Figure 2.5 agrees very well with the results reported in other references[9,16].

Table 2.1 The Propagation Velocities of Ultrasonic Wave in Different Solid Materials. (The Values in the Bracket are Uncertainties)

| Materials | Brass | Aluminum | Nylon | Iron |
|---|---|---|---|---|
| Velocity (m/s) | 4289(9) | 6391(20) | 2594(5) | 5877(10) |
| Reference(m/s) | 4300 | 6350 | 2620 | 5850 |

The propagation velocities of an ultrasonic wave in many different solid materials were measured by the method described by Equation (2.2). The results of the measurements are listed in Table 2.1. As a comparison, the values reported from reference are also listed in Table 2.1. From Table 2.1, we can see that the experimental results of this study agree well with the reported values. It is noted that the time difference $\Delta t$ in these measurements was chosen as the time difference between the "leading edge" of the water pulse and that of the transmission pulse for all tested samples. The leading edge is defined as the first motion of the ultrasound pulse in the measured waveform[58]. Figure 2.6 shows a typical leading edge of an ultrasound pulse. Even

though in many medical and industrial non-invasive detection systems the "leading edge" method is widely used in the measurement of pulse transmission transit time, it creates a big problem in the determination of the transit time in dissipative materials. A detailed discussion will be given in the next chapter.

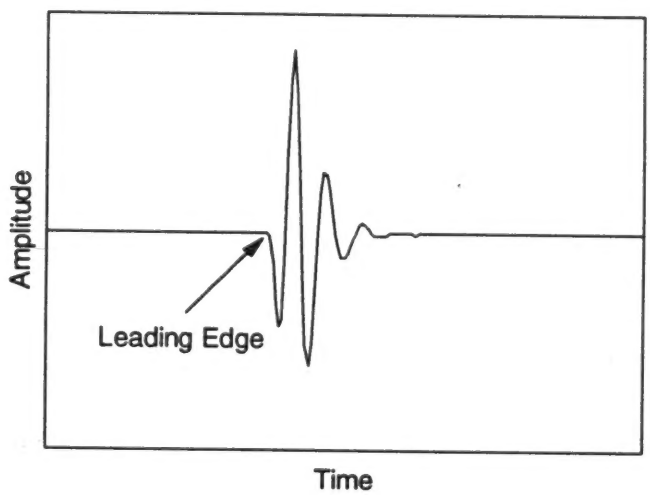


Figure 2.6 A typical "leading edge" of an ultrasound pulse

## 2.3 Measurements of Attenuation

The attenuation of an ultrasonic wave can be roughly defined as the loss of the beam energy during travel through the medium. Many factors can result in the attenuation of the ultrasonic wave. They can be classified into two types: (1) redirection of beam energy due to reflections on the boundaries of the medium and scattering inside the medium, (2)

absorption, where beam energy is converted into heat. If an ultrasonic wave travels in a medium, its intensity will be reduced as a function of distance due to the attenuation process. The expression for the plane wave beam intensity as a function of distance in a medium can be written as:

$$I(x) = I_0 e^{-ux} \tag{2.3}$$

where $I_0$ is the intensity at $x=0$ and $I(x)$ is the intensity at a depth $x$. $u$ is the intensity attenuation coefficient. For amplitude, the expression can be written:

$$A(x) = A_0 e^{-\alpha x} \tag{2.4}$$

where $A_0$ and $A(x)$ are the amplitude at $x=0$ and $x$, and $\alpha$ is the amplitude attenuation coefficient. The relation between the intensity attenuation coefficient and amplitude attenuation coefficient is:

$$u = 2\alpha \tag{2.5}$$

It is frequently convenient to express attenuation coefficients as logarithmic dB units, thus:

$$\alpha(dB) = 10 \log_{10}\left(\frac{I_0}{I(x)}\right) \tag{2.6}$$

In an experimental system, the attenuation of the ultrasonic wave is measured relative to the coupling medium, water. The ultrasonic wave generated by the transmitter travels through the coupling medium (water) and test sample and finally reaches the receiver. The possible attenuation of the ultrasonic wave includes: beam spreading, reflections from

water-sample boundaries, attenuation in the water and attenuation in the test sample. What we are really interested in this experiment is the measurement of the attenuation in the test sample, therefore the other factors that cause the attenuation of the beam need to be as small as possible. The beam spreading and the attenuation of the ultrasonic wave in water were tested by measuring the pulse amplitudes at different transmitter-receiver distances (from 3cm to 8cm). The results show that the beam spreading and attenuation in water is less than 1% and therefore can be ignored. There are two reflection surfaces for the test sample. For non-dissipative materials, the reflections from these two surfaces can be corrected by simple calculation of the reflection coefficients for each surface.

The attenuation coefficient for the test sample is usually a function of wave frequency, because absorption and scattering are both frequency-dependent processes. The ultrasonic pulse contains a specific range of frequencies, therefore it is possible to measure the attenuation as a function of wave frequency by spectral analysis. In spectral analysis, the fast Fourier transformation (FFT) is applied to the measured water pulse and the sample waveforms. The detailed FFT theory and method will be described in Appendix II. By FFT, the amplitude spectra of the water pulse and sample pulse can be obtained and the attenuation can be calculated from:

$$Attenuation(dB) = 20\,log\left(\frac{A_o(f)}{A_s(f)}\right) \qquad (2.7)$$

where $A_o(f)$ and $A_s(f)$ are the amplitude spectra of the water pulse and transmission pulse respectively. The above equation includes the loss due to the reflections from the two

surfaces of the sample. In most cases, the reflections can be deduced from equation 2.7 by calculation of the amplitude reflection coefficient. If the reflection coefficients of two surfaces are assumed to be $t_1$ and $t_2$, the attenuation can be calculated by:

$$Attenuation(dB) = 20\,log\left(\frac{A_o(f)}{A_s(f)}\right) - 20\,log\left(t_1 t_2\right) \qquad (2.8)$$

$t_1$ and $t_2$ are frequency independent in most cases and can be written as:

$$t_1 t_2 = \frac{4 z_1 z_2}{\left(z_1 + z_2\right)^2} \qquad (2.9)$$

where $z_1$ and $z_2$ are acoustic impedences of the water and sample material and can be expressed as:

$$z_1 = \rho_w V_w \qquad (2.10)$$

$$z_2 = \rho_s V_s \qquad (2.11)$$

where $\rho_w$ and $\rho_s$ are the densities of the water and sample material, and $V_w$ and $V_s$ are the propagation velocities in the water and sample.

In order to test the ability of this system to measure attenuation, 5 blocks of rubber phantoms were tested. The rubber phantoms were made of the same material but had different thicknesses (from 0.876 to 2.375 cm). Rubber is a dissipative material, its attenuation coefficient (attenuation normalized by thickness) is a linear function of wave

frequency. Therefore the attenuation in these rubber phantoms should be proportional to their thickness. Figure 2.7 shows the recorded waveforms of the ultrasonic pulse traveling through the rubber phantoms as well as the water pulse. The amplitude spectra of the waveforms were obtained by FFT and the attenuation was calculated by equation 2.5. For the rubber material, the density is 1.4 $kg/m^3$ and the propagation velocity is 1.76 km/s. The measured attenuation of the ultrasonic wave in the rubber phantoms as a function of wave frequency is shown in Figure 2.8. From Figure 2.8, we can clearly see that the attenuation of ultrasonic waves is a linear function of wave frequency (0.2 to 1.2 MHz) in the effective frequency range (0.15 to 1.4 MHz). Here the effective frquency is determined from amplitude spectrum of the transmission signal (above 20% of peak value). Linear least squares fitting was applied on those attenuation curves over the effective frequency range and the slopes plotted as a function of thickness in Figure 2.9. From Figure 2.9, the attenuation coefficient of the rubber material is about 18.7 dB/cm-MHz, which is very close to the reported value of 16.0 dB/cm-MHz for rubber material [16]. Since the minimum difference in thickness among the rubber phantoms is only about 0.2 cm, this system demonstrates at least 4 dB resolution for attenuation measurement.

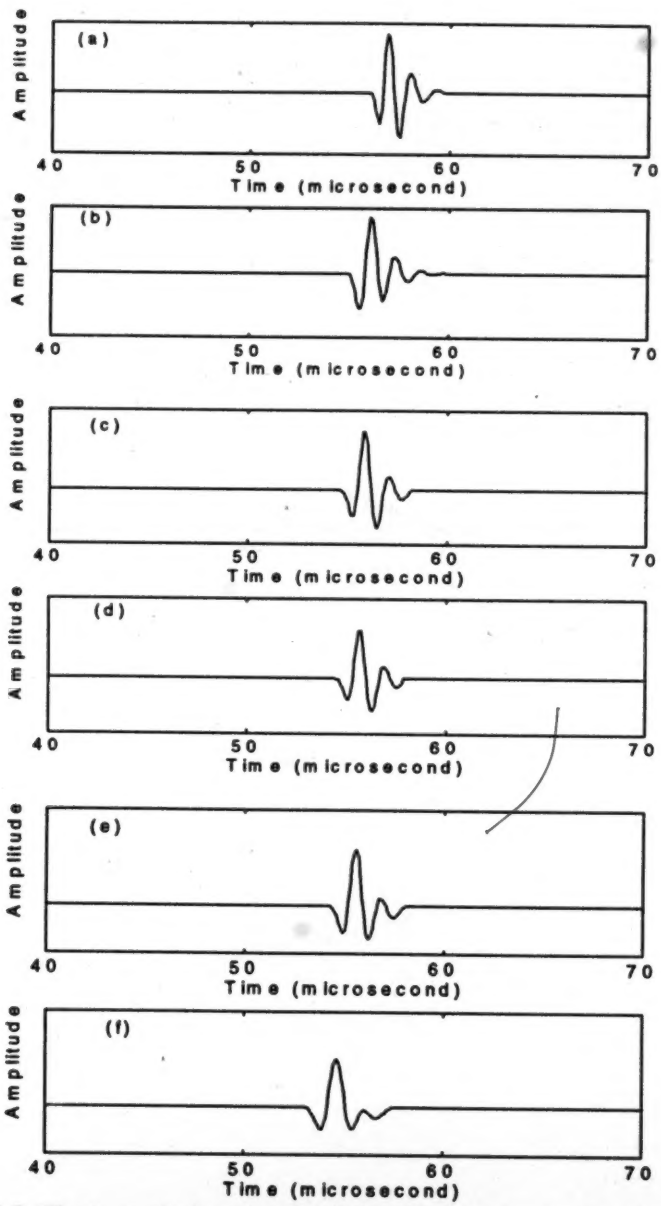


Figure 2.7 The transmission signals of the ultrasound pulse 5 rubber phantoms.
(a) water pulse, (b) thickness=0.876cm, (c) thickness=1.092cm,
(d) thickness=1.226cm, (e) thickness=1.407cm, (f) thickness=2.375cm
(The distance between the two transducers is 7.5 cm)

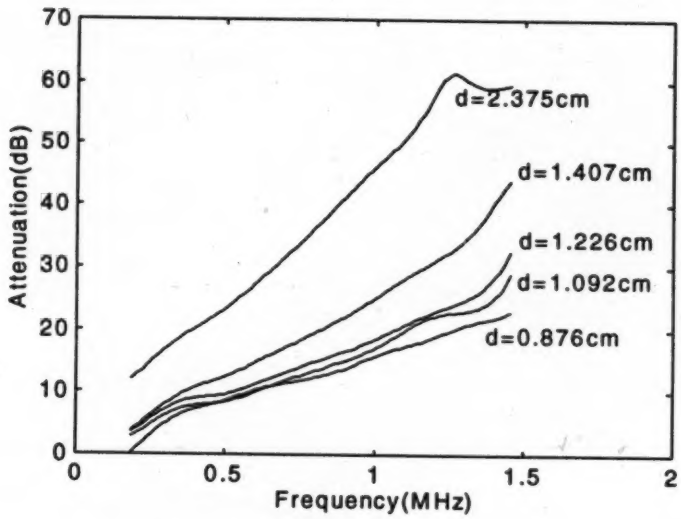


Figure 2.8 The attenuation of 5 rubber phantoms as the functions of wave frequency

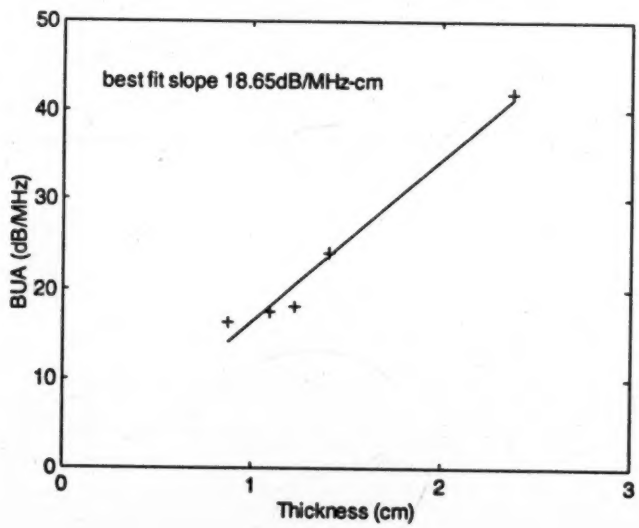


Figure 2.9 The ultrasonic attenuation in the rubber is a linear function of thickness

# Chapter Three : Propagation Velocity Measurement in The Frequency Domain

## 3.1 The difficulty in Determination of the Pulse Transit Time in the Dissipative Material

In chapter 2, the method of measuring propagation velocity of an ultrasonic wave in the time domain was described. In the time domain, the transmission transit time was determined by measuring the time difference between the "leading edges" of the water pulse and the transmission pulse. There are other ways of defining the transit time of the pulse in the time domain, such as zero crossing and thresholding[56]. The zero crossing method measures the time differences between consecutive zero crossing point pairs of the water pulse and the transmission pulse. As shown in Figure 3.1, there are 4 zero crossing point pairs that can be used to determine the transmission transit time for a brass sample. The propagation velocity of the ultrasonic wave in the medium is an objective quantity that describes the acoustic properties of the medium, therefore the results of all possible methods must be consistent. Let's compare the results of zero crossing and the leading edge in a brass sample. The transmission transit times obtained from the leading edges and the 4 zero crossing point pairs are listed in Table 3.1. From Table 3.1, we can see that the results are very consistent. Generally speaking, using leading edge methods to determine the transmission transit time in elastic materials such as metals and glasses provides accuracy, because the

Table 3.1 The Transmission Time in a Brass Sample (2.54cm) Determined by Leading Edge and Zero Crossing Points

| | *Leading Edge* | *1st zero crossing* | *2nd zero crossing* | *3rd zero crossing* | *4th zero crossing* |
|---|---|---|---|---|---|
| Time Diff. (μs) | 11.25 | 11.20 | 11.23 | 11.29 | 11.24 |

transmission pulse is only very slightly modified by the medium. Actually the leading edge and zero crossing methods are based on the assumption that the shape of the pulse does not change

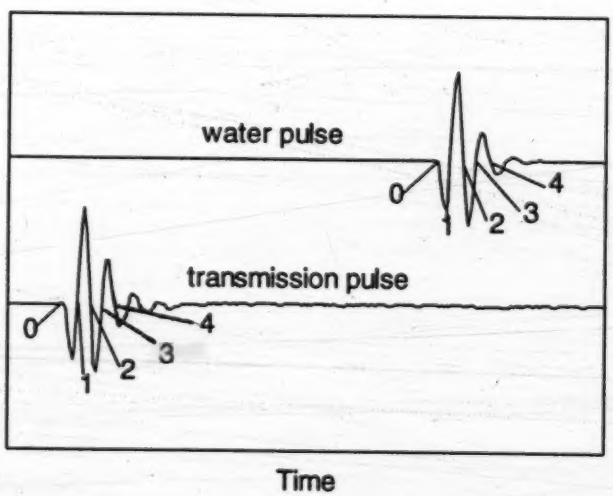


Figure 3.1 The leading edges and zero crossing points for the water pulse and transmission pulse through a brass sample (2.54cm)

after traveling through the sample. This assumption is not true for dissipative materials such as rubber and cancellous bone. Another example is provided. Figure 3.2 shows the leading edge and 4 zero crossing point pairs between the transmission pulse of a rubber phantom and the water pulse. In Table 3.2 the transit times obtained from the leading edge and 4 zero crossing point pairs are listed . We find that the results from the leading edge and 4 zero crossing pairs are not consistent, the discrepancy between

Table 3.2 The Transmission Time in Rubber Phantom Determined by the Leading Edge and Zero Crossing Points

| | *Leading Edge* | *1st zero crossing* | *2nd zero crossing* | *3rd zero crossing* | *4th zero crossing* |
|---|---|---|---|---|---|
| Time Diff. (μs) | 1.42 | 1.15 | 1.08 | 1.00 | 0.95 |

the leading edge and last zero crossing point pair being 66%. This results in a considerable variation in the determination of the propagation velocity of the ultrasonic wave in the rubber phantom. The reason for this inconsistency is possibly due to the attenuation occurring in the medium, which significantly modifies the shape of the pulse and correlates with the dispersion effect. In order to determine accurately the propagation velocity in dissipative material, the physical concept of propagation velocity of an ultrasonic wave must be understood.

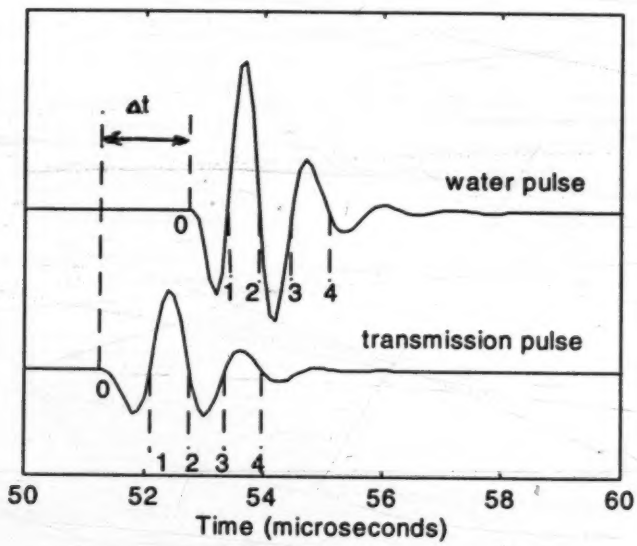


Figure 3.2 The leading edges and zero crossing points of the water pulse and the transmission pulse through a rubber phantom (0.986cm)

In physics only two distinct wave velocities are clearly defined for traveling waves: phase velocity, which is the velocity of a sinusoidal wave at single frequency, and group velocity, which is the velocity with which the amplitude envelope of a wave packet travels. A broadband ultrasonic pulse used in this experiment contains many sinusoidal waves with a frequency range from 0.1 MHz to 1.6 MHz. In a dissipative medium, these sinusoidal waves may travel with different phase velocities due to the dispersion caused by medium. Therefore the concept of phase velocity to describe the wave propagation in a medium has more physical significance.

There are many possible ways to determine the phase velocity of acoustic waves in dissipative material. For pulse transmission techniques, phase spectral analysis provides a more convenient approach to phase velocity measurement. In this chapter, the phase spectral analysis method of measuring phase velocity distributions in the broadband ultrasonic pulse will be introduced. As an example of the application of the phase spectral analysis, a detailed procedure to obtain the phase velocity distributions in a rubber phantom is presented.

### 3.2 The Phase Spectral Analysis Method

The phase spectral analysis method used in this study is based on the work of Wolfgang Sachse[52].

The signals of water and sample pulses detected by the receiver are both the functions of time and can be expanded as the summations of many plane waves:

$$f(t) = \int F(\omega) e^{-i\omega t} d\omega \qquad (3.1)$$

$$g(t) = \int G(\omega) e^{-i\omega t} d\omega \qquad (3.2)$$

where $f(t)$ and $g(t)$ are the water pulse and the sample pulse, $F(\omega)$ and $G(\omega)$ are their Fourier amplitudes, and $\omega$ is the angular frequency of the wave. In this experimental system, the water pulse is the pulse generated by the transmitter traveling through the water between the transducers, therefore $F(\omega)$ can be written:

$$F(\omega) = A(\omega)e^{-i\frac{\omega L}{V_w}} \tag{3.3}$$

where $A(\omega)$ is the amplitude of $\omega$ frequency generated by the transmitter, $V_w$ is the propagation velocity of the wave in water, which is assumed to be a constant for all frequencies because we know that the dispersion in water is very small, and $L$ is the distance between the transducers. By the same method, the Fourier amplitude of the sample wave can be written:

$$G(\omega) = A(\omega)e^{-i\omega\left(\frac{L-d}{V_w} + \frac{d}{V_s(\omega)}\right)} \tag{3.4}$$

where $d$ is the thickness of sample and $V_s(\omega)$ is the phase velocity of a sinusoidal wave at frequency $\omega$ in the sample. Comparing Equation 3.3 and Equation 3.4, we have:

$$G(\omega) = F(\omega)e^{-i\omega d\left(\frac{1}{V_s(\omega)} - \frac{1}{V_w}\right)} \tag{3.5}$$

The phase difference between the water pulse and the sample pulse can be defined as:

$$\Delta\Phi(\omega) = -\omega d\left(\frac{1}{V_s(\omega)} - \frac{1}{V_w}\right) \tag{3.6}$$

From Equation 3.6, the phase velocity can be calculated by:

$$V_s(\omega) = \frac{\omega d}{-\Delta\Phi(\omega) + \frac{\omega d}{V_w}} \tag{3.7}$$

The phase difference $\Delta\Phi(\omega)$ is the key in the calculation of phase velocity and can be obtained from the Fourier amplitudes of water and sample pulses. The Fourier amplitudes of water and sample pulses are complex quantities and can generally be written:

$$F(\omega) = F_1(\omega) + iF_2(\omega) \qquad (3.8)$$

and

$$G(\omega) = G_1(\omega) + iG_2(\omega) \qquad (3.9)$$

where $F_1(\omega)$ , $G_1(\omega)$ , $F_2(\omega)$ and $G_2(\omega)$ are all real quantities. The phase difference equals:

$$\Delta\Phi(\omega) = tan^{-1}\left(G_2(\omega)/G_1(\omega)\right) - tan^{-1}\left(F_1(\omega)/F_2(\omega)\right) \qquad (3.10)$$

The Fourier amplitudes of the water pulse and the sample pulse can be obtained by performing FFT on each of the waveforms. As described in the previous chapter, each waveform contains 1024 data points with 100ns steps. When using equation 3.10 to calculate the phase difference, the computation algorithm limits the value of the $tan^{-1}$ function from $-\pi$ to $\pi$. Thus, discontinuities of $\pi$ will occur whenever the magnitude of $\Delta\Phi(\omega)$ becomes less than zero or greater than $2\pi$. This can be corrected by adding or subtracting the amount of shift to render the phase shift spectrum continuous[32].

### 3.3 An Example:The Phase Velocity Measurement for a Rubber Phantom

The waveforms of a pulse traveling through a rubber phantom (thickness is 0.876 cm) and the water pulse are shown in Figure 3.2. The phase spectra analysis method was used to determine the phase velocities in this medium. FFT was performed on both transmission and water pulses. From equation 3.10, the phase difference spectrum was calculated by a program written in Matlab. In order to correct the $\pi$ shift in the phase difference spectrum, the *unwrap* function was used. The *unwrap* function was designed in Matlab to correct the $\pi$ shift by adding multiples of $\pm 2\pi$ when absolute shifts are greater than $\pi$. Figure 3.3(a) and (b) show the phase difference spectrum before and after correction. The use of the *unwrap* function may cause $\pm 2n\pi$ uncertainty at low frequencies because the spectral contents of the ultrasonic

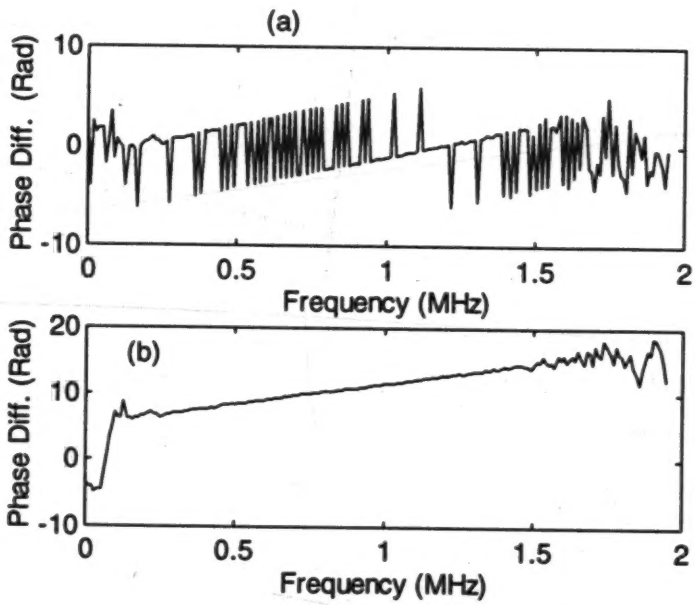


Figure 3.3 The phase difference spectrum. (a) before unwrap, (b) after unwrap

pulse do not extend all the way to zero frequency. This error can be eliminated by using the nearly linear behavior of the phase difference spectrum. First, using the data points within the usable range of frequencies (0.2 MHz to 1.2 MHz ), the y-axis intercept is calculated from the least squares fit to the data and compared with $\pm 2n\pi$. If there is a $\pm 2n\pi$ error, for example, the calculated y-axis intercept is close to $2n\pi$, and the correct phase difference spectrum is then obtained by subtracting or adding $2n\pi$. For the rubber phantom, the phase difference spectrum before and after correction is shown in Figure 3.4. The corrected phase difference spectrum is then used to calculate the phase velocities using equation 3.7. The phase velocities in the rubber phantoms within the bandwidth of the transducer are shown in Figure 3.5. From Figure 3.5, we can see that the dispersion in the rubber is very small, the variation among the phase

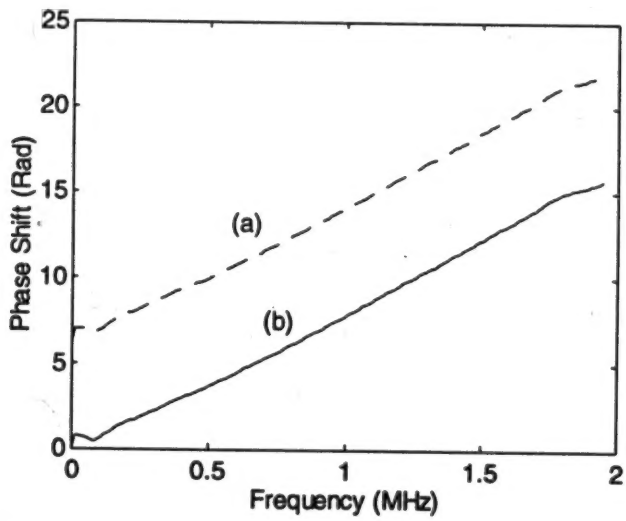


Figure 3.4 The phase difference spectrum in a rubber phantom. (a) before correction, (b) after correction

velocities are mainly due to the errors in the FFT. Therefore the ultrasonic waves contained in the pulse are approximately traveling with the same velocity.

### 3.4 Discussion about the Dispersion in the Dissipative Medium

The ultrasonic pulse has very small dispersion when it travels through the rubber phantom. According to the dispersion theory of acoustic waves in a dissipative material, the phase velocity of the acoustic wave is related to the attenuation by Kramers-Kronig relation (K-K). In the general K-K relation, it is required that the attenuation be known over all the frequencies. The simpler form of K-K relation, known as the local approximation, can be written[22]:

$$\frac{1}{V_s(\omega)} = \frac{1}{V_s(\omega_0)} - \frac{2}{\pi}\int_{\omega_0}^{\omega} \frac{\alpha_s(\omega')}{\omega'^2} d\omega' \qquad (3.11)$$

where $V_s(\omega_0)$ and $V_s(\omega)$ are respectively the phase velocities at frequencies $\omega_0$ and $\omega$. The $\alpha_s(\omega)$ is the attenuation coefficient with unit of Np/cm. Where the Np represents neper which is a unit used for expressing the ratio of two analogous quantities, the number of nepers is the nature logarithm of this ratio.

From the K-K relations, we know that the phase velocity will increase with the frequency if the attenuation is not zero. From chapter 2, we know that the attenuation in the rubber phantom is a linear function of frequency and the attenuation coefficient can be approximately expressed as:

$$\alpha(f) = A \times f \qquad (3.12)$$

As mentioned in chapter 2, the $A$ is measured to be 20 dB/cm-MHz. This is equivalent to 2.3Np/cm-MHz. Using equation 3.12 and equation 3.11, the velocity dispersion can be calculated over the effective frequency range of the pulse. From 0.2 MHz to 1.1 MHz, the phase velocity increases about 2.5% by K-K relations. This 2.5% phase velocity increase is very difficult to detect in our experiment because of the unequal error distributions of the FFT. The relative uncertainties of the signal are subject to redistribution after FFT. The minumum uncertainty occurs at maximum amplitude. From the amplitude spectrum, we know that the maximum amplitude is at 0.75 MHz for the transmission signal, and minumum amplitudes occur at low and high frequency ends. Therfore, the effective range of frequency is taken as the frequency range between 0.2 to 1.2 MHz with minimum uncertainty at 0.75 MHz. In Figure 3.5, the phase velocities obtained experimentally are compared with those obtained by the K-K relations. From Figure 3.5, we can see that the experimental results are consistent with the theoretical predictions, even though accurate dispersion can not be determined experimentally.

### 3.5 Transmission Delay Time

The transmission transit time for an ultrasonic pulse is defined as the time difference between transmission and water pulses. Since the dispersion relateded to the attenuation is very small, the waves contained in the pulse travel with almost the same

velocity in the medium. When a single frequency sinusoidal wave travels through the medium, the medium will modify the phase of the wave. As the result of this modification, the phase of a sinusoidal wave will be "delayed" in the time domain. The transmission delay time can be defined as:

$$\Delta t = \frac{\Delta\Phi(\omega)}{\omega} \tag{3.13}$$

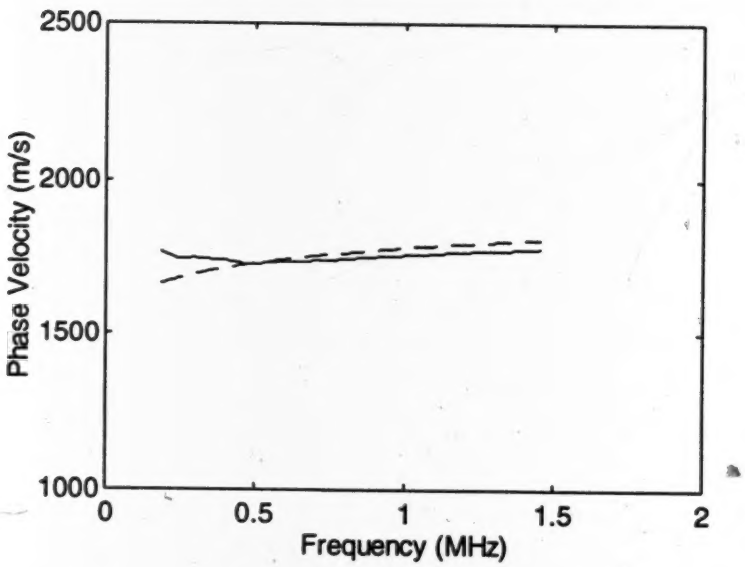


Figure 3.5 The phase velocity in rubber phantom. solid line: experiment, dashed line: K-K relation

For a pulse, Equation (3.13) actually defines a time delay spectrum. It is very interesting to compare the transmission delay time with the pulse transmission transit

time. In a rubber phantom, the transmission delay time can be obtained by averaging the transmission delay times over the frequency range of the pulse (0.1 MHz to 1.5 MHz). The transmission delay time is 1.01 μs. The pulse transmission transit time has not strictly been defined for dissipative material. Table 3.2 lists all the transmission transit times obtained from the leading edge method and the zero crossing method. By comparing, we find that the transmission delay time is between the pulse transmission transit times obtained from second zero crossing and third zero crossing measurements. No theory has ever proved that there is a relationship between the transmission delay time and the pulse transit time. However, it was found that the pulse transit time obtained from maximum convolution between water pulse and transmission pulse has a significantly correlation with the transmission delay time[44].

# Chapter Four : The Theory of Ultrasonic Wave Propagation in Fluid Filled Porous Solid Materials

The fundamental theory that describes the propagation of acoustic waves in fluid-filled porous materials is known as Biot's theory[7,8]. Biot's theory discusses the interactions of the solid frame with the viscous fluid induced by the acoustic wave as well as the influences of those interactions on the propagation modes of the acoustic wave. In this chapter, the basic idea of Biot's theory and the fundamental wave equations to describe the propagation of an acoustic wave will be introduced. In reality, a medium will always have finite size. To describe the behavior of an acoustic wave on the surface of a medium, the boundary conditions need to be known. In this chapter, open cell boundary conditions will be discussed.

## 4.1 Biot's Theory

Biot's theory was proposed by M. A. Biot in 1956. It is a theory that describes acoustic wave propagation in a macroscopically homogeneous and isotropic fluid filled porous material. The basic assumptions of Biot's theory are: (1) there exist volumes in the medium that are large compared to pore sizes but small compared to a wavelength in the medium, (2) the movements of each volume can be described by the average displacement of the fluid $U(\bar{r},t)$ and the solid frame $\bar{u}(\bar{r},t)$. The equations of motion are[34]:

$$\rho_{11}\frac{\partial^2\vec{u}}{\partial^2}+\rho_{12}\frac{\partial^2\vec{U}}{\partial^2}=P\nabla(\nabla\cdot\vec{u})+Q\nabla(\nabla\cdot\vec{U})-N\nabla\times(\nabla\times\vec{u})+bF(\omega)\left(\frac{\partial\vec{U}}{\partial}-\frac{\partial\vec{u}}{\partial}\right) \qquad (4.1)$$

and

$$\rho_{22}\frac{\partial^2\vec{U}}{\partial t^2}+\rho_{12}\frac{\partial^2\vec{u}}{\partial t^2}=R\nabla(\nabla\cdot\vec{U})+Q\nabla(\nabla\cdot\vec{u})-bF(\omega)\left(\frac{\partial\vec{U}}{\partial t}-\frac{\partial\vec{u}}{\partial t}\right) \qquad (4.2)$$

For the cases in which the solid skeletal frame is a single component homogenous material, $P$, $Q$, and $R$ are generalized elastic coefficients which can be related to the bulk modulus of fluid $K_f$, the bulk modulus of solid $K_s$, the bulk modulus of the skeletal frame $K_b$ and to $N$ which is the shear modulus of the skeletal frame.

$$P=\left\{\frac{(1-\Phi)\left(1-\Phi-\frac{K_b}{K_s}\right)K_s+\Phi\frac{K_s}{K_f}K_b}{1-\Phi-\frac{K_b}{K_s}+\Phi\frac{K_s}{K_f}}\right\}+\frac{4}{3}N \qquad (4.3)$$

$$Q=\frac{\left(1-\Phi-\frac{K_b}{K_s}\right)\Phi K_s}{1-\Phi-\frac{K_b}{K_s}+\Phi\frac{K_s}{K_f}} \qquad (4.4)$$

$$R=\frac{\Phi^2K_s}{1-\Phi-\frac{K_b}{K_s}+\Phi\frac{K_s}{K_f}} \qquad (4.5)$$

Here $\Phi$ is the porosity (fluid volume fraction). In the absence of the electrochemical interfacial effect between fluid and solid, the $K_b$ and $N$ become independent of what fluid is in the pores.

The density terms $\rho_{11}$, $\rho_{22}$ and $\rho_{12}$ in the equations of motion are related to the density of solid $\rho_s$ and density of fluid $\rho_f$ by:

$$\rho_{11} + \rho_{12} = (1 - \Phi)\rho_s \qquad (4.6)$$

$$\rho_{22} + \rho_{12} = \Phi\rho_f \qquad (4.7)$$

$$\rho_{12} = -(\Lambda - 1)\rho_f \qquad (4.8)$$

Here $\Lambda > 1$ is called the structure factor or tortuosity, which is a purely geometrical quantity independent of solid and fluid densities. The remaining parameters govern attenuation. b is related to the viscosity of the fluid $\eta$ and permeability of the solid frame k:

$$b = \frac{\eta\Phi^2}{k} \qquad (4.9)$$

$F(\omega)$ is a function that describes the relation between the viscous skin depth and the effective damping:

$$F(\omega) = \frac{1}{4}\frac{\kappa T(\kappa)}{\left[1 - 2T(\kappa)/j\kappa\right]} \qquad (4.10)$$

where

$$\kappa = a\left(\omega\rho_f / \eta\right)^{1/2} \qquad (4.11)$$

and

$$T(\kappa) = \frac{ber'(\kappa) + jbei'(\kappa)}{ber(\kappa) + jbei(\kappa)} \qquad (4.12)$$

where $a$ is the average pore size, and *ber()* and *bei()* are zero order and first order Kevin functions[7,8]. The viscous skin depth is defined as:

$$\delta = \sqrt{\frac{2\eta}{\omega\rho_f}} \qquad (4.13)$$

therefore $\kappa$ is equal to:

$$\kappa = \sqrt{2} \times \frac{a}{\delta} \qquad (4.14)$$

In the equations of motion (4.2) and (4.3), three basic coupling effects between the fluid and the solid frame are described. They are: inertial coupling, viscous coupling and static elastic coupling. The inertial coupling was described by the equations in $\rho_{11}$, $\rho_{22}$, $\rho_{12}$ terms. The inertial parameter $\Lambda$ is included in those mass coefficients. Physically, the inertial coupling corresponds to the fact that the saturated fluid does not flow through straight capillaries in the porous medium but follows a sinuous path through the porous network. The inertial interaction force is proportional to the relative acceleration of the fluid and the solid frame. The viscous coupling corresponds to the viscous force excerted by the fluid on the solid frame when the viscous fluid

flows within the pores. The viscous force is proportional to the relative velocity of the fluid and the solid frame. The static elastic coupling corresponds to the elastic moduli changes when the solid phase and fluid phase are interpenetratable.

The solutions to equations of motion (4.1) and (4.2) can be approached by two limited cases according to the wave frequency. The low frequency limit is the case where the viscous skin depth is much greater than the average pore size, therefore the fluid is totally locked to the solid frame. The medium behaves like a single system. The acoustic wave will propagate in two modes (longitudinal and transverse) and suffers high absorption in the medium. The solutions to the equations of motion in this case are diffusive. The high frequency limit is the case that the viscous skin depth is much smaller than average pore size, therefore only a small portion of the fluid is viscously locked to the solid frame. In this case the acoustic wave will propagate in three modes (two longitudinal and one transverse), as well be shown in the following section.

### 4.2 High Frequency Limit Solutions

For the high frequency limit, $\delta << a$, so we have:

$$\kappa \to \infty,\ T(\kappa) \to \frac{1+j}{\sqrt{2}} \tag{4.15}$$

and

$$F(\omega) \to \frac{\kappa}{4}\left(\frac{1+j}{\sqrt{2}}\right) \tag{4.16}$$

Because $F(\omega)$ is multiplied by a first order time derivative in the equations of motion, and $F(\omega) \propto (\omega)^{1/2}$, this term becomes very small compared to the other terms in the equations and can be ignored. The equations (4.1) and (4.2) can therefore be written:

$$\rho_{11}\frac{\partial^2 \bar{u}}{\partial t^2} + \rho_{12}\frac{\partial^2 \bar{U}}{\partial t^2} = P\nabla(\nabla \cdot \bar{u}) + Q\nabla(\nabla \cdot \bar{U}) - N\nabla \times (\nabla \times \bar{u}) \qquad (4.17)$$

$$\rho_{22}\frac{\partial^2 \bar{U}}{\partial t^2} + \rho_{12}\frac{\partial^2 \bar{u}}{\partial t^2} = R\nabla(\nabla \cdot \bar{U}) + Q\nabla(\nabla \cdot \bar{u}) \qquad (4.18)$$

For the shear wave, we have:

$$\nabla \cdot \bar{u} = 0,\ \nabla \cdot \bar{U} = 0 \text{ and } \nabla \times \bar{u} \neq 0 \qquad (4.19)$$

the wave equations (4.17) and (4.18) become:

$$\rho_{11}\frac{\partial^2 \bar{u}}{\partial t^2} + \rho_{12}\frac{\partial^2 \bar{U}}{\partial t^2} = -N\nabla \times (\nabla \times \bar{u}) \qquad (4.20)$$

$$\rho_{22}\frac{\partial^2 \bar{U}}{\partial t^2} + \rho_{12}\frac{\partial^2 \bar{u}}{\partial t^2} = 0 \qquad (4.21)$$

If we assume $\bar{u} = u(x)\hat{j}$, because

$$\nabla \times (\nabla \times \bar{u}) = -\frac{\partial^2 u}{\partial x^2}\hat{j} \qquad (4.22)$$

the wave equations can be reduced to:

$$\rho_{11}\frac{\partial^2 u}{\partial t^2} + \rho_{12}\frac{\partial^2 U}{\partial t^2} = N\frac{\partial^2 U}{\partial x^2} \qquad (4.23)$$

and

$$\rho_{22}\frac{\partial^2 U}{\partial t^2}+\rho_{12}\frac{\partial^2 u}{\partial t^2}=0 \qquad (4.24)$$

For a single frequency wave $u(x,t)=u(x)e^{-i\omega t}$, the equation for the propagation is:

$$\left(\rho_{11}-\frac{{\rho_{12}}^2}{\rho_{22}}\right)\frac{\partial^2 u}{\partial t^2}=N\frac{\partial^2 u}{\partial x^2} \qquad (4.25)$$

The propagation velocity for the shear wave can be obtained:

$$V_{shear}=\sqrt{\frac{N}{(1-\Phi)\rho_s+\left(1-\frac{1}{\Lambda}\right)\Phi\rho_f}} \qquad (4.26)$$

Associated with the propagation of the shear wave, the motions of the solid frame and the fluid are in phase.

For the longitudinal wave,

$$\nabla\cdot\vec{u}\neq 0,\ \nabla\cdot\vec{U}\neq 0 \text{ and } \nabla\times\vec{u}=0 \qquad (4.27)$$

assume the solutions for the equations (4.1) and (4.2) are:

$$\vec{u}=u(x,t)\hat{i},\ U=U(x,t)\hat{i} \qquad (4.28)$$

the wave equations become:

$$\rho_{11}\frac{\partial^2 u}{\partial t^2}+\rho_{12}\frac{\partial^2 U}{\partial t^2}=P\frac{\partial^2 u}{\partial x^2}+Q\frac{\partial^2 U}{\partial x^2} \qquad (4.29)$$

$$\rho_{22}\frac{\partial^2 U}{\partial t^2}+\rho_{12}\frac{\partial^2 u}{\partial t^2}=R\frac{\partial^2 U}{\partial x2}+Q\frac{\partial^2 u}{\partial x^2} \qquad (4.30)$$

for single frequency waves:

$$u(x,t)=Ae^{j(\omega t-kx)} \quad \text{and} \quad U(x,t)=Be^{j(\omega t-kx)} \qquad (4.31)$$

substitute (4.31) into (4.29) and (4.30) we have:

$$\left(k^2P-\omega^2\rho_{11}\right)A+\left(k^2Q-\omega^2\rho_{12}\right)B=0 \qquad (4.32)$$

$$\left(k^2Q-\omega^2\rho_{12}\right)A+\left(k^2R-\omega^2\rho_{22}\right)B=0 \qquad (4.33)$$

Because $A$ and $B$ should not be equal to zero at the same time, the equations that determine the propagation modes can be written:

$$\begin{vmatrix}\left(k^2P-\omega^2\rho_{11}\right) & \left(k^2Q-\omega^2\rho_{12}\right)\\ \left(k^2Q-\omega^2\rho_{12}\right) & \left(k^2R-\omega^2\rho_{22}\right)\end{vmatrix}=0 \qquad (4.34)$$

Here

$$k^2=\left(\frac{\omega}{V}\right)^2 \qquad (4.35)$$

The propagation velocities can be obtained:

$$V_{1,2}=\sqrt{\frac{2\left(PR-Q^2\right)}{\Delta\pm\sqrt{\Delta^2-4\left(\rho_{11}\rho_{22}-\rho_{12}{}^2\right)\left(PR-Q^2\right)}}} \qquad (4.36)$$

and

$$\Delta = R\rho_{11} + P\rho_{22} - 2Q\rho_{12} \tag{4.37}$$

The theory predicts two longitudinal waves in the medium. Because $V_1 < V_2$ The wave propagating with velocity $V_1$ is named the slow wave and the other the fast wave. It is very interesting to see how the fluid and solid frame move corresponding to these two waves. From equations (4.32) and (4.33), we find that the amplitude of the displacement for the solid frame $A$, and the amplitude of the displacement for the fluid $B$ generally have the relation:

$$A = rB \tag{4.38}$$

where

$$r = \frac{k^2Q - \omega^2\rho_{12}}{k^2P - \omega^2\rho_{11}} \tag{4.39}$$

Substituting (4.36) into (4.39), it is very easy to prove that for the fast wave $r > 0$ and for the slow wave $r < 0$. This indicates that the motions of the solid frame and the fluid are in phase for the fast wave mode and out of phase by 180 degrees for the slow wave. It should be noted that each wave mode is simultaneously present in both the fluid and solid frame.

### 4.3 Boundary Conditions

Biot's theory describes the acoustic wave propagation in fluid filled porous materials. In most experimental cases, the sample has finite size and the acoustic wave is

generated from a source outside the sample. In order to understand how the longitudinal wave converts from a single propagation mode outside the sample into two propagation modes inside the sample, the boundary conditions must be established. For elastic porous samples, there are usually two types of boundary conditions depending on whether the surface is open or sealed. In our experiments, the surfaces of the sample were open, with same fluid filled outside and inside the sample. Therefore our discussion is just limited to the open surface situation.

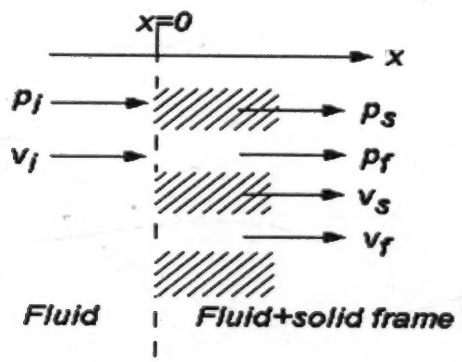


Figure 4.1 Cross-section of an open surface

For an open cell surface, as shown in Figure 4.1, the fluid in the sample is connected to the fluid outside the sample. Let the particles of the solid frame have velocity $v_s$, the particles of the fluid in the internal field has velocity $v_f$ and the fluid in the external field have velocity $v_i$. At the surface the normal volume velocity per unit area must be continuous[10], therefore at $x=0$, we have:

$$v_s(1-\Phi)+v_f\Phi=v_i \tag{4.40}$$

To disallow infinite accelerations, the pressure in the external field must equal to both the pressure of the fluid in the pore and the frame normal stress at the surface[10], therefore at $x=0$, we get:

$$(1-\Phi)p_i=p_s \tag{4.41}$$

and

$$\Phi p_i=p_f \tag{4.42}$$

where $p_i$, $p_s$ and $p_f$ are the pressures on the external field, solid frame and fluid in the pore. It should be noted that the porous material is assumed to be homogenous so that the surface porosity is equal to the volume porosity. Equations (4.40), (4.40) and (4.41) give the boundary conditions of an open surface sample. The acoustic transport properties of the sample can be studied based on these boundary conditions.

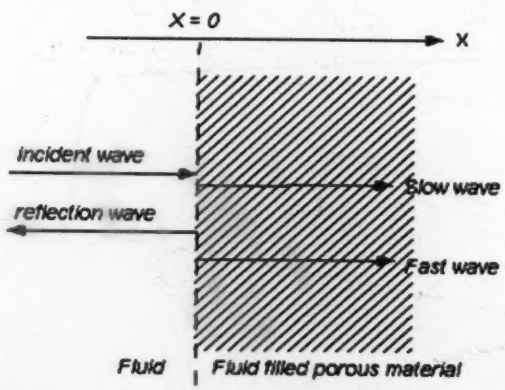


Figure 4.2 The waves generated on an open surface

Let's first consider an open surface of a semi-infinite porous medium (Figure 4.2). When a plane longitudinal acoustic wave strikes the surface from the external fluid ($x<0$), the external wave field will contain the incident and reflected waves. For normal incidence, the external field can be written as:

$$U(x,t) = L_1 e^{j(\omega t - k_f x)} + L_2 e^{j(\omega t + k_f x)} \quad \text{for } x<0 \qquad (4.43)$$

where $U(x,t)$ is the displacement of the fluid. The internal field ($x>0$) contains two wave modes, and each mode will propagate in both the solid frame and the fluid. The acoustic field can be written as:

$$u(x,t) = r_1 B_1 e^{i(\omega t - k_1 x)} + r_2 B_2 e^{i(\omega t - k_2 x)} \qquad (4.44)$$

for the solid frame and

$$U(x,t) = B_1 e^{i(\omega t - k_1 x)} + B_2 e^{i(\omega t - k_2 x)} \qquad (4.45)$$

for the fluid. In (4.44) and (4.45), $u(x,t)$ and $U(x,t)$ are the average displacements of the solid frame and the fluid, $k_1$ and $k_2$ are the propagators of the slow wave and fast wave modes, and $r_1$ and $r_2$ are defined by Equation (4.39). The acoustic pressure and the particle velocity of the external field are:

$$p(x,t) = -K_f \frac{\partial U}{\partial x} \qquad (4.46)$$

and

$$v = \frac{\partial U}{\partial t} \tag{4.47}$$

where $K_f$ is the bulk modulus of the fluid. In the internal field, the stress and the velocity of motion of the solid frame are:

$$P_s = -\left( P\frac{\partial^2 u}{\partial x^2} + Q\frac{\partial^2 U}{\partial x^2} \right) \tag{4.48}$$

$$v_s = \frac{\partial u}{\partial t} \tag{4.49}$$

The pressure and the velocity of motion of the fluid are:

$$p_f = -\left( R\frac{\partial U}{\partial x} + Q\frac{\partial u}{\partial x} \right) \tag{4.50}$$

$$v_f = \frac{\partial U}{\partial t} \tag{4.51}$$

Using boundary conditions (4.40), (4.41) and (4.42), the transmission and reflection coefficients of the wave on the surface can be obtained. It should be noted that the wave mode has been converted from a single longitudinal mode in the external field into two longitudinal modes on the surface.

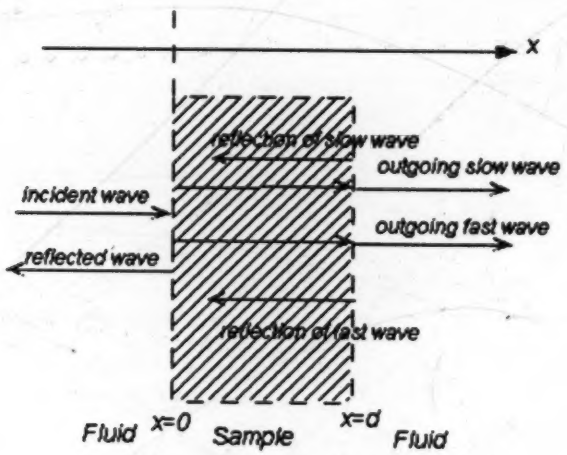


Figure 4.3 The acoustic wave transmission through a finite sample

For the experimental arrangement of pulse transmission technique, there are two such surfaces on the sample as shown in Figure 4.3. One is the input surface and the other is the output surface. The input wave has been converted into the fast and slow wave on the input surface. In the medium, the fast wave and slow wave propagate independently. On the output surface $x=d$, the displacment of the solid frame and the displacement for the fast wave are:

$$u_1 = r_1 B_1 e^{-ik_1 x} + r_1 B_1 R_1 e^{ik_1 x} \qquad (4.52)$$

and

$$U_1 = B_1 e^{-ik_1 x} + B_1 R_1 e^{ik_1 x} \qquad (4.53)$$

where $R_1$ is the amplitude reflection coefficient of the fast wave on the output surface. The external wave field for the fast wave is:

$$U = De^{-ik_f x} \tag{4.54}$$

Using same boundary conditions (4.40), (4.41) and (4.42), the transmission coefficient of the fast wave on the output surface can be obtained. The transmission coefficient of the slow wave can be obtained in the same way. The detailed procedure is given in Appendix I.

# Chapter Five: The Experimental Studies of the Ultrasonic Transport Properties of Water-Saturated Aluminum Foams

Biot's theory described the general behavior of acoustic wave propagation in a fluid filled solid porous material and predicts two longitudinal propagation modes for the acoustic wave. A lot of experimental effort has been made to detect these propagation modes in various fluid filled porous materials such as glass beads[34,46], polyurethane foam[10], sedimentary rocks and sands[11]and cancellous bone[28]. In most of these cases only one longitudinal mode has been detected and in a very few cases both the fast and slow wave modes were observed at the same time. Since porous solid materials behave quite differently from their solid form, it is impossible to derive their acoustic properties from the properties of the bulk material. The importance of Biot's theory is that it not only predicts two longitudinal waves in the medium, but also provides a useful theory to understand acoustic wave propagation in the complex two phase system and therefore enables us to calculate the acoustic properties of the medium.

In this chapter, the experimental results of the ultrasonic study of the water-saturated aluminum cellular forms will be presented. The original initiative for this study was not intended to detect two longitudinal propagation modes. The major purpose of the study was an attempt to establish a simple experimental model to explore the acoustic transport properties of cancellous bone. The cellular aluminum foam is very similar to

cancellous bone in that they both have an open cell structure. When the aluminum foam is saturated with water, the whole composite medium should have a lot of similarities to the marrow filled cancellous bone. On the other hand, the cell structure of the aluminum foam is much simpler than the structure of the natural cancellous bone. The bulk material of the aluminum foam is homogenous elastic metal. Most of the physical parameters of the aluminum foam are known or easy to estimate, thus the calculations of the acoustic properties from Biot's theory is straight forward.

## 5.1 The Cellular Aluminum Foam Samples

The cellular aluminum foam is a very recently developed engineering material. Its bulk material is 7010 aluminum alloy which is a homogenous, isotropic and elastic metal. The major feature of this material is its high strength and low density. The aluminum foam samples used in this study were provided by the EGR company (USA) in 2"×2"×1" (5.0 cm×5.0 cm×2.5cm) blocks. The porosity and the cell sizes of the samples can be designed independently over a specific range. The cell sizes of all the samples in this study were fixed at 40 cells per inch, with the porosities ranging from 88% to 95% (12% to 5% density). The matrix of the cells and ligaments are completely repeatable, regular and uniform throughout. Here the cell is defined as a minimum repeatable volume which includes a solid part ligament and a void part(pore). The porosity is the volume percentage of the void part in each cell. a typical cellular aluminum foam sample is shown in Figure 5.1.

## 5.2 The Experimental Method and Procedure

The broadband pulse transmission technique was used for the test of the aluminum samples. The detailed experimental arrangement has been described in chapter 2. The dry samples were cleaned in an ultrasonic bath for about 1 hour and then immersed in degassed water.

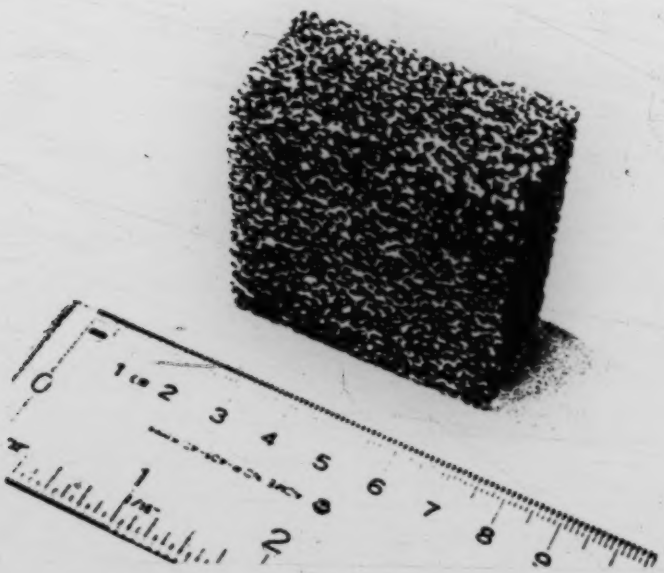

Figure 5.1 The cellular aluminum sample (40 PPI)

Before measurement, the prepared samples were moved from degassed water to the water tank without exposure to air. Water temperature was measured by a mercury thermometer. The distance between the two transducers was fixed at 7.5 cm. The samples

were tested along their length (5.08 cm) direction with surfaces parallel to the surfaces of the transducers. The distance between the sample and transmitter is 1.5 cm.

## 5.3 Results

(a) Waveforms

The waveforms of an ultrasonic pulse through samples of 95%, 93%, 90% and 88% porosities are shown in Figure 5.2 (a) to (d) respectively. For comparison, the water pulse is also shown in each figure. From Figure 5.2 (d), we can see clearly that two pulses appear in the received signal for the 88% porosity sample. The first pulse travels faster and the second pulse travels slower than the water pulse. The two received pulses are very similar except their amplitudes. The amplitude of the first arrival is smaller than that of the second arrival. These two pulses can be identified as the fast and the slow waves respectively . The prediction of Biot's theory appears to have been proved here. For the 95% porosity sample (Figure 5.2(a)), the received waveform is complex. The amplitude of the first arrival is very small, and can only be detected by very large gain of the digital oscilloscope, saturating the main body of the waveform. The second arrival contains two oscillations. The first oscillation is completely in phase with the water pulse and has obvious shorter period than that of the second one. From the wave form of the 88% porosity sample we know that the slow wave pulse has a similar pulse shape with that of the fast wave, therefore, the observed second arrival in the 95% porosity sample can be assumed to be the slow wave partially overlapped with another wave pulse. It is not

difficult to distinguish the slow wave from the "third" unknown wave pulse. This unknown wave pulse will be discussed in Section 5.4 below. Figure 5.2 (b) and (c) show the waveforms of the ultrasonic pulse traveling through 95% and 90% porosity samples. The "third" unknown wave pulse still appears in the waveform of each sample, but the amplitude decreases with the decrease of the porosity

(b) Measurements of the Propagation Velocities

The propagation velocities of both the fast and the slow waves in the water-saturated samples can be measured by the phase analysis method which has been described in Chapter 3. Each received signal contains two pulses as well as the noise due to scattering and reverberation. In order to do phase analysis, it is necessary to use temporal windows to isolate the slow wave pulse as well as the fast wave. For clean pulses like in Figure 5.2 (d), the temporal window width was chosen to just cover each pulse and the rest of the points in the time domain were set to zero. For complex waveforms like in Figure 5.2(a) to (c), it is very difficult to chose an appropriate temporal window to separate the slow wave with the unknown "third" wave pulse, because they are overlapped. For simplicity, the temporal windows, in these cases, were chosen to cover the second oscillations of the second arrival. It must be noted that part of the "third" unknown pulse was also included in the temporal window for each waveform.

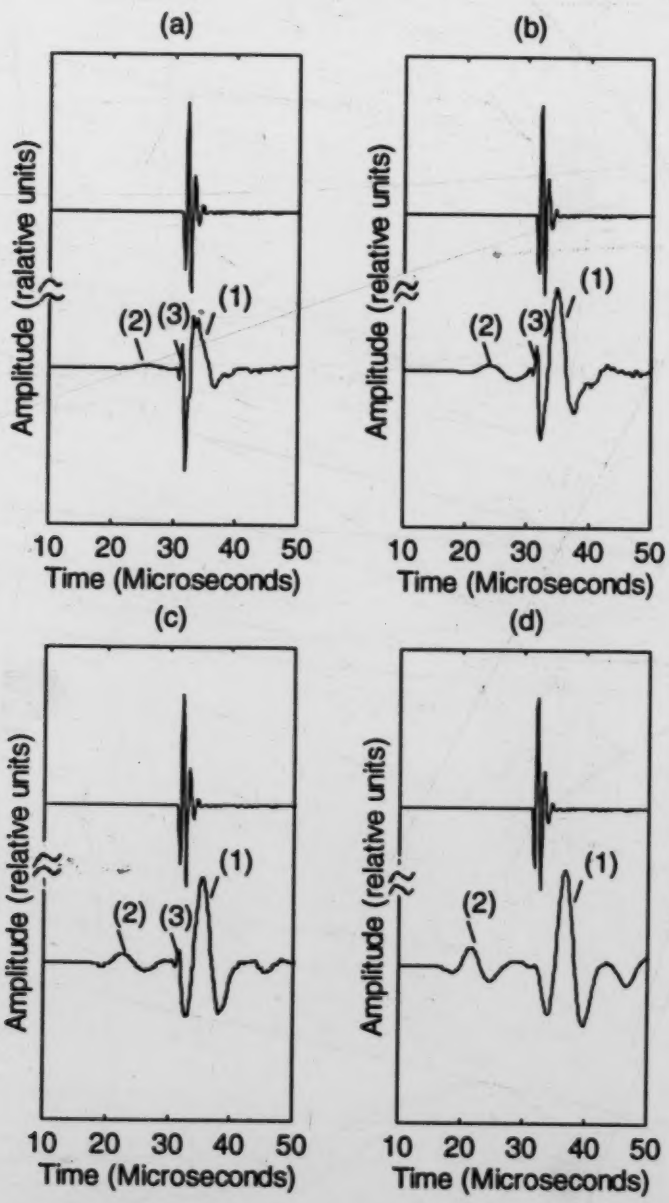


Figure 5.2 The waveforms of the transmission pulses through (a) 95% porosity sample, (b) 93% porosity sample, (c) 90% porosity sample, (d) 88% porosity sample. In each waveform, top: water pulse, bottom: (1) slow wave, (2) fast wave, (3) unknown third wave.

The phase velocities of each isolated pulse over the frequency range covered by the amplitude spectrum can be obtained by the phase spectrum method described in Chapter 3. Figure 5.3 (a) to (d) show the results of the measurements. The results tell us important information about ultrasonic wave propagation in water-saturated aluminum foams: the dispersions of both the slow wave and fast wave are very small. The propagation velocities can be represented by the average value over the covered frequency range.

TABLE 5.1 The Velocities of Fast and Slow Waves in the Samples

| Density ($kg/m^3$) | Porosity | Velocity of Fast Wave (km/s) | Velocity of Slow Wave (km/s) |
|---|---|---|---|
| 136 | 95% | 1.79 ±0.06 | 1.41±0.05 |
| 190 | 93% | 1.82 ±0.05 | 1.37±0.04 |
| 271 | 90% | 1.98±0.04 | 1.34±0.04 |
| 325 | 88% | 2.09±0.03 | 1.30±0.03 |

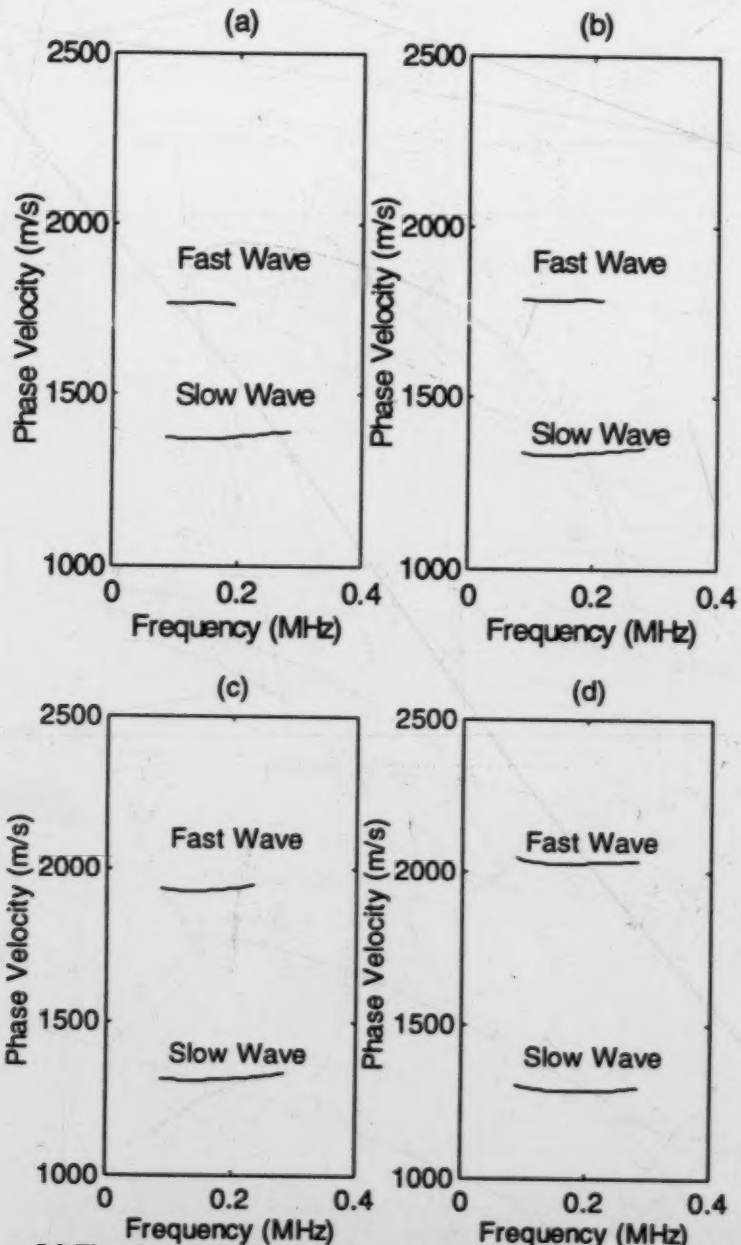


Figure 5.3 The phase velocities obtained from transmission pulses (a) for the 95% porosity sample, (b) for the 93% porosity sample, (c) for the 90% porosity sample, (d) for the 88% porosity sample.

These values are listed in Table 5.1.

(c) Amplitude Spectra

FFT can give both the phase and amplitude spectra for each isolated pulse. The phase spectra were used to calculate phase velocities. For each phase spectrum, the corresponding amplitude spectrum was used to identify the effective frequency range of the spectrum. Figure 5.4 (a) to (d) show these amplitude spectra. From Figure 5.4 we can see that the amplitude distributions of the fast and the slow waves in each sample behave in a very similar way: they are both restricted in a very narrow low frequency range (0.1MHz to 0.3 MHz) and peak values at about 0.15 MHz. The amplitude spectra of 95%, 93% and 90% porosity samples contain high frequency portion, which is due to the contamination by the unknown "third" wave, because the temporal windows were not able to separate the slow wave pulse completely.

(d) BUA

From the amplitude spectra, the attenuation of the ultrasonic wave as a function of the wave frequency can also be obtained. Since the input wave pulse has been converted into a fast wave pulse and a slow wave pulse, the attenuation have to be redefined. For convenience, the attenuation for the fast wave and slow wave is defined as:

$$\alpha_1(f) = 20\log_{10}\left(\frac{A_1(f)}{A_0(f)}\right) \qquad (5.1)$$

and $$\alpha_2(f) = 20\log_{10}\left(\frac{A_2(f)}{A_0(f)}\right) \qquad (5.2)$$

where $A_1$(f) and $A_2(f)$ are the amplitude spectra of the fast wave and slow wave. Equations (5.1) and (5.2) include the loss due to reflections. The attenuation as the function of wave frequency for all test samples is shown in Figure 5.5 (a) to (d). From Figure 5.5, we can see that the attenuation of the fast and slow waves in the water-saturated aluminum foams are strongly frequency dependent. Attenuation is not a linear function of the wave frequency.

**5.4 Discussions**

The experimental results of the broadband ultrasonic studies of water-saturated aluminum foams have been presented. The measured waveform of the 88% porosity sample shows a typical medium response to the input ultrasonic pulse. In the 95%, 93% and 90% porosity samples, an unknown "third" pulse was observed. This unknown pulse is very likely due to the "free" fluid (water) in the medium. As analyzed above, the viscous and inertial couplings between the solid frame and the fluid are very weak, therefore in very high porosity sample, there is not enough solid material to "hold" the all the fluid if the length of the sample is limited. The "free" water forms many straight water paths in the medium. As a result, only part of the fluid is coupled with the solid frame and part of the

fluid is free. The input pulse can propagate in the free water directly without interacting with the solid frame but can also propagate through the water which is coupled with

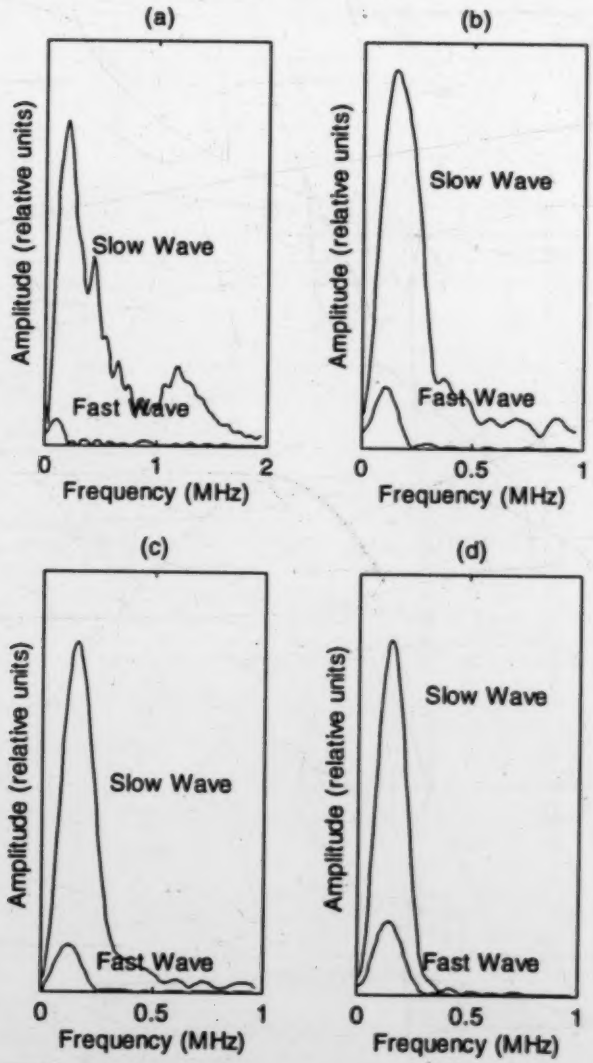


Figure 5.4 The amplitude spectra for the transmission pulse through (a) 95% porosity sample, (b) 93% porosity sample, (c) 90% porosity sample (d) 88% porosity sample.

(a)

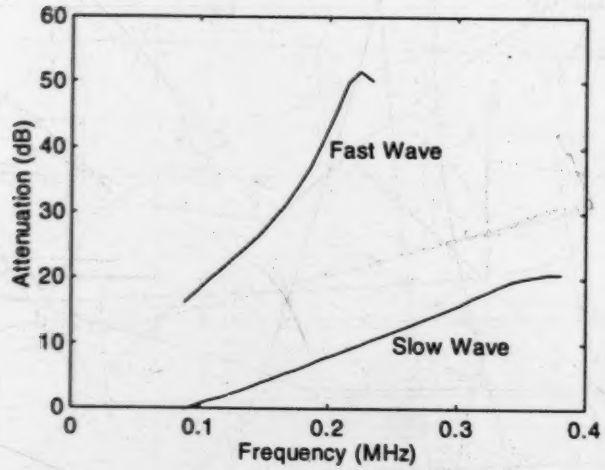
Attenuation (dB)
Frequency (MHz)
Fast Wave
Slow Wave
0
10
20
30
40
50
60
0.1
0.2
0.3
0.4

(b)

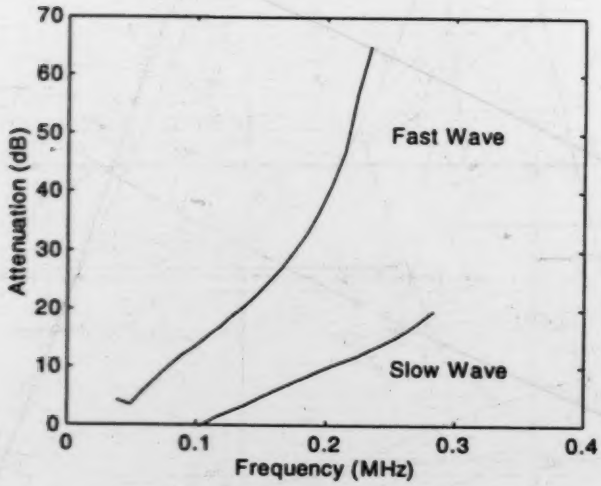
Attenuation (dB)
Frequency (MHz)
Fast Wave
Slow Wave
0
10
20
30
40
50
60
70
0.1
0.2
0.3
0.4

(c)

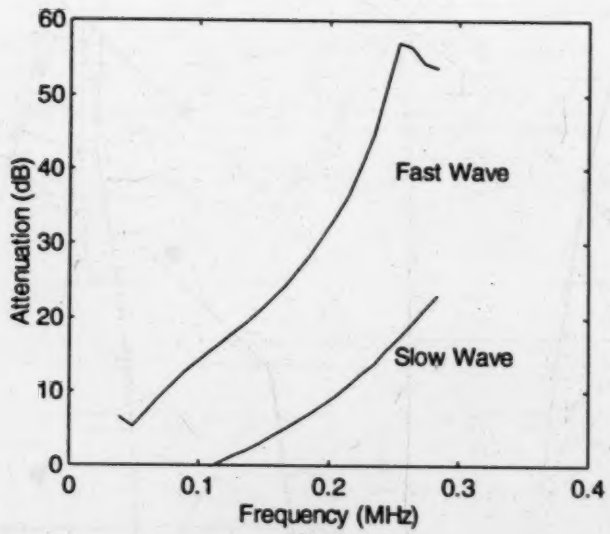


(d)

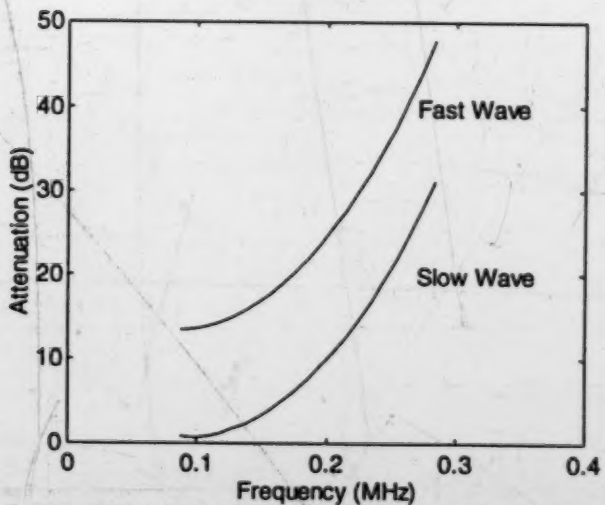


Figure 5.5 The BUA in (a) 95% porosity sample, (b) 93% porosity sample (c) 90% porosity sample, (d) 88% porosity sample

the solid frame. This will result in the presence of two overlapped wave pulses in the observed waveform. The pulse which travels through the free water does not suffer the same scattering loss as the coupled wave does, therefore it will maintain its high frequency feature similar to the input pulse. This unknown pulse, which we would call a "leaking pulse", is actually just an artifact in a very high porosity sample, but its existence will change the coupling picture of Biot's theory, because in the theory, the fluid is assumed to be totally coupled with the solid frame in a medium of infinite length.

The fast and the slow wave pulses are both restricted to a very narrow low frequency range. Since the viscous interaction in the medium is very small, the attenuation is therefore mainly due to scattering. The amplitude of the slow wave is larger than that of the fast wave. This suggests that our experimental arrangement is more favourable to the excitation of the slow wave mode. Since both inertial and viscous couplings in the medium are very weak, the fast wave is largely determined by the properties of the solid frame. Similarly, the slow wave is largely determined by the properties of water. When an input ultrasonic pulse interacts with the surface of the sample, because the surface of the sample is open, the solid part and the fluid part on the sample are both excited. If the surface has the same porosity as the medium, the fluid part occupies about 90 percent of the boundary surface and the solid part only 10 percent. As a result, the incident wave is converted primarily into a slow wave mode. The detailed theoretical analysis of the experimental results will be given in the next chapter.

## 5.5 Experiments on the Gelatine-Water Mixture Filled Aluminum Foams

The gelatine-water mixture that is investigated in this section is a material that has been used as a bone marrow mimic in many bone phantoms[13]. The acoustic properties of a gelatine-water is very close to bone marrow, but the viscosity is about 10 times less than that of bone marrow( Viscosity of gelatine-water mixture (11g powder in 150 ml water) is about 0.014 poise)[13]. The major difference between water and gelatine-water is that the latter is not a simple fluid phase material. It is very interesting to study the ultrasonic transport properties of the gelatine-water filled aluminum foams. This study can provide very useful information about the interactions between gelatine-water and the aluminum frame.

(1) The acoustic properties of gelatine-water mixtures

The gelatine-water materials were obtained by adding different amounts of dry gelatine powder to water in the temperature of 40 ℃. For the ultrasonic test, the concentration of gelatine power should be chosen as a compromise between the increased mechanical stiffness at high concentration and maintaining a relatively flexible fluid at low concentration. After many tests, it was found that adding 10g gelatine powder to 300 ml water achieved the best result. The ultrasonic test system for the gelatine-water mixture is shown in Figure 5.6. In this system, two identical P wave ultrasonic transducers were mounted on two oppose sides of a plastic box ( 3"×3"×3"). Before the test, water filled

in the box. The ultrasonic pulse traveling through water only was first recorded as a reference. Then water was replaced by the gelatine-water mixture in fluid phase, and

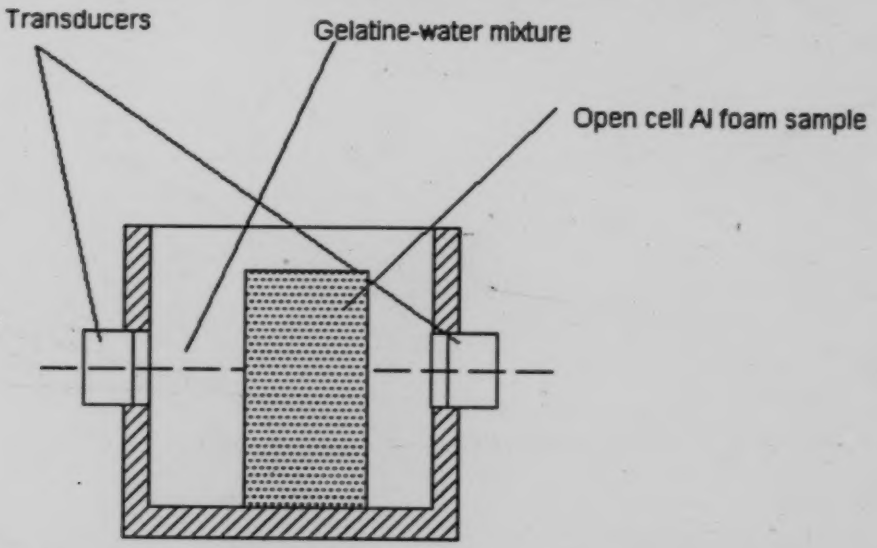


Figure 5.6 The Experimental System Designed for Gelatine-Water Filled Aluminum Foams

ultrasonic signals were initially recorded while the mixture was in the fluid phase. After the mixture formed the gelatinate phase, the ultrasonic signal was recorded again. The temperatures of the mixture and of the water reference medium were monitored by a electronic thermometer during the measurement process. Figure 5.7 shows the ultrasonic waveforms of the gelatine-water mixture in the fluid phase and the gelatinate phase. From Figure 5.7, we can see there is no difference between the signals of the fluid phase and the gelatinate phase except a time delay which is due to the temperature difference. The

temperatures were measured as 36 °C at fluid phase and 21 °C at gelatinate phase. This temperature difference will cause a 0.3 μs time difference. The amplitudes of two pulses

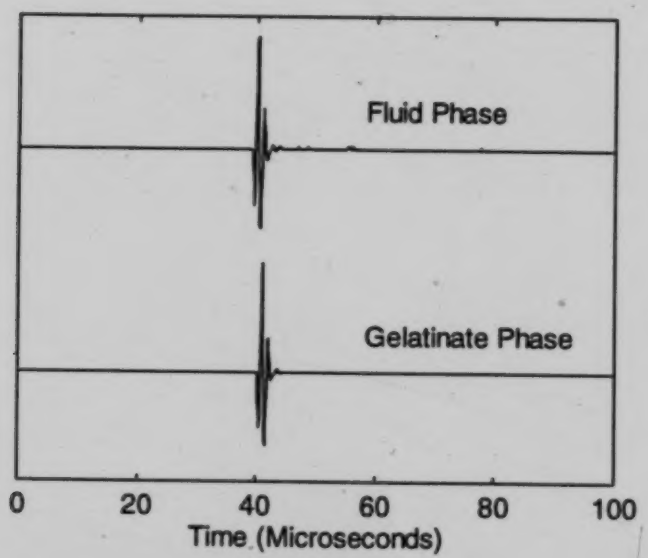


Figure 5.7 The ultrasonic signals in gelatine-water mixture. Top: in fluid phase Bottom: in Gelatinate Phase

are almost same. This means that the attenuation of the ultrasonic wave due to the phase change is very small and can be ignored. Comparing the ultrasonic signal in the gelatine-water mixture with the ultrasonic signal in water, we found that they are exactly identical, which means that the acoustic properties of the gelatine-water mixture are the same as that of water fluid.

(2) The ultrasonic signal in gelatine-water mixture filled aluminum foams

A 90% porosity cellular aluminum foam was saturated with the gelatine-water mixture in the fluid phase in the testing box. The ultrasonic transmission waveforms were recorded as shown in Figure 5.8. From Figure 5.8, we found that the transmission waveforms in gelatine-water mixture (for both fluid phase and gelatinate phase) filled aluminum foam are almost identical to the transmission waveform of water-saturated aluminum foam as shown in Figure 5.2 (c). Two propagation modes can be identified from the waveforms.

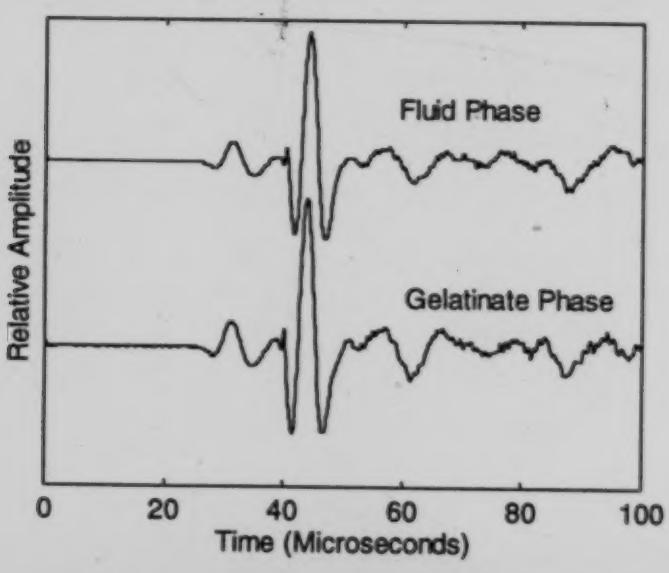


Figure 5.8 The Transmission Waveforms in Gelatine-Water Mixture Filled Cellular Aluminum Foam (90% Porosity Sample). Top: The Mixture in Fluid Phase, Bottom: The Mixture in Gelatinate Phase

The fast wave pulses of the two waveforms are identical but there is a very slight shift between slow wave pulses which is due to the temperature difference. Similar results were obtained from the ultrasonic tests of gelatine-water filled aluminum foams with 95%, 93%

and 88% porosity samples. Table 5.2 lists the results. These results show that the acoustic properties of gelatine-water filled aluminum foams are the same as those of the water - saturated aluminum foams, even though the gelatine-water is not a perfect fluid. Since the viscosity of gelatine-water mixture is very close to that of water, the effect of viscous coupling can not be observed in the experiments.

Table 5.2 The Wave Propagation Velocities in Gelatine-Water Mixture Filled Al Foams

| Porosity | Propagation Velocities (km/s) (mixture in fluid phase) | | Propagation Velocities (km/s) (mixture in gelatinate phase) | |
|---|---|---|---|---|
| | fast wave | slow wave | fast wave | slow wave |
| 95% | 1.78 | 1.40 | 1.78 | 1.39 |
| 93% | 1.82 | 1.37 | 1.82 | 1.37 |
| 90% | 1.96 | 1.34 | 1.97 | 1.34 |
| 88% | 2.05 | 1.31 | 2.05 | 1.30 |

Table 5.3 The Wave Propagation Velocities in Gelatine-Water Mixture

| | Propagation Velocity (km/s) |
|---|---|
| Fluid Phase | 1.51 |
| Gelatinate Phase | 1.48 |

The conclusion drawn from the above experimental results is that the acoustic behavior of a gelatine-water mixture trapped in the pores of an aluminum foam is exactly the same as that of water, regardless of whether it is in a fluid phase or gelatinate phase.

# Chapter Six :Theoretical Studies of the Ultrasonic Transport Properties of Water-Saturated Aluminum Foams

The experimental results of the broadband ultrasonic studies of water-saturated aluminum foams show the characteristics of ultrasonic wave propagation in fluid-filled porous materials. In this chapter, a detailed theoretical study of ultrasonic wave propagation in the water-saturated aluminum foams will be presented. This study is based on the Biot's theory summarized in Chapter four.

## 6.1 The Mechanical Properties of Cellular Aluminum Foams

In order to understand the acoustic transport properties of the water-saturated aluminum foam, the mechanical properties of the dry material must be known. The most important mechanical parameters of the dry material, which influence its acoustic transport properties, are the elastic moduli of the skeleton (structure). Since the cellular aluminum foam is an artificial material, its mechanical properties have been studied and tested by the manufacturer. Ashby[2] summarized a common character of many man-made porous materials such as metal foams and open cell polyurethane. When a foam is compressed, the strain response of the foam is characterized by the stress-strain curve as shown in Figure 6.1. At low strain, the foam deforms in a linear-elastic behavior. With increasing strain, the stress-strain curve reaches plateau, and the deformation of the foam is almost

at constant stress. Corresponding to this part of curve, the cells of the foam begin to collapse. With the further increase of strain, the deformation of the foam reaches a

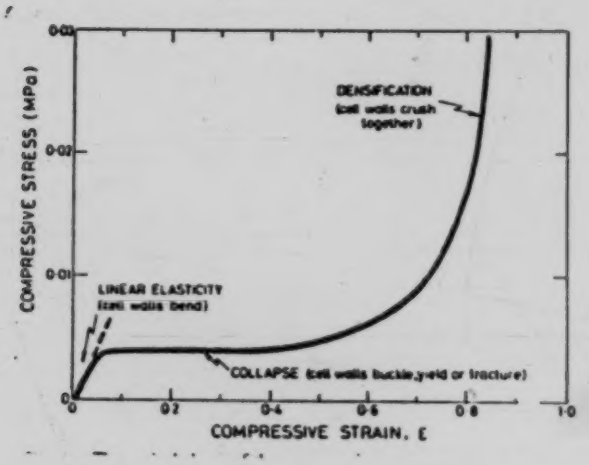


Figure 6.1 The relation of stress and strain in a cellular metal foam

region where all the cell walls crush together. Because the stress disturbance of an acoustic wave usually is very small, the dry foam response to the acoustic wave is in the linear region of the stress-strain curve.

In the linear-elastic region of the stress-strain curve, the elastic moduli ($K_b$ for bulk and $N$ for shear) of the foam can be expressed as:

$$K_b = K_s C_1 \left( \frac{\rho_b}{\rho_s} \right)^n \qquad (6.1)$$

and $$N = N_s C_2 \left( \frac{\rho_b}{\rho_s} \right)^n \qquad (6.2)$$

where $C_1$ and $C_2$ are constants, $K_s$ and $N_s$ are the bulk and shear moduli of the bulk material, and $\rho_b$ and $\rho_s$ are the densities of the foam and bulk material. The parameter $n$ is a constant which depends upon the structure of the foam. For isotropic foam, $n$=2. The mechanical tests of many metal foams show that the constants $C_1$ and $C_2$ are both very close to 1.

### 6.2 The Viscous Coupling in the Water-Saturated Aluminum Foam

Viscous interaction between the solid frame and the fluid is an important factor that influences the acoustic properties of many fluid filled porous materials. The viscous coupling between the solid frame and the fluid is described by the viscous penetration depth, which is defined as:

$$\delta = \sqrt{\frac{2\eta}{\rho_f \omega}} \qquad (6.3)$$

where $\eta$ and $\rho_f$ are, respectively, the viscosity and the density of the water, and $\omega$ is the angular frequency of the wave. The viscous penetration depth is a frequency dependent parameter. For water, the viscosity and density are 0.01 poise and 1000 kg/m$^3$. In an experiment, the ultrasonic wave frequency covers a range from 0.1 MHz to 1.5 MHz. The

viscous penetration depth therefore can be calculated from equation 6.3. The calculated viscous depth of water is about 2 μm at 0.1 MHz frequency and 0.6 μm at 1.5 MHz frequency. For the aluminum foam used in this experiment, the cell size of each aluminum foam sample is fixed at 40 cells per inch, corresponding to a dimension of 0.63 mm. The pore size is abut 0.55mm for the 88% porosity sample and 0.6mm for the 95% porosity sample. The penetration depth is much smaller than the pore size in each sample, which means that only a very thin layer of the fluid (water) is locked to the solid frame and most of the fluid in the pore is viscously free. This analysis shows that the viscous coupling in the water-saturated aluminum foam is very small, and therefore all the discussions in Chapter 4 for the high frequency approximation can be used to calculate the phase velocities in the water-saturated aluminum foams. In Biot's theory, the only wave energy dissipation process in fluid-filled porous materials is due to the viscous interaction. In water-saturated aluminum foam, this interaction is very small and can be ignored. The main influence of viscous interaction on wave propagation is the dispersion of the phase velocity. In our experiments, the phase velocities for both fast and slow waves in all tested samples had very small dispersion, and this fact agreed with this analysis.

### 6.3 The Inertial Coupling in Water-Saturated-Aluminum Foams

In Biot's theory, the structure factor $\Lambda$ is an important parameter that determines the inertial coupling between the solid frame and the fluid. As described in Chapter 4, in the case where the viscous coupling can be ignored, the structure factor $\Lambda$ is a real number

and always greater than 1. The structure factor Λ only depends on the geometry of the pores and the porosity. Berryman[6, 48] theoretically derived the relationship between Λ and porosity in the case of isolated spherical solid particles in the fluid:

$$\Lambda = \frac{1}{2} + \frac{1}{2}\left(\frac{1}{\Phi} + 1\right) \qquad (5.4)$$

where Φ is the porosity of the medium. This equation can be used to estimate the structure factor in isotropic porous materials such as consolidated and unconsolidated glass beads. For anisotropic materials, Williams[61] proposed a general formula:

$$\Lambda = \frac{1}{2} + R\left(1 + \frac{1}{\Phi}\right) \qquad (6.5)$$

where $R$ is a parameter which depends on the geometry of the pores. For the cellular aluminum foam, the pore structure is not absolutely spherical (R<0.5), but the magnitude of the structure factor can be estimated by the following formula:

$$\Lambda = \frac{1}{2} + 0.3\left(1 + \frac{1}{\Phi}\right) \qquad (6.6)$$

Considering that the porosities of the aluminum foams range from 88% to 95%, the structure factors for the aluminum foam samples are between 1.15 and 1.09, which are close to 1. That means the inertial coupling between water and the aluminum frame is not very strong.

### 6.4 The Propagation Velocities of Ultrasonic Wave

The propagation velocity of the ultrasonic wave in the water-saturated aluminum foams can be calculated from the Biot's theory. The physical parameters required for the calculation are listed in Table 6.1. From the analysis above, the structure factor $\Lambda$ is the only unknown parameter. In the calculation, $\Lambda$ is determined by fitting the calculated propagation velocities with the experimental values. The calculated propagation velocities and fitted $\Lambda$ values are listed in Table 6.2. For comparison, the experimental results are also listed in Table 6.2. From Table 6.2, we can see that results of the theoretical calculations agree very well with the experimental results except for the 95% sample. The fitted $\Lambda$ values are reasonable. The discrepancy between the calculated values and the experimental values for the 95% porosity sample is most likely due to the presence of the "leaking" wave pulse.

Table 6.1 The Basic Physical Parameters of the Water-Saturated Aluminum Foams

| | |
|---|---|
| Bulk Modulus of Solid Material $K_s$ | 83.1 GPa |
| Shear Modulus of Solid Material $N_s$ | 25.9 GPa |
| Bulk Modulus of Fluid $K_f$ | 2.19 GPa |
| Density of Fluid (water) $\rho_f$ | 1000 Kg/m$^3$ |
| Density of Solid Material $\rho_s$ | 2710 Kg/m$^3$ |
| Viscosity of Fluid (water at 20 °C) $\eta$ | 0.01 Poise |

Table 6.2 The Velocities of Fast and Slow Waves in the Samples

| Density (Kg/m$^3$) | $\Phi$ | $\Lambda$ | Velocity of Fast Wave (m/s) Experiment | Theory | Velocity of Slow Wave (m/s) Experiment | Theory |
|---|---|---|---|---|---|---|
| 136 | 95% | 1.02 | $1.79\times10^3$ | $1.60\times10^3$ | $1.41\times10^3$ | $1.34\times10^3$ |
| 190 | 93% | 1.03 | $1.82\times10^3$ | $1.75\times10^3$ | $1.37\times10^3$ | $1.39\times10^3$ |
| 271 | 90% | 1.08 | $1.98\times10^3$ | $1.95\times10^3$ | $1.34\times10^3$ | $1.34\times10^3$ |
| 325 | 88% | 1.14 | $2.06\times10^3$ | $2.09\times10^3$ | $1.30\times10^3$ | $1.31\times10^3$ |

## 6.5 Ultrasonic Transport Properties and *r* Values

(1) Transport Properties

An input wave is converted into a slow wave ,a fast wave and a reflection wave on the input surface of a sample. The fast and slow waves propagate in the medium independently, therefore the transmission coefficients of the fast wave and slow wave can be defined as:

$$T_f = t_{f1} t_{f2} \tag{6.7}$$

$$T_s = t_{s1} t_{s2} \tag{6.8}$$

where $t_{f1}$ and $t_{f2}$ are the amplitude transmission coefficients of the fast wave on the input and output surfaces, and $t_{s1}$ and $t_{s2}$ are the amplitude transmission coefficients of the slow wave on the input and output surfaces. On the input surface, $t_{f1}$ and $t_{s1}$ are defined as:

$$t_{f1} = \frac{A_f}{A_0} \tag{6.9}$$

$$t_{s1} = \frac{A_s}{A_0} \tag{6.10}$$

where $A_f$ and $A_s$ are the amplitudes of the fast and slow waves created on the input surface. $A_0$ is the amplitude of the input wave. These transmission coefficients can be calculated from the boundary conditions discussed in Chapter four. A detailed derivation can be found in Appendix I. If the medium is dissipative, the transmission coefficients are usually complex, which means the transmission waves will have a phase shift with respect

to the input wave on the input surface. Let's consider a non-dissipative case. The calculated amplitude transmission coefficients are listed in Table 6.3

Table 6.3 The Calculated Transmission Coefficients for a Non Dissipative Water-Saturated Al Foams

| | $T_f$ | $T_s$ |
|---|---|---|
| 95% porosity | 0.24 | 0.70 |
| 93% porosity | 0.29 | 0.64 |
| 90% porosity | 0.32 | 0.61 |
| 88% porosity | 0.34 | 0.59 |

$T_f$ and $T_s$ represent the conversion efficiencies of the fast and slow waves in the medium. The data show that the water-saturated aluminum foams are more inclined to transmit or convert to the slow wave mode. This agrees with experimental observations.

(2) The Relation Between the Motions of the Solid Frame and the Fluid

Corresponding to the fast and slow waves, the motions of the solid frame and the fluid are coupled together. The displacements of the solid frame and the fluid have a linear relation as shown in Equation (4.38). In Equation (4.38), the $r$ coefficient is the ratio of the displacement amplitudes of the solid frame and the fluid. The calculated $r$ coefficients for both the fast and the slow waves are listed in Table 6.4. The $r$ coefficients are negative for the slow wave and positive for the fast wave. This means the motions of the solid frame and the fluid are in phase for the fast wave and out of phase by 180 degrees for the slow wave. The absolute values of $r$ for the slow wave are smaller than 1, and greater than 1 for

the fast wave. This means the slow wave is dominated by the motion of the fluid and the fast wave is dominated by the motion of the solid. The acoustic properties of the medium are more like these of the fluid for the slow wave and more like those of the solid frame for the fast wave.

Table 6.4 The Calculated *r* Coefficients

| | Slow Wave | Fast Wave |
|---|---|---|
| 95% porosity | -0.712 | 2.24 |
| 93% porosity | -0.601 | 3.67 |
| 90% porosity | -0.575 | 3.77 |
| 88% porosity | -0.462 | 3.88 |

### 6.6 The Acoustic Scattering in the Water-Saturated Aluminum Foam

Biot's theory appears to be the most generally effective theory for two component systems where one is a fluid. In the previous discussions in this chapter, the experimental results of the broadband ultrasonic tests of the water-saturated aluminum foams have been shown to be well described as a special case of Biot's theory. One of the fundamental predictions of the theory: two longitudinal propagation modes, has been observed. The theoretical calculations agree very well with the experimental observations. Unfortunately, the attenuation of the acoustic wave, which is an important aspect of the wave propagation, is not described very well by Biot's theory. In the theory, the only wave

energy dissipation process is the viscous interaction between the solid frame and the fluid (poroelastic attenuation). Rasolofosaon[49] modified Biot's theory and introduced another type of attenuation process: viscoelastic attenuation, which is due to the viscoelastic properties of the solid frame. In the water-saturated aluminum foams, the solid frame is totally elastic and the viscous penetration depth of water is much smaller than the average pore size. Therefore the two attenuation processes in the theory are supposed to be very small and can be ignored. The most fundamental attenuation process in the inhomogenous medium; scattering, is not described in the theory at all, because the two phase components in the medium are assumed coupled together and the wave can travel across the interface between the solid frame and the fluid in two wave modes without any redirection. This does not agree very well with the experimental results. In the experiment, the attenuation of the input pulse in the medium is very high and shows a strong wave frequency dependence especially in the high frequency range. In order to evaluate the role of scattering processes in wave propagation, the scattering wave for the 90% porosity sample was measured by rotating the receiver (detection direction) perpendicular to the wave propagation direction. The observed scattering waveform is shown in Figure 6.2. The corresponding amplitude spectrum is shown in Figure 6.3. The frequency range of the scattering wave is mainly in the high frequency portion. This agrees very well with the experimental observation that the frequency range of the transmission wave (either fast wave or slow wave) is restricted in the low frequency portion. Of course the spectrum of scattering wave (Figure 6.3) does not give the accurate information about scattering wave

because the amplitudes of the input pulse and the frequency response of the receiver has the similar spectrum as the profile of the Figure 6.3. But this fact at least suggests that the scattering process is the major attenuation source in the water-saturated aluminum foam. Water-saturated aluminum foam is not a perfect medium as described in Biot's theory. The theory assumes that the average pore size is much smaller than the wavelength so that the motions of the solid frame and the fluid can be described by their average displacements and the wave "sees" the medium as a coupled homogenous medium. If the acoustic wavelength is smaller than or of the same order of magnitude as the pore size, the coupling effects of Biot's theory is broken down, the medium simply behaves like a random inhomogenous medium, and the wave will suffer high scattering loss when

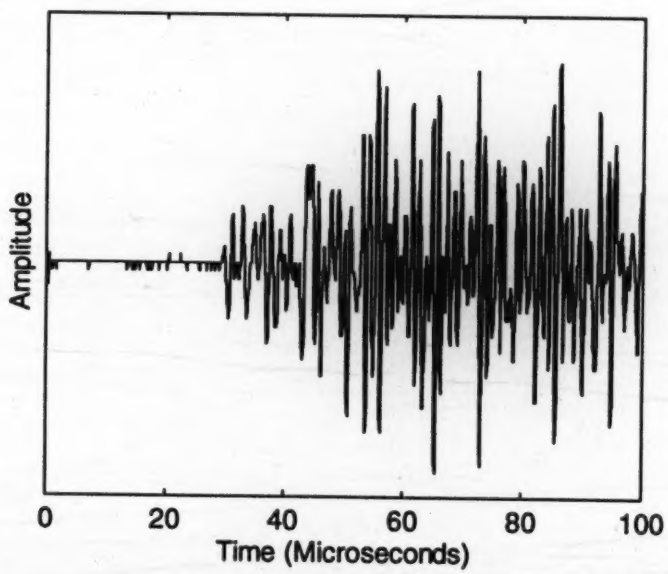


Figure 6.2 The scattering wave measured in 90% porosity sample (Rotating the receiver 90 degree with the propagation direction).

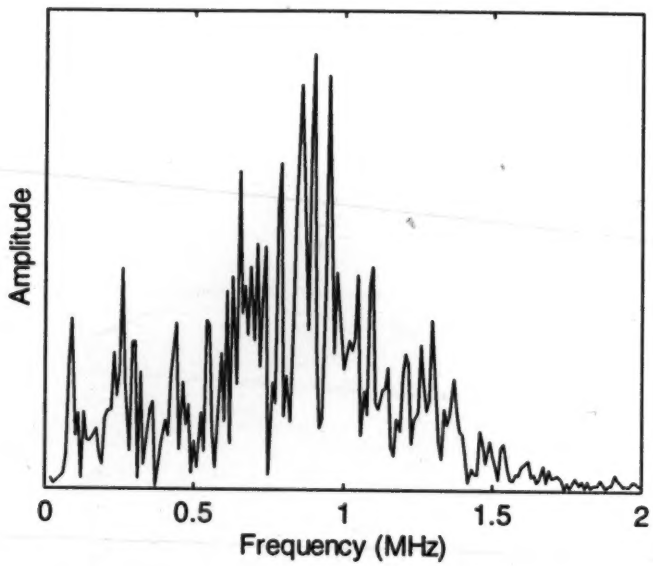


Figure 6.3 The amplitude spectrum of the scattering wave in 90% porosity sample

traveling in the medium. The aluminum foams used in this experiment have average pore size about 0.55mm to 0.6mm. If we assume the propagation velocity of the ultrasonic waves is 2000 m/s for the fast wave and 1500m/s for the slow wave, then at 1.5 MHz frequency, the ultrasonic wavelength is 1.3 mm for the fast wave and 1.0 mm for the slow wave. At 0.15 MHz frequency, the ultrasonic wavelength is 13 mm for the fast wave and 10 mm for the slow wave. Obviously at low frequency , the basic assumptions in Biot's theory are barely satisfied and at high frequency, because the wavelength has same order of magnitude as the pore size, the assumption is not true. In order to use Biot's theory to

explain the experimental results of the ultrasonic wave propagation in the water saturated aluminum foams, an attenuation model must be implemented.

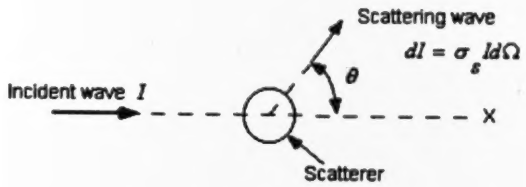


Figure 6.4 Illustration of the scattering of a wave by a single scatterer

(1) The Single Scattering Model

The basic physical principles of sound scattering are well known, but their extension to three dimensional fluid-filled solid porous material is still in its infancy. Although the situation is certainly complicated, a number of simplified models may approach this problem. Fry[19] proposed a single scattering model to describe the attenuation of an ultrasonic wave in the human skull bone. The basic idea of Fry's proposal is that the boundaries between the fluid and the solid form many scatterers which are randomly distributed in the medium, and when a wave strikes one of these, a portion of the incident power is scattered out. The attenuation coefficient of the ultrasonic wave can be derived from the scattering cross section of a single scatterer.

The single discrete scatterer model is shown in Figure 6.4. The scattering of a sound wave by a single discrete scatterer with simple geometry can be calculated by many methods. In the limit that the bodies of the scatterers are either very small or very large

with respect to the wavelength, the calculations are exact. In intermediate cases, it is much more complicated[15]. Since the transmission pulses observed in water saturated aluminum foam are in the very low frequency range where the wavelength is much larger than the pore size, the approach where the scatterers are much smaller than the wavelength is very useful.

Let's considering a plane acoustic wave propagating in a medium with bulk modulus $K_1$ and density $\rho_1$. If a scatterer in the medium has bulk modulus $K_2$ and density $\rho_2$, then when the plane wave is incident upon the scatterer, the power $P$ which is removed from the wave by the scattering process is related to the total scattering cross section, $\sigma$, to the incident intensity $I$ by:

$$P = \sigma I \tag{6.11}$$

The cross section is defined as:

$$\sigma = \int \sigma_s' d\Omega \tag{6.12}$$

where the $\sigma_s'$ is the scattering cross section scattered per unit solid angle or differential scattering cross section. If the scatterer is penetrable sphere, the scattering cross section per unit solid angle can be derived as[15,30]:

$$\sigma_s' = \frac{1}{9}\left(\frac{2\pi}{\lambda}\right)^4 a^6 \left[\frac{K_2 - K_1}{K_1} + \frac{3\rho_2 - 3\rho_1}{2\rho_2 + \rho_1}\cos\theta\right]^2 \tag{6.13}$$

where $a$ is the radius of the scatterer, $\theta$ is the angle between the incident wave and the scattering direction in which the differential scattering cross section is defined, and $\lambda$ is the wavelength.

Equation (6.13) is valid only in the limit of the scatterer being small with respect to the wavelength, and is defined as the Raleigh scattering region. From (6.13), we see that the scattering is proportional to the fourth power of the wave frequency and is strongly dependent upon the radius of the scatterer. The scattering wave contains two components: an isotropic scattering term due to the difference in compressibility (bulk modulus), and a dipole non-isotropic term due to the difference in densities. Integration of (6.13) all over space yields the total scattering cross section:

$$\sigma = \frac{2\pi}{9}\left(\frac{2\pi}{\lambda}\right)^4 a^6 \left[\left(\frac{K_2 - K_1}{K_1}\right)^2 + 3\left(\frac{K_2 - K_1}{K_1}\right)\left(\frac{\rho_2 - \rho_1}{2\rho_2 + \rho_1}\right) + 3\left(\frac{\rho_2 - \rho_1}{2\rho_2 + \rho_1}\right)^2\right] \qquad (6.14)$$

(2) The Scattering Attenuation Coefficient

Assume the number density of the scatterer in the medium is $n$. When the wave travels through the medium by $dx$, the attenuation loss of the wave intensity is:

$$dI = n\sigma I dx \qquad (6.15)$$

The attenuation coefficient of wave intensity is $n\sigma$ . Therefore the amplitude attenuation coefficient is:

$$\alpha = \frac{1}{2} n\sigma \qquad (6.16)$$

For the porous solid, the scatterer density can be calculated from the average pore size. If the average pore size is $d$, and the geometry of the pore is spherical, the number density of the scatterer is[19]:

$$n = \frac{1}{V} = \frac{1}{\frac{1}{3}\pi\left(\frac{d}{2}\right)^3} \tag{6.17}$$

(3) Implementation of the Single Scattering Model into Biot's Theory

In Biot's theory, scattering is not discussed. Fortunately the scattering model described above can be implemented into the theory. This can be accomplished by modifying the elastic moduli of the medium. Before the implementation, however, it is necessary to discuss the concept of the dynamic elastic moduli of the medium.

(a) The Dynamic Moduli of the Medium

Wave propagation in a medium is actually the result of the elastic response of the medium to stress. If a static stress is applied to the medium, the medium responds with a deformation (strain). For an elastic medium, the deformation is a linear function of the stress. The linear coefficient between the stress and the strain is called the static elastic modulus of the medium. But for a stress that changes rapidly with time, the deformation of the medium is not usually in phase with the stress due to attenuation. Therefore the dynamic elastic modulus of the medium is usually a complex quantity even for a perfect

elastic medium. This dynamic response of the medium determines how an acoustic wave propagates.

Suppose the dynamic elastic modulu of a medium is: $K' = K(1 + i\delta)$ and $N' = N(1 + i\delta)$[12], where $K$ and $N$ are the static elastic moduli and $\delta$ is a dimensionless number that represents the attenuating part of the medium. (the complex parts of $N'$ and $K'$ are assumed the same for simplicity). For most media, $\delta << 1$. The propagation velocity of the acoustic wave can be written:

$$V = \sqrt{\frac{K' + \frac{4}{3}N'}{\rho}} \qquad (6.18)$$

Since $\delta << 1$, Equation (6.18) can be written:

$$V = \sqrt{\frac{\left(K + \frac{4}{3}N\right)(1 + i\delta)}{\rho}} = V_0\sqrt{1 + i\delta} \approx V_0\left(1 + \frac{1}{2}i\delta\right) \qquad (6.19)$$

where

$$V_0 = \sqrt{\frac{K + \frac{4}{3}N}{\rho}} \qquad (6.20)$$

The propagator of the wave is:

$$k = \frac{\omega}{V} = \frac{\omega}{V_0\left(1 + \frac{1}{2}i\delta\right)} \approx k_0\left(1 - \frac{1}{2}i\delta\right) \qquad (6.21)$$

and $$k_0 = \frac{\omega}{V_0} \qquad (6.22)$$

The amplitude attenuation coefficient can therefore be obtained:

$$\alpha = \frac{\omega}{2V_0}\delta \qquad (6.23)$$

(b) The Dynamic Moduli of the Aluminum Foam

There are two types of elastic moduli that determine the static behavior of the solid porous material: the elastic moduli of the solid material itself $K_s$ and $N_s$ , the bulk moduli of the structure (skeleton) $K_b$ and $N_b$ , which are quantities that depend on the spatial arrangement of the bulk material as well as on $K_s$ and $N_s$. For most porous solids, $K_b$ and $N_b$ are not equal to zero and their relation with $K_s$ and $N_s$ are as shown in equation (6.1) and (6.2). But for some porous solids such as unconsolidated glass beads and sands, even though their $K_s$ and $N_s$ are very large, their $K_b$ and $N_b$ are almost equal to zero because the particles in the media do not form elastic structures[34]. When an acoustic wave propagates in a porous solid, the dynamic behavior of the medium is mainly determined by $K_b$ and $N_b$.

For the aluminum foam, since the bulk material itself is a homogenous elastic material, the acoustic attenuation in the material itself is very small and can be ignored. Therefore $K_s$ and $N_s$ are considerated to be real quantities. The attenuation of the wave in the medium comes primarily from the structure, therefore $K_b$ and $N_b$ can be written as:

$$K'_b = K_b(1 + i\delta) \qquad (6.24)$$

$$N'_b = N_b(1 + i\delta) \tag{6.25}$$

For the dry material (voids are considered as vacuum), the propagation velocity of the longitudinal acoustic wave is:

$$V = \sqrt{\frac{K'_b + \frac{4}{3}N_b}{\rho_b}} \tag{6.26}$$

where $\rho_b$ is the density of the aluminum foam. The attenuation coefficient can be expressed as:

$$\alpha = \frac{\omega}{2V_0}\delta \tag{6.27}$$

and

$$V_0 = \sqrt{\frac{K_b + \frac{4}{3}N_b}{\rho_b}} \tag{6.28}$$

By the same way, the attenuation coefficient for a shear wave can also be obtained. Since shear waves and longitudinal waves are two different kinds of waves, their attenuation in the dry porous material are different. For convenience, in this simulation, they are treated as the same ( same $\delta$ ).

(c) Implementation of the Scattering Model

As mentioned above, the acoustic attenuation in the water-saturated aluminum foam is due to scattering, therefore the parameter $\delta$ is mainly determined by this and can be related to the scattering cross section by Equations (6.16) and (6.27):

$$\delta = \frac{n\sigma V_0}{\omega} \tag{6.29}$$

For the dry aluminum foam, the propagation velocity of the longitudinal acoustic wave can be calculated by equation (6.26). $K_b$ and $\rho_b$ are given by:

$$K_b = K_s(1-\Phi)^2 \tag{6.30}$$

and

$$\rho_b = \rho_s(1-\Phi) \tag{6.31}$$

Therefore :

$$V_0 = V_s(1-\Phi)^{1/2} \tag{6.32}$$

where $V_s$ is the propagation velocity of the acoustic wave in the aluminum bulk material and $\Phi$ is the porosity of the foam. The scatterer density n in the aluminum foam can be calculated by Equation (6.17). The radius of the spherical scatterer in the model is assumed to be 0.3 mm, therefore n is about $8.8\times10^3$ $cm^{-3}$ . Because the pore sizes of the aluminum foams are very close (from 0.55mm to 0.63mm), the scatterer density n can be assumed to be the same for all the tested samples. The scattering cross section $\sigma$ can be calculated from Equation(6.14). Equation(6.14) can be written as a frequency dependent function :

$$\sigma = \frac{2\pi}{9}\left(\frac{\omega}{V_0}\right)^4 a^6\left[\left(\frac{K_f-K_s}{K_s}\right)^2 + 3\left(\frac{K_f-K_s}{K_s}\right)\left(\frac{\rho_f-\rho_s}{2\rho_f+\rho_s}\right) + 3\left(\frac{\rho_f-\rho_s}{2\rho_f+\rho_s}\right)^2\right] \tag{6.33}$$

since we have $$\lambda f = V_0 \tag{6.34}$$

The densities and elastic moduli of the aluminum bulk material and water can be found in Table 6.1. When the aluminum foam is saturated by water, the elastic properties of the medium are determined by $K_b$ , $N_b$ as well as other real moduli shown in Equations (4.3), (4.4) and (4.5). Implementation of complex $K_b$ and $N_b$ in Biot's theory will result in complex propagation velocities for both fast and slow waves. For each complex propagation velocity, the real part represents the phase velocity of the wave and the imaginary part represents the attenuation.

### 6.7 The Numerical Simulations of the Transmission Signals

The transmission signal of the ultrasonic pulse through the water-saturated aluminum foams can be reproduced from the simulation of the acoustic properties of the medium using the Biot's theory and a single scattering model. At the input surface of the sample, the input pulse is converted into fast and slow wave pulses by boundary conditions described in Chapter 4. In the medium, both the fast wave and the slow wave travel with the velocities determined by Biot's theory and lose their wave energy as determined by the imaginary parts of the complex propagators. At the output surface, both waves transmit through the surface according to the boundary conditions.

(1) Simulation Strategy

A numerical simulation of the transmission signal for the ultrasonic pulse traveling through the water-saturated aluminum foams was performed based on the above theory. The

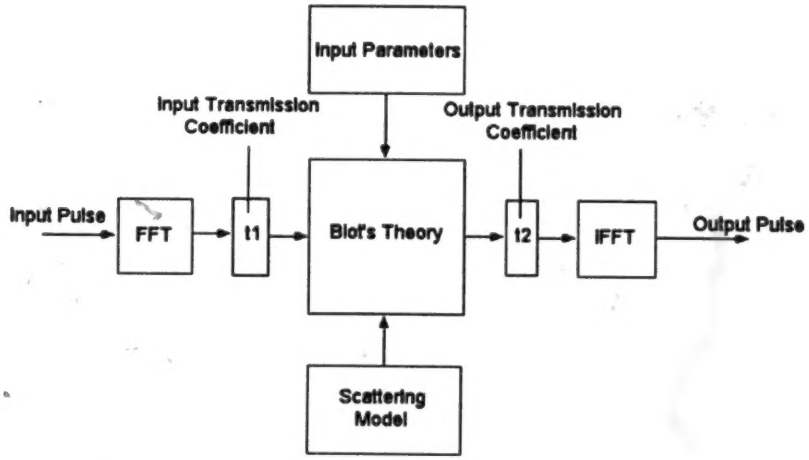


Figure 6.5 The strategy for the numerical simulation. The input pulse is a water pulse

simulation strategy is shown in Figure 6.5, in which the boundary conditions described in chapter 4 are included. A program was developed to perform the numerical simulations. In this program, the structure factor $\Lambda$ and porosity $\Phi$ are set to be the input parameters, which represent the characteristics of the samples. The input pulse is the water pulse shown in Figure 2.6. FFT was performed on the input pulse and the output pulse was obtained by inverse FFT to the processed data. During simulation, the Fourier component of the water pulse was corrected by a $2\pi fL/V_w$ phase shift. The detailed theory is given in Appendix V.

(2) Results

Simulation of the transmission pulses in the 88% porosity sample without implementation of scattering model was first performed. The result is shown in Figure 6.6. Without considering attenuation, the input pulse is split into fast and slow wave pulses. The fast

and slow wave pulses have the same pulse shape as that of input pulse. The calculated transmission coefficients in Table 6.3 determine the amplitudes of the fast and slow wave pulses. Compared with the experimental result, Biot's theory gives a good prediction of the output waves in the time domain.

With implementation of the scattering model, three samples with porosities 88%, 90% and 93% were simulated. The results are shown in Figure 6.7 (a) to (c). The corresponding experimental results are also shown in each figure. It must be noted that the waveforms of experiments contain noise and reverberation signal after the main pulses, but in the simulation, these effects were not included. From these results, we can see that the calculated wave shapes, amplitudes and arrival times for both fast and slow waves in 88% and 90% porosity samples are almost identical to the experimental results. For the 93% density sample, the discrepancies between experimental result and theory is obvious. The reason for this is due to the "leaking" wave pulse. The solid frame and the fluid are not perfectly coupled in the medium.

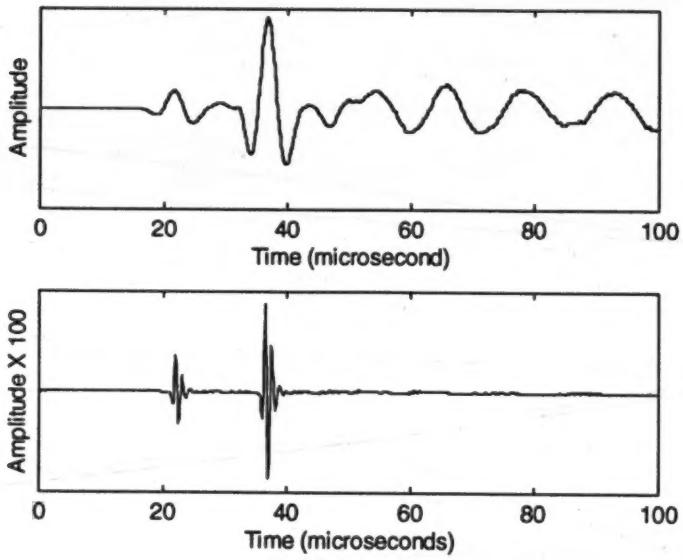


Figure 6.6 The simulated transmission pulses for 88% porosity sample without considering scattering attenuation. Top: experiment. Bottom: theory

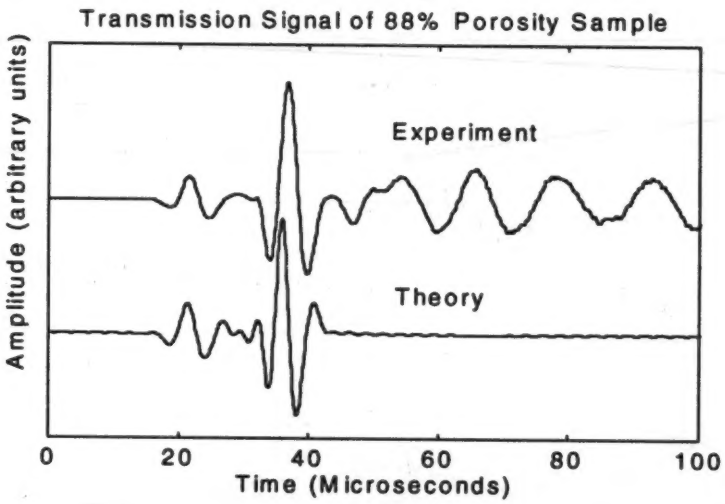


Figure 6.7 (a) The simulation of the transmission pulses in the88% porosity sample. Top: Experiment, Bottom: Theory

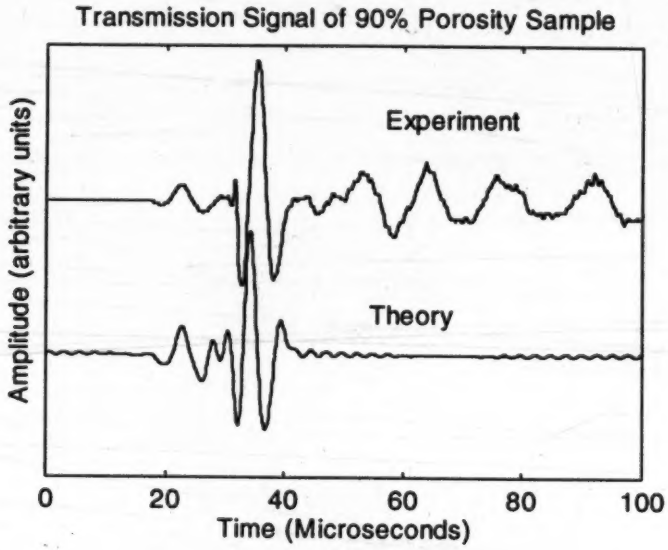


Figure 6.7(b) The simulation of the transmission pulses in the 90% porosity sample. Top: Experiment. Bottom: Theory

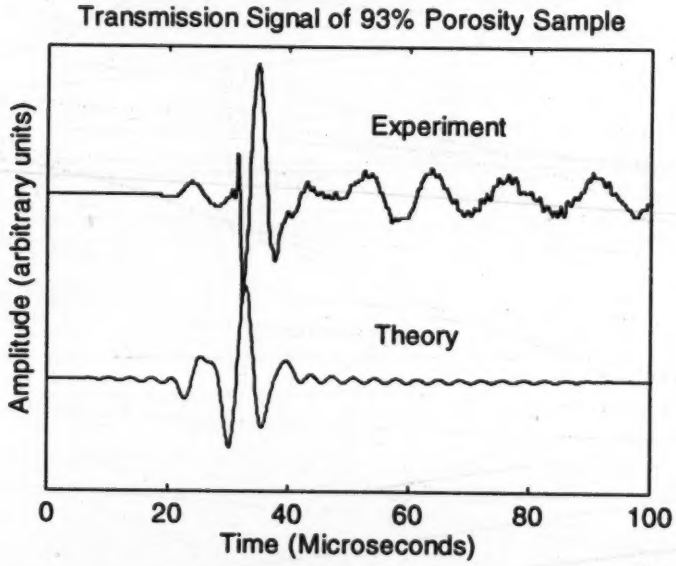


Figure 6.7 (c) The siumlation of the transmission pulses in the 93% porosity sample. Top:Experiment, Bottom: Theory

### 6.8 Discussions

In the simulation, a single scattering model is used. For the scattering theory, the single scattering model is only good when the density of scatterer is lower than 5%. When the density of the scatterer is greater than 5%, the single scattering approximation is not appropriate because of the influence of multiple scattering. Implementation of a multiple scattering model in Biot's theory is ideal, but it would be very difficult. However, the implementation method used in this research can be extended to any scattering model, because it is independent on the theoretical model.

By implementation of an attenuation model, the attenuation of both the fast wave and slow waves can be quantitatively described. During simulation, it is found that the attenuation of both the fast wave and the slow wave are dependent on the structure factor $\Lambda$. This indicates that the internal interactions between the solid frame and the fluid play an important role in wave attenuation.

# Chapter Seven: Ultrasonic Studies of Other Cancellous Bone Phantoms

The development of cancellous bone phantoms has become, in itself, an intensive research project in recent years. The propose of this research has been to provide an objective standard for the commercial machines built for diagnosis of osteoporosis. In the clinical environment there is a distinction between test objects and phantoms. A test object is designed to evaluate equipment performance while a phantom is designed to mimic the material properties of a natural tissue with a particular reference to the parameter to be measured. The water-saturated or gelatine-water mixture filled aluminum foams are the phantoms we designed and used to investigate the mechanism of ultrasonic wave propagation in cancellous bone with particular interest in the two wave propagation model. From studies of these types of phantoms, the wave propagation properties of fluid filled porous materials can be fully understood and, most importantly, the physical model for this study can be extended to explain the acoustic properties of other cancellous bone phantoms and cancellous bone. However, the water-saturated aluminum foams do not mimic all the material properties of cancellous bone. For instance, in cancellous bone , the most interested bone parameter is porosity or bone density. The porosity of cancellous bone ranges from 65% for a healthy bone to 95% for a osteoporotic bone[42]. Attempts to find an appropriate bone phantom are still in a development stage. In this chapter, the ultrasonic tests of several cancellous bone phantoms will be presented

**7.1 Experiments of bovine bone samples**

4 pieces of bone samples with different thickness were obtained from bovine femora. After removal of bone marrow, the specimens were immersed in water for a week. Ultrasonic tests of those bone specimens were performed on the experimental system which was described in Chapter two. The waveforms of transmission signals in those bone specimens are shown in Figure 7.1. BUA and SOS for each bone sample were obtained from the transmission signal. The results were summarized in Table 7.1.

From Table 7.1 we can see that there is almost no correlation between the ultrasonic parameters (nBUA and SOS) and the bone density. nBUA is the BUA value normalized by the thickness. Only one pulse was found in the waveform of the transmission signal for all 4 tested samples. This pulse, according to the analysis of Biot's theory, is the fast wave pulse. The slow wave was not detected in these experiments. In most of the ultrasonic in-vitro studies of cancellous bone, only one pulse was detected from a transmission signal except in one special case[28]. To extend the physical model established in this project to cancellous bone, detailed information about fundamental parameters of cancellous bone such as the structure factor has to be known. Table 7.2 lists some bone parameters reported by other researchers and the physical parameters of water-saturated aluminum foams. It must be noted that the bulk material of cancellous bone is not readily available in nature, and the values listed in Table 7.2 were obtained from cortical bone[42]. From Table 7.2, we can see that the viscous coupling in the cancellous bone is still very small with respect to the average pore size, so the viscous coupling effect

can be ignored. The structure factor, which determines the inertial coupling, is very complicated in cancellous bone due to the anisotropy. The observation of two longitudinal propagation modes in the cancellous bone was reported only in the case that the inertial coupling effect is very small[28,43].

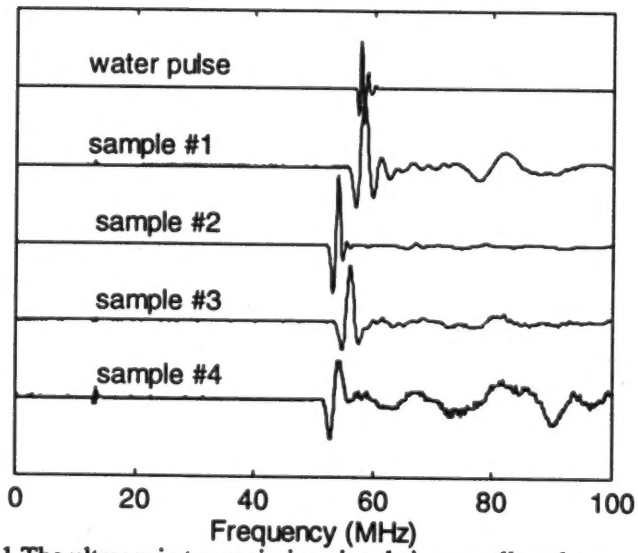


Figure 7.1 The ultrasonic transmission signals in cancellous bone sample

Table 7.1 The Measured Parameters of Bovine Cancellous Bone Sample

| | Sample#1 | Sample#2 | Sample#3 | Sample#4 |
|---|---|---|---|---|
| Thickness(cm) | 0.742 | 1.58 | 1.85 | 2.13 |
| Density(kg/m$^3$) | 660 | 680 | 703 | 720 |
| Porosity (%) | 63 | 62 | 61 | 59 |
| SOS (km/s) | 1.631 | 1.723 | 1.649 | 1.814 |
| nBUA (dB/cm MHz) | 31.8 | 35.4 | 24.4 | 40.5 |

Table 7.2 The Physical Parameters of the Cancellous Bone and Water-Saturated Al Foams

| | Cancellous Bone | Water-Saturated Al foam |
|---|---|---|
| Density of the bulk Material | 1800kg/m$^3$ | 2700kg/m$^3$ |
| Bulk modulus of the Bulk Material | $1.96\times10^{10}$ Pa | $8.31\times10^{10}$ Pa |
| Shear Modulus of the Bulk Material | $5.83\times10^{9}$ Pa | $2.59\times10^{10}$ Pa |
| Density of the Fluid | 960kg/m$^3$ | 1000kg/m$^3$ |
| Viscosity of the Fluid | 1.459 poise | 0.01 poise |
| Average Pore Size | 0.3-0.6 mm | 0.55-0.63 mm |
| Viscous Penetration Depth | 69μm (at 1MHz) | 5.6μm (at 1MHz) |

## 7.2 Rubber block model

The simplest cancellous bone phantom can be made by drilling a number of identical straight holes into a "cortical bone mimic" block. The diameter of the holes determines the

pore size and porosity of the phantoms. In order to test this type of approach, two phantoms were made. For each phantom, 36 straight holes were drilled in a 2"×2"×1" rubber block (hockey puck). The diameter of holes is 1 mm for a 4.3% porosity phantom and 2.5 mm for a 27.3% porosity phantom. Figure 7.2 shows the diagram of this type of phantom. The phantoms were saturated by water in the water tank, and then tested along the axis of the cylindrical holes in the experimental set-up. Figure 7.3 and Figure 7.4 show the transmission signals of the ultrasound pulse in these two phantoms. For comparison, the water pulse and the transmission signal through a rubber block (0 porosity) was also shown in each figure.

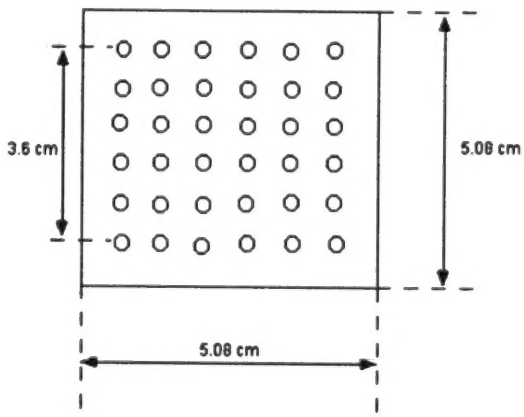


Figure 7.2 A diagrammatic representation of the rubber block model phantoms in this study

From Figure 7.3 and Figure 7.4, we can see clearly that the transmission signal for each phantom contains two pulses, one due to ultrasonic wave propagation in the rubber, in which the wave suffers attenuation and travels with a velocity that is faster than that of

water, and the other is due to a wave propagating through the water path in the phantom. The second pulse does not suffer any attenuation. The ratio of the two pulses depends on the

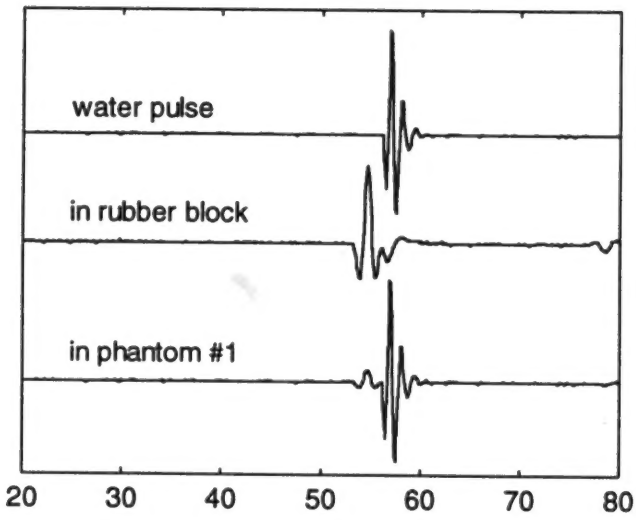


Figure 7.3 The transmission pulse in phantom #1 (2mm hole diameter)

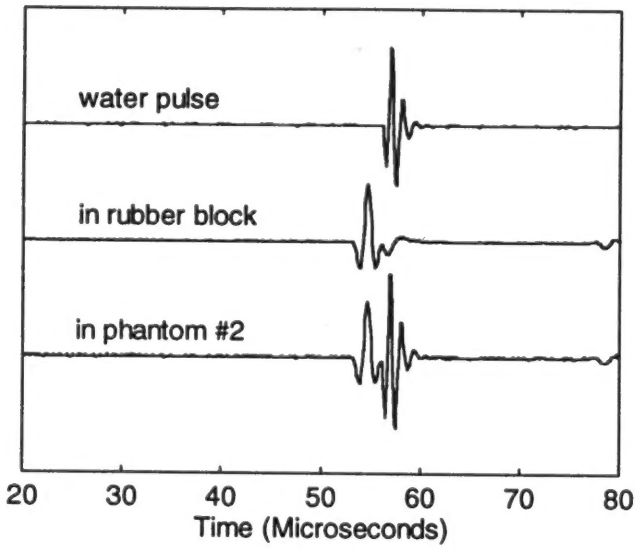


Figure 7.4 The transmission pulse in phantom #2 (1mm hole diameter)

diameter of the holes.

The experimental results of the rubber block phantoms demonstrate the case that there is not any coupling in the porous material. In this case, the wave propagates in both the solid material and the fluid independently. The geometry of the phantom determines the amplitude of the transmission pulses.

### 7.3 The Vancouver Phantom

The Vancouver phantoms are cancellous bone mimics built for quality assurance and cross-calibration of commercial ultrasound machines. The detailed technical information

about these phantoms is not available because it is the subject of a patent application. From our knowledge, these phantoms are reticulated vitreous carbon foams filled with a heavy USP grade oil. The porosity of this type of material is over 99%. Three phantoms with attenuation characteristics in the range of cancellous bone were tested in this project. The Vancouver phantoms have been tested on 3 different types of commercial ultrasound machines. Table 7.3 lists test results of these three phantoms by three different commercial machines and our experimental system. From Table 7.3, we can see that the results are not very consistent. Our results are close to those tested on the Sahara and uBUA575+ machines. The BUA values were all obtained from linear regression between 0.2 to 0.6 MHz.

The ultrasonic transmission waveforms in these phantoms are interesting. Figure 7.5 shows the waveforms. Figure 7.6 shows the curves of attenuation against wave frequency. From Figure 7.6, we found that the attenuation in the phantom is not a linear function of wave frequency, therefore the BUA values (slope of the curve) depend on the frequency range of linear regression. From the waveforms shown in Figure 7.5, we find that the main pulses in all waveforms arrive almost at the same time. This means the ultrasonic wave propagation velocities in the reticulated vitreous carbon foams are almost the same. The time shift between the water pulse and the transmission pulse is believed to be mainly due to the perspex walls of the phantom and the filling oil. Since the porosities of the reticulated vitreous carbon foams are over 99% and the thickness of the foams are about 1 inch, according to the analysis in Chapter 5, the main pulses of the transmission

waveforms are "leaking wave" pulses. The fast wave and slow wave can not be detected in these phantoms. It is worthy to note that a similar effect has also been reported by Nicholson[43] on cancellous bone. Nicholson reported that the main pulse of transmission signals in some of vertebral bone samples (tested along the weight bearing direction) is very close to the water pulse and the fast wave (Nicholson called it the "bar wave") can only be observed by saturating the main body of the waveform. Since the "leaking wave" only reflects the acoustic properties of the fluid in the sample, the elastic behavior of the solid material can not be determined from the transmission signals.

**7.4 Rubber Test Objects**

Three rubber test objects with different densities and elastic properties built for the calibration of ultrasound machines were tested using our experimental system. Table 7.4 lists the test results . These results can be used to compare with other ultrasound systems.

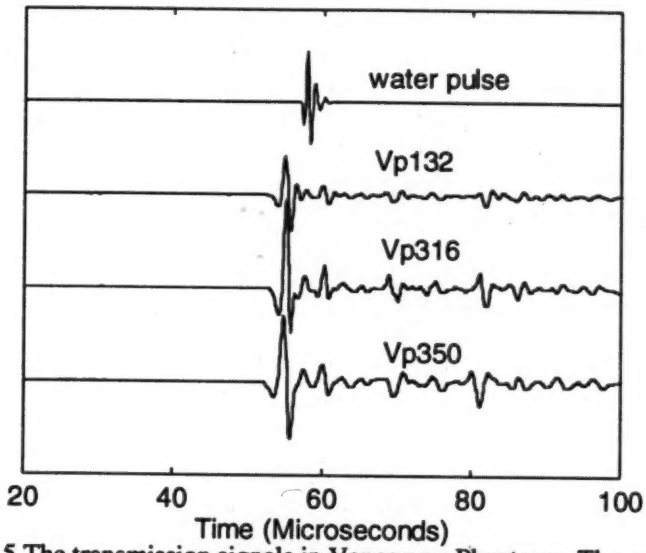


Figure 7.5 The transmission signals in Vancouver Phantoms, The water pulse is shown at the top.

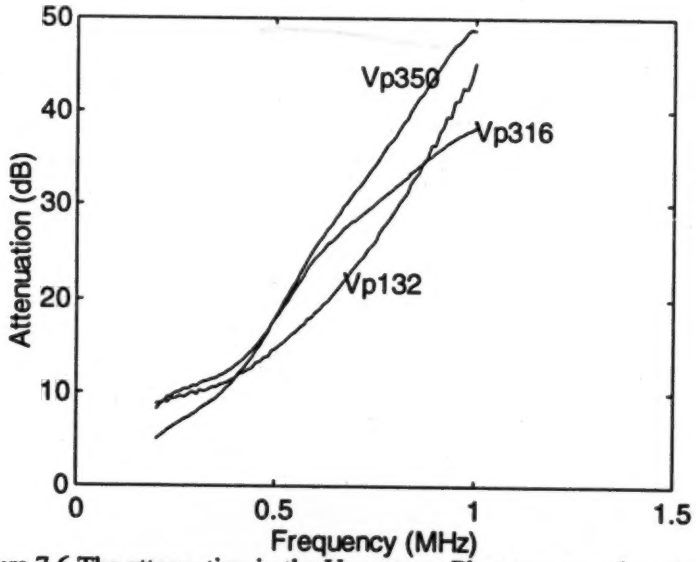


Figure 7.6 The attenuation in the Vancouver Phantoms as a function of wave frequency.

Table 7.3 The Comparison of the BUA Test Results of Vancouver Phantoms on Different Systems. The Unit of BUA : dB/MHz (fitting from 0.2 to 0.6 MHz)

| Vancouver Phantom | VP132 | VP316 | VP350 |
|---|---|---|---|
| uBUA 575+ | 38.25 | 53.75 | 67 |
| Achilles+ | 80 | 91.5 | 103 |
| Sahara | 26.7 | 44.35 | 60.375 |
| This System | 24.1 | 37.8 | 51.1 |

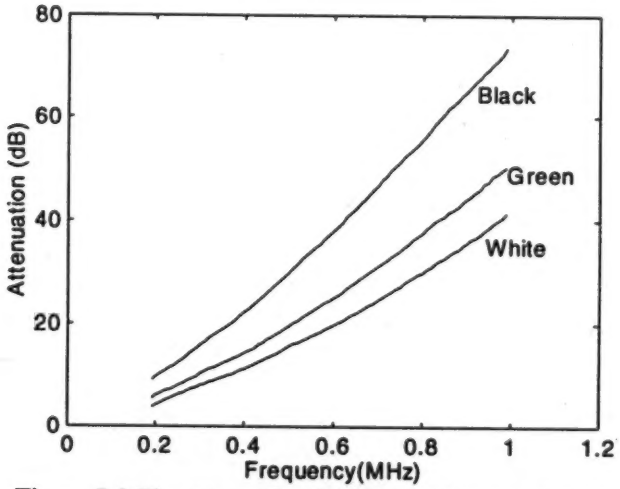


Figure 7.8 The attenuation in three rubber test objects.

Table 7.4 The test results of three rubber test objects

| Test Object | BUA (dB/MHz) (0.2 to 0.8 MHz) | BUA(dB/MHz) (0.2 to 0.6 MHz) |
|---|---|---|
| Black | 76.5 | 70.1 |
| Green | 51.8 | 46.7 |
| White | 41.7 | 38.1 |

**7.5 Discussions**

Developing a cancellous bone phantom is very difficult work. From the experimental results presented in this chapter, we can see that the ultrasonic transport properties of tested bone phantoms are not very close to those of cancellous bone samples. Fortunately, the detected waveforms can be explained by the theoretical model established in this study. The inconsistency in the results of the BUA test on Vancouver Phantoms highlights the problem of different operating performance among commercial ultrasound machines.

# Chapter Eight : Conclusion

## 8.1 Further Work

The diagnosis of osteoporosis using broadband ultrasound is still very much in a development stage. The major difficulty is to establish robust quantitative correlation between the ultrasonic parameters and the bone parameters. Since measured ultrasonic parameters are related to wave propagation, the physical model of wave propagation in cancellous bone is very important. This work established a physical model based on Biot's theory. The experimental results on ultrasonic studies of water-saturated aluminum foams agree very well with this model. In future experiment, this physical model needs to be further tested in the low porosity range(50% to 80%). To describe the attenuation behaviour of the water-saturated aluminum foams, the multiple-scattering model should be implemented. To extend this model to cancellous bone, which has more complicated microstructure than that of the aluminum foam, further work has to be done on investigating cancellous bone parameters. From the analysis of the coupling effects in cancellous bone, we know that the viscous coupling between the solid bone frame and bone marrow is very small. Therefore the major coupling effects are static elastic and inertial couplings. The structure factor, which is an important bone parameter proposed by Biot's theory, determines the inertial coupling in the bone. Since the pore structure of cancellous bone is anisotropic, the structure factor depends on both porosity and the wave propagation direction. From the results of ultrasonic studies on the Vancouver

phantoms we can predict that in the highly osteoporostic bone (over 95% porosity), the ultrasound signal detected is most likely a "leaking wave", because the structure factor in the highly osteoporostic bone is almost 1, no matter the complexity of the pore structure. In the range of medium porosity, the inertial coupling effect is usually strong. However, because of the anisotropy of the microstructure, the structure factor depends on the orientation of the trabeculea. There are still some cases where the inertial coupling is very weak. For instance, the trabeculea of vertebral bone is more anisotropic than other cancellous bone (heel bone for example)[44]. Its trabeculea roughly align along the weight bearing direction. It is therefore easy to understand that the structure factor along this direction is very small with respect to other directions. The inertial coupling along this direction is very weak. As a result, it is very possible to observe two propagation modes in the transmission waveform. For these two propagation modes, they could be either uncoupled modes(similar to the rubber block model) or coupled modes (like in the water-saturated aluminum foams), which depend on the spatial arrangement of trabeculea. In the isotropic cancellous bone, the spatial arrangement of trabeculea is random, therefore the structure factor depends on porosity only. In the case of strong inertial coupling, the slow wave mode has been "pushed" to a very low propagation velocity and is very difficult to detect. So the main pulse observed in the transmission waveform is expected to be the fast wave. This agrees with most of the observations. A linear correlation between the ultrasonic parameters and porosity is likely in this situation. The predictions from the above analysis need to be experimentally proven. However, it is obvious that the structure

factor plays an important role in the determination of ultrasonic properties of cancellous bone. Even though the structure factor is not a new parameter, it has been ignored in most of the previous cancellous bone studies. Further work needs to be done on the experimental measurements of the structure factor in cancellous bone. The experimental methods of measuring the structure factor in porous materials have been proposed by many researchers[10,48], but have never been used in cancellous bone. Using the measured structure factor to correct the correlation between the measured ultrasonic parameters and the porosity can give more accurate information about the mechanical properties of cancellous bone.

## 8.2 Conclusions

This thesis demonstrates that the propagation of an ultrasonic wave in the water-saturated aluminum foams obeys the theory proposed by Biot. The two longitudinal wave modes predicted by the theory were successfully detected experimentally. In addition to the two propagation modes, another wave, which is due to the decoupling of the water with the aluminum frame was also detected in the high porosity samples. Except for the high porosity samples, the experimental results agree very well with the theoretical analysis based on the Biot's theory. In addition to the experimental observations, this project has provided a detailed description of ultrasonic wave propagation in fluid-filled porous material. The physical description of the conversion of the modes at the input surface, the propagation of two wave modes in the medium, and transportation of the waves through

the output surface, have been established in this study. From the analysis of this study, the major attenuation source of ultrasonic waves in the medium is scattering. By implementation of a scattering model into Biot's theory, the transmission pulses can be reproduced by numerical simulation.

Although this study has established a physical model to describe the ultrasonic transport properties of water-saturated aluminum foams, there is more to be done in the application of this physical model to the cancellous bones.

# Appendix I: The Transmission Coefficients on An Open Cell Surface

Boundary conditions for an open cell surface have been given in Chapter Four. A water-saturated aluminum foam sample in this experimental set-up has two surfaces, one is the input surface on which the input wave has been converted into two forward propagation modes and a backward reflection wave. The other is the output surface, from which both the fast and the slow wave travel through the boundary. A portion of the wave energy will be reflected back into the medium. In this appendix, a detailed calculation of the transmission coefficients will be given.

(1) Input surface

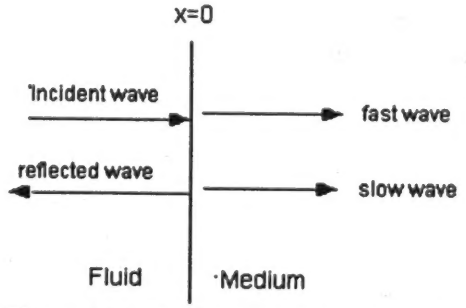


Figure A1.1 The input surface of sample

The surface is assumed to be at $x=0$. For $x<0$, the wave field in the external field is:

$$U(x,t) = L_1 e^{i\left(\omega t - k_f x\right)} + L_2 e^{i\left(\omega t + k_f x\right)} \qquad (1)$$

The external velocity field and pressure field can be written as:

$$p_i(x,t) = -K_f \frac{\partial U}{\partial x} = ik_f K_f \left( L_1 e^{i\left(\omega t - k_f x\right)} - L_2 e^{i\left(\omega t + k_f x\right)} \right) \quad (2)$$

and

$$v_i(x,t) = \frac{\partial U}{\partial t} = i\omega \left( L_1 e^{i\left(\omega t - k_f x\right)} + L_2 e^{i\left(\omega t + k_f x\right)} \right) \quad (3)$$

For $x>0$, the displacements of the solid frame and the fluid can be written as:

$$u(x,t) = r_1 B_1 e^{i\left(\omega t - k_1 x\right)} + r_2 B_2 e^{i\left(\omega t - k_2 x\right)} \quad (4)$$

and

$$U(x,t) = B_1 e^{i\left(\omega t - k_1 x\right)} + B_2 e^{i\left(\omega t - k_2 x\right)} \quad (5)$$

The internal pressure field and velocity field for solid frame can be written:

$$P_s(x,t) = -\left(p\frac{\partial u}{\partial t} + Q\frac{\partial U}{\partial t}\right) = ik_1\left(r_1 P + Q\right)B_1 e^{i\left(\omega t - k_1 x\right)} + ik_2\left(r_2 P + Q\right)B_2 e^{i\left(\omega t - k_2 x\right)} \quad (6)$$

and

$$v_s = \frac{\partial u}{\partial t} = i\omega \left( r_1 B_1 e^{i\left(\omega t - k_1 x\right)} + r_2 B_2 e^{i\left(\omega t - k_2 x\right)} \right) \quad (7)$$

The internal pressure field and velocity field of the fluid are:

$$P_f(x,t) = -\left(R\frac{\partial U}{\partial t} + Q\frac{\partial u}{\partial t}\right) = ik_1\left(r_1Q + R\right)B_1 e^{i\left(\omega t - k_1 x\right)} + ik_2\left(r_2Q + R\right)B_2 e^{i\left(\omega t - k_2 x\right)} \tag{8}$$

and

$$v_f = \frac{\partial U}{\partial t} = i\omega\left(B_1 e^{i\left(\omega t - k_1 x\right)} + B_2 e^{i\left(\omega t - k_2 x\right)}\right) \tag{9}$$

At x=0, using the boundary conditions given by equations (4.40), (4.41) and (4.42), the following equations can be obtained:

$$L_1 + L_2 = \left[(1-\Phi)r_1 + \Phi\right]B_1 + \left[(1-\Phi)r_2 + \Phi\right]B_2 \tag{10}$$

$$k_f K_f (1-\Phi)\left(L_1 - L_2\right) = k_1\left(r_1P + Q\right)B_1 + k_2\left(r_2P + Q\right)B_2 \tag{11}$$

$$k_f K_f \Phi\left(L_1 - L_2\right) = k_1\left(R + r_1Q\right)B_1 + k_2\left(R + r_2Q\right)B_2 \tag{12}$$

From equations (10), (11) and (12), the amplitude transmission coefficients for the fast and slow waves can be obtained:

$$t_{f1} = \frac{B1}{L_1} = \frac{2C_1}{C_1C_4 - C_2C_3} \tag{13}$$

$$t_{s1} = \frac{B_2}{L_2} = \frac{-2C3}{C_1C_4 - C_2C_3} \tag{14}$$

where:

$$C_1 = \frac{k_1}{k_f K_f}\left[r_1P + R + \left(1 + r_1\right)Q\right] + \left[r_1(1-\Phi) + \Phi\right] \tag{15}$$

$$C_2 = \frac{k_2}{k_f K_f}\left[r_2 P + R + \left(1 + r_2\right)Q\right] + \left[r_2\left(1 - \Phi\right) + \Phi\right] \tag{16}$$

$$C_3 = \frac{k_1}{1 - \Phi}\left(r_1 P + Q\right) - \frac{k_1}{\Phi}\left(R + r_1 Q\right) \tag{17}$$

$$C_4 = \frac{k_2}{1 - \Phi}\left(r_2 P + Q\right) - \frac{k_2}{\Phi}\left(R + r_2 Q\right) \tag{18}$$

(2) Output Surface

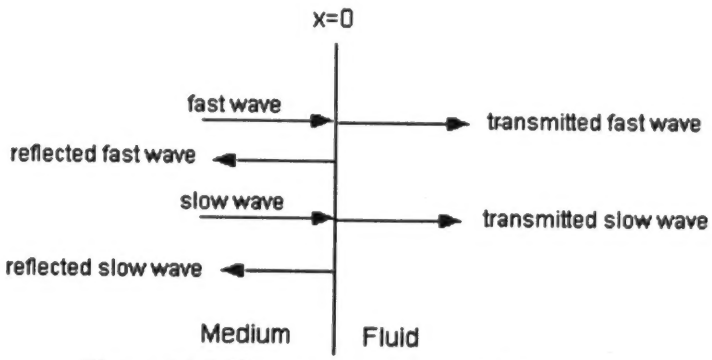


Figure A1.2 The waves on output surface

Figure A1.2 shows the waves on the output surface. Since the fast and slow waves propagate independently in the medium, the transmission problem for each wave can be treated separately. For the fast wave, the internal wave field can be written:

$$u_s = r_1 B_1 e^{i\left(\omega t - k_1 x\right)} + r_1 E e^{i\left(\omega t + k_1 x\right)} \tag{19}$$

$$U = B_1 e^{i\left(\omega t - k_1 x\right)} + E e^{i\left(\omega t + k_1 x\right)} \tag{20}$$

Therefore the pressure and velocity fields for the solid frame are:

$$p_s = ik_1\left(r_1 P + Q\right)B_1 e^{i\left(\omega t - k_1 x\right)} - ik_1\left(r_1 P + Q\right)B_1 e^{i\left(\omega t + k_1 x\right)} \tag{21}$$

$$v_s = i\omega r_1 B_1 e^{i\left(\omega t - k_1 x\right)} + i\omega r_1 E e^{i\left(\omega t + k_1 x\right)} \tag{22}$$

The pressure and velocity fields for the fluid are:

$$p_f = ik_1\left(R + r_1 Q\right)B_1 e^{i\left(\omega t - k_1 x\right)} - ik_1\left(R + r_1 Q\right)B_1 e^{i\left(\omega t + k_1 x\right)} \tag{23}$$

$$v_f = i\omega B_1 e^{i\left(\omega t - k_1 x\right)} + i\omega E e^{i\left(\omega t + k_1 x\right)} \tag{24}$$

In the external field, the wave can be written as:

$$U = De^{i\left(\omega t - k_f x\right)} \tag{25}$$

and the pressure and velocity fields can therefore be written:

$$p = ik_f K_f De^{i\left(\omega t - k_f x\right)} \tag{26}$$

and

$$v = i\omega De^{i\left(\omega t - k_f x\right)} \tag{27}$$

Using the boundary conditions, the following equations can be obtained:

$$D = \left[r_1\left(1 - \Phi\right) + \Phi\right]\left(B + E\right) \tag{28}$$

$$\left(1 - \Phi\right)K_f k_f D = k_1\left(r_1 P + Q\right)\left(B_1 - E\right) \tag{29}$$

$$\Phi k_f K_f D = k_1\left(R + r_1 Q\right)\left(B_1 - E\right) \tag{30}$$

From equations (28), (29) and (30) the transmission coefficient can be obtained:

$$t_{2f} = \frac{D}{B_1} = \frac{2}{\left[\dfrac{1}{r_1(1-\Phi)+\Phi} + \dfrac{K_f k_f}{k_1\left(r_1 P + R + r_1 Q + Q\right)}\right]} \tag{31}$$

In the same way, the transmission coefficient of the slow wave can also be obtained:

$$t_{2s} = \frac{D}{B_2} = \frac{2}{\left[\dfrac{1}{r_2(1-\Phi)+\Phi} + \dfrac{K_f k_f}{k_2\left(r_2 P + R + r_2 Q + Q\right)}\right]} \tag{32}$$

# Appendix II: Fast Fourier Transformation

(1) Algorithm

The Fourier transformation of a finite discrete vector can be performed by application Fast Fourier transformation algorithm. If x is a vector with N data points, the Fast Fourier transformation of x is:

$$X(k) = \sum_{j=1}^{N} x(j)\omega_N^{(j-1)(k-1)} \qquad (1)$$

where

$$\omega_N = e^{-\frac{2\pi i}{N}} \qquad (2)$$

The inverse fast Fourier transformation is:

$$x(j) = \frac{1}{N}\sum_{k=1}^{N} X(k)\omega_N^{-(j-1)(k-1)} \qquad (3)$$

(2) Applications

A common use of Fast Fourier transformation is to find the frequency components of a signal measured in the time domain. For example, an ultrasonic signal is measured in a time domain as shown in Figure 2A.1. This waveform contains 1024 data points. The time interval between two adjacent data points is 0.1 μs. After fast Fourier transformation, 1024 data points in frequency domain are obtained, but only the first half of those data

points (512) are meaningful frequency components, the other half are only symmetric. The frequency range covered by those 512 components is:

$$\Delta f = \frac{1}{2\Delta t} = \frac{1}{2 \times 0.1\mu s} = 5MHz \qquad (4)$$

and the frequency interval of two adjacent frequency components can be determined by:

$$\delta f = \frac{\Delta f}{512} = 0.0097656MHz \qquad (5)$$

The Fourier component of a waveform in the time domain is usually a complex number, which contains the information for amplitude and phase. The amplitude distribution of the waveform in Figure 2A.1in the frequency domain is shown in Figure 2A.2.

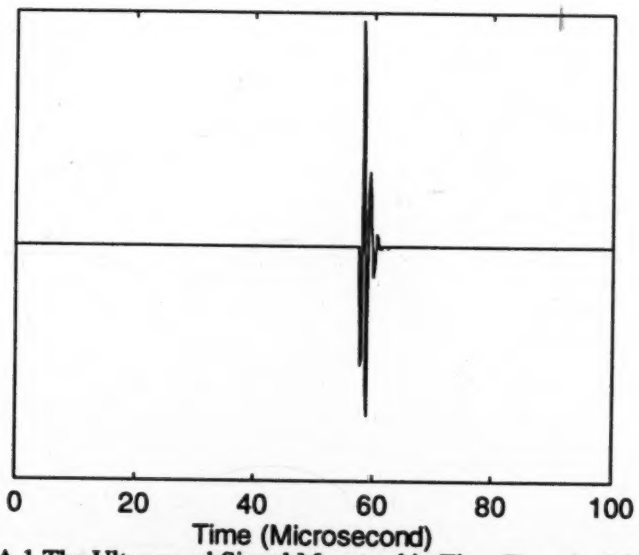


Figure 2A.1 The Ultrasound Signal Measured in Time Domain (1024 data points, time interval between two adjacent points is 0.1μs)

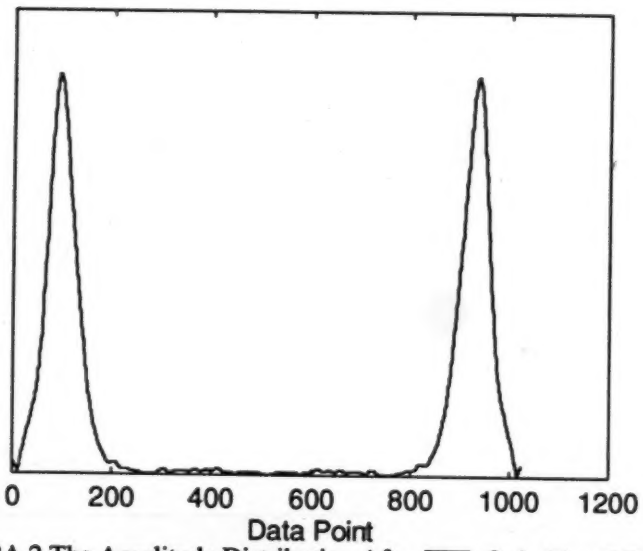


Figure 2A.2 The Amplitude Distribution After FFT, Only First 512 Data Points are Meaningful.

# Appendix III : The Waveforms in Various Solid Materials

(1) In Copper Block (1.78 cm). The distance between transducers: 7.0 cm

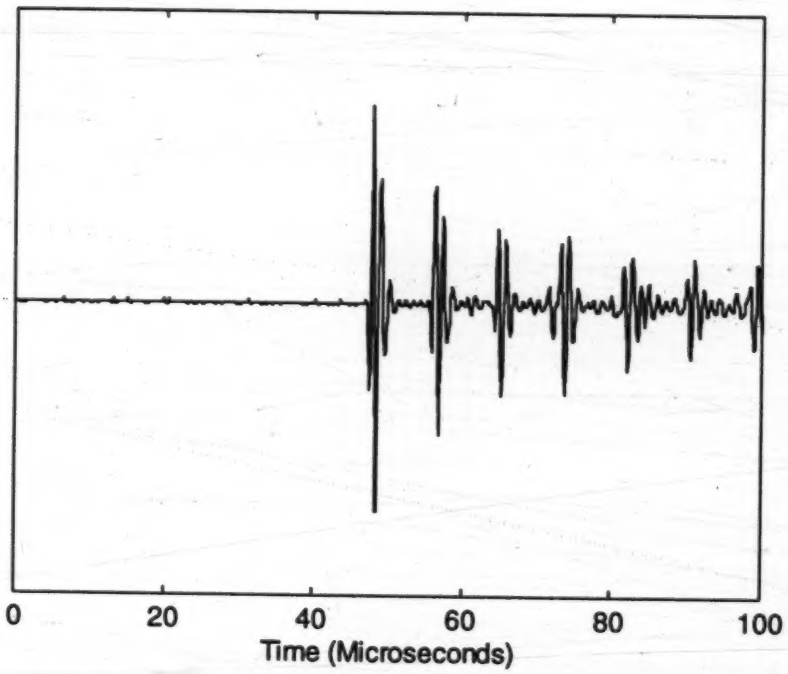

(2) In Steel Block (1.78 cm). The distance between transducers: 7.0 cm

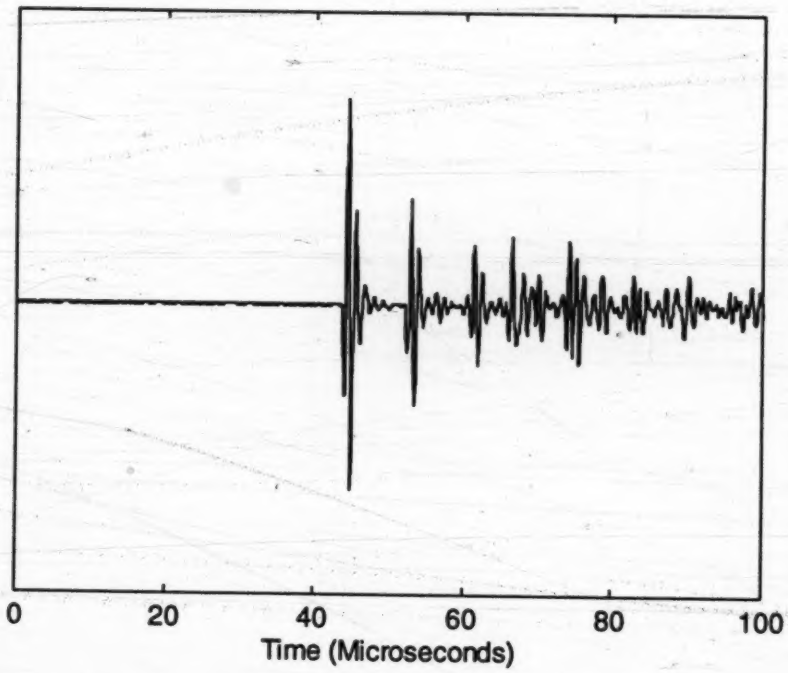

(3) In Nylon Block (1.5 cm). The distance between transducers: 7.5 cm

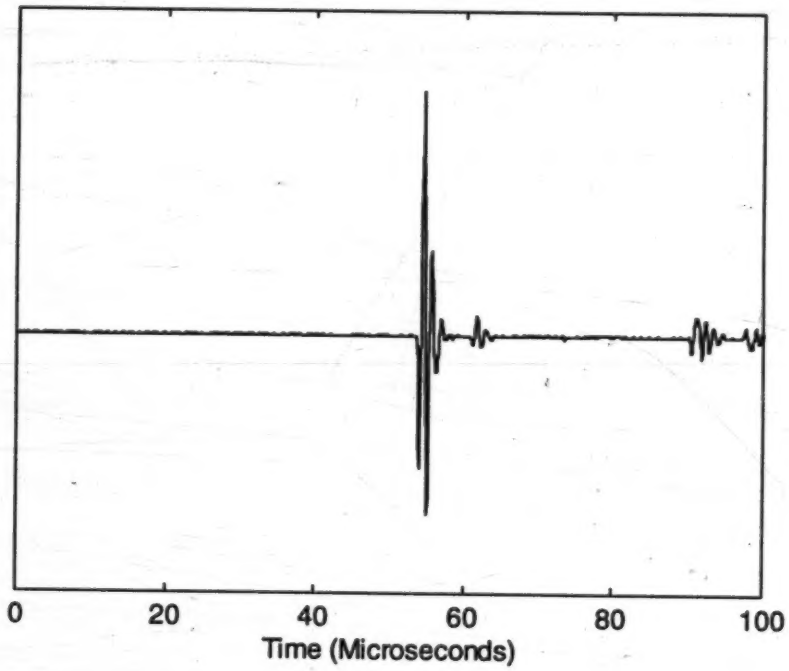

# Appendix IV: The Schematics of Pulse Generator (Main Circuit)

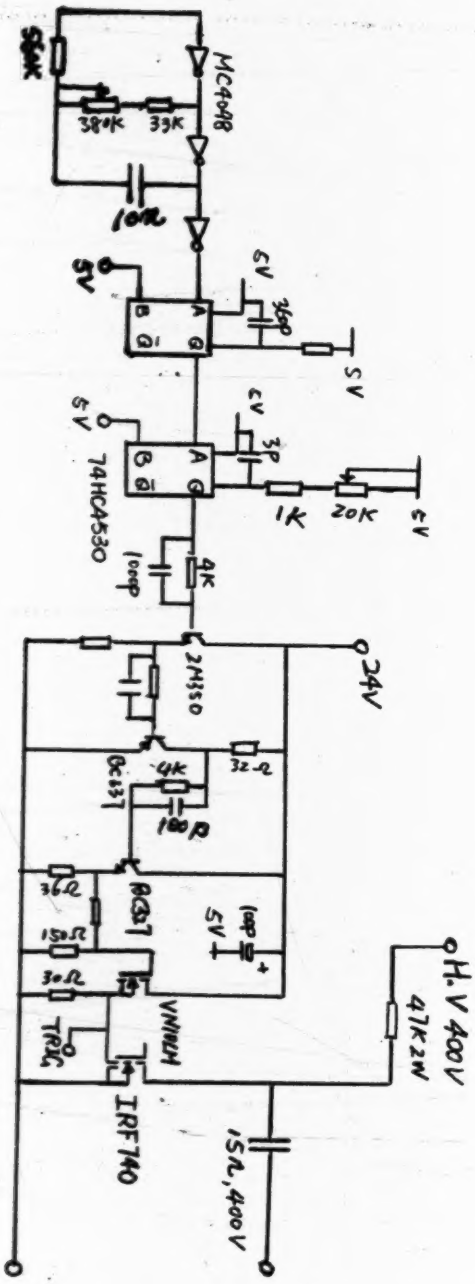

# Appendix V: The Detailed Discussion about Numerical Simulation

The numerical simulation of a received output signal from water-saturated aluminum foam was performed by the following method.

The input pulse was the received water pulse, which is denoted as $f(t)$. By fast Fourier transformation, the Fourier component $F(\omega)$ is obtained, which represents the amplitude of a sinusoidal wave with angular frequency $\omega$ contained in a water pulse. The attenuation of the ultrasound wave in water is assumed to be zero. If a water-saturated aluminum sample is inserted between the transducers, the input wave pulse is converted into the fast and slow wave pulses on the input surface. The fast and slow wave pulses of output waveform are assumed as $g_1(t)$ and $g_2(t)$ with corresponding Fourier components $G_1(\omega)$ and $G_2(\omega)$. Since the propagation velocities of the fast and slow waves in the sample are different from the propagation velocity in water, we have following relations:

$$G_1(\omega) = t_{f1}t_{f2}F(\omega)e^{-i\left[k_1 L - \left(\frac{\omega L}{V_w}\right)\right]} \qquad (1)$$

$$G_2(\omega) = t_{s1}t_{s2}F(\omega)e^{-i\left[k_2 L - \left(\frac{\omega L}{V_w}\right)\right]} \qquad (2)$$

Where $k_1$ and $k_2$ are the complex propagators calculated from Biot's theory, $L$ is the thickness of the sample, $t_{f1}$ and $t_{s1}$ are the transmission coefficients of the fast and slow waves on the input surface, $t_{f2}$ and $t_{s2}$ are the transmission coefficients of the fast and slow waves on the output surface and $\omega$ is the angular frequency of the ultrasound wave. The propagators $k_1$ and $k_2$ can be calculated from Biot's theory by the equations 4.35 and 4.36. If attenuation is ignored, the k1 and k2 are real values which just contain the information of propagation velocities of the fast and slow waves. The transmission coefficients $t_{f1}$, $t_{s1}$, $t_{f2}$ and $t_{s2}$ can be calculated from equations given in Appendix I. If the scattering model is implemented in Biot's theory, $k_1$ and $k_2$ become complex values, which contain the information for both propagation velocities and attenuation of the fast and slow waves. The complex transmission coefficients cause a constant phase shift of the fast and slow waves, but do not influence the amplitudes. The output fast and slow wave pulses can be obtained by inverse Fourier transformations:

$$g_1(t) = iFFT\left(G_1(\omega)\right) \qquad (3)$$

$$g_2(t) = iFFT\left(G_2(\omega)\right) \qquad (4)$$

# References


1. J. F. Allard, C. Depollier and A. L'Esperance, "Observation of the Biot slow wave in a plastic foam of high flow resistance at acoustic frequency," J. Appl. Phys. **59**, 3367-3370 (1986)
2. M. F. Ashby, "The Mechanical properties of Cellular Solids," Metallurigcal Transactions A **14A**, 1755-1769 (1983)
3. R. B. Ashman, J. D. Corin and C. H. Turner, "Elastic properties of cancellous bone: Measurement by an ultrasonic technique," J. Biomech. **20**, 979-986 (1987)
4. R. B. Ashman and J. Y. Rho, "Elastic modulus of trabecular bone material," J. Biomech. **21**, 177-181 (1988)
5. P. P. Antich, J. A. Anderson, R. B. Ashman, J. E. Dowdey, J. Gonzales, R. C. Murry, J.E. Zerwekh and C. Y. C. Pak, "Measurement of mechanical properties of bone material in vitro by ultrasonic reflection: methodology and comparision with ultrasound transmission," J. bone and mineral research **6**, 417-426 (1991)
6. J. G. Berryman, "Confirmation of Biot's theory," Appl. Phys. Lett. **37**, 382-384 (1980)
7. M. A. Biot, "Theory of propagation of elastic wave in a fluid-saturated porous solids I: Low-frequency range," J. Acoust. Soc. Am. **28**, 168-178 (1956)
8. M. A. Biot, "Theory of propagation of elastic wave in a fluid-saturated porous solids II: Higher-frequency range," J. Acoust. Soc. Am. **28**, 179-191 (1956)
9. J. Blitz, "Ultrasonics: Method and Applications," (Butterworth & Co, London, 1971),
10. J. S. Bolton and E. R. Green, "Normal incidence sound transmission through double-panel systems lined with relatively stiff, partially recticulated polyurethane foam," Appl. Acoustics **39**, 23-51 (1993)
11. F. A. Boyle and N. P. Coritos, "Experimental detection of a slow acoustic waves in sedment at shallow grazing angles," J. Acoust. Soc. Am. **91**, 2615-2619 (1992)

12. V. Bucur and I. Bohnke, "Factors affacting ultrasonic measurements in soild wood," Ultrasonics, Vol 30, 198-212, (1994)

13. A. J. Clarke, J. A. Evans, J. G. Truscott, R. Miller and M. A. Smith, "A phantom for quantitative ultrasound of trabecular bone," Phys. Med. Biol. **39**, 1677-1687 (1994)

14. F. Cosman, B. Herrington, S. Himmelstein and R. Lindsay, "Radiographic Absorptiometry: A simple method for determination of bone mass," Osteoporosis Int. **2**, 34-38, (1991)

15. C. M. Coulam, J. J. Erikson, and A. E. James Jr., "The physical basis of medical imaging" Appleton-Century-Crofts, New York, (1981)

16. D. Ensminger, "Ultrasonic: Fundamentals, Technology, Applications," (Marce Dekker, New York, 1988)

17. F. G. Evans, "Mechanical Properties of Bone," (Charles Thomas, Springfield, 1973)

18. W. D. Evans, E. O. Crawley, J. E. Compston, C. Evans and G. M. Green, "A Comparision of broadband ultrasonic attenuation with single photon absorptiometry and quantitative computed tomography for the measurement of bone mineral content," in *Ultrasonic Studies of Bone*, IOP Short Meetings Series **No.6**, (Bristol: IOPP 1987)

19. F. J. Fry and J. E. Barger, "Acoustical properties of the human skull," J. Acoust. Soc. Am. **63**, 1676-1590 (1978)

20. G. D. Fullerton, J. A. Zagzebski, "Medical physics of CT and ultrasound: tissue imaging and characterization," AAPM, AIP, (1980)

21. M. A. Greenfield, "Current status of physical measurement of the skeleton," Med. Phys, 19, No.6 1349-1357, (1992)

22. L. W. Goldman and J. B. Fowlkes, "Medical CT and Ultrasound: Current Technology and Applications," (Advanced Medical Publishing, 1995)

23.C. C. Gluer, C. Y. Wu, M. Jergas, S. A. Goldstein and H. K. Genant, "Three quantitative ultrasound parameters reflect bone structure," Calcif. Tissue Int. **55**: 46-52, (1994)

24 C. L. Gordon, C. E Webber, J. D. Adachi and N. Christoforou, "In vivo assessment of trabecular bone structure at the distal radiu from high-resolution computed tomography images", Phys. Med. Biol. **41**, 495-508 (1996)

25. T. P. Harrigan, M. Jasty, R. W. Mann and W. H. Harris, "Limitations of the continuum assumption in cancellous bone," J. Biomech. 21(4), 269-275

26. B. Hartmann and J. Jarzynski, "Ultrasonic hysteresis absorption in polymers," J. Appl. Phys. **43**, 4304-4312 (1972)

27. R. Hodgskinson, C. F. Njeh, M. A. Whitehead and C. M. Langton, "The non-linear relationship between BUA and porosity in cancellous bone," Phys. Med. Biol. **41**, 2411-2420 (1996)

28. A. Hosokawa and T. Otani, "Ultrasonic wave propagation in bovine cacellous bone," J. Acoust. Soc. Am. **101** 558-562 (1997)

29. A. Huddleston, "Quantitative method in bone densitometry," (Kluwer Academic Publisher, Boston, 1988)

30. A. Ishimaru, "Wave propagation and scattering in random media," Vol. 1, (Academic Press, New York, 1978)

31 S. A. Jackson, A. G. Cartwright, and D. Lewis, "The morphology of bone mineral crystals," Calcif. Tiss. Res. **25** 217-222 (1978)

32. H. Jeong and D. K. Hsu, "Experimental analysis of porosity-induced ultrasonic attenuation and velocity change in carbon composites," Ultrasonics **33**, 195-203 1995

33. Q. Ji, L. H. Le, L. J. Fillipow and S. A. Jackson, "Ultrasonic wave propagation in water-saturated cellular aluminum foams," Accpted by Ultrasonics

34. D. L. Johnson and T. J. Plona, "Acoustic slow waves and the consolidation transition," J. Acoust. Soc. Am. **72**, 556-564 (1982)

35. M. Kleerekoper, D. A. Nelson, M. J. Flynn, A. S. Pawluszka, G. Jacobsen, and E. L. Peterson, "Comparision of radiographic absorptiometry with dual-energy x-ray absorptiometry and quantitative computed tomography in normal older white and black women," J. of Bone and Mineral Research, **9** No.11,1745-1749, (1994)

36. R. Lakes, H. S. Yoon and L. Katz,"Ultrasonic wave propagation and attenuation in wet bone," J. Biomech., **9**, 407 (1976)

37. C. M. Langton, S. B. Palmer and R. W. Porter, "The measurement of broadband ultrasonic attenuation in cancellous bone," Eng. Med. **13**, 89-91 (1984)

38. C. M. Langton, A. V. Ali, C. M. Riggs, G. P. Evans and W. Bonfield, "A contact method for the assessment of ultrasonic velocity and broadband attenuation in cortical and cancellous bone," Clin. Phys. Physiol. Meas. **11** 243-249 (1990)

39. C. M. Langton, "Critical analysis of the ultrasonic interrogation of bone and future developments," in *Ultrasonic Studies of Bone*, IOP Short Meetings Series **No. 6,** (Bristol: IOPP 1987)

40. Y. Lu, "Effects of random fluctuations in ply mechanical properties on ultrasound propagation in a laminated solid layer," Ultrasonics, Vol 33, 332-354 (1995)

41. M. L. Mckelvie and S. B. Palmer, "The interaction of ultrasound with cancellous bone," in *Ultrasonic Studies of Bone*, IOP Short Meetings Series **No. 6**, (Bristol: IOPP 1987)

42. M. L. Mckelvie and S. B. Palmer, "The interaction of ultrasound with cancellous bone," Phys. Med. Biol. **36**, 1331-1340 (1991)

43. P. H. F. Nicholson, M. J. Haddaway and M. W. J. Davie, "The dependence of ultrasonic properties on orientation in human vertebral bone," Phys. Med. Biol. **39**, 1013-1024 (1994)

44. P. H. F. Nicholson, G. Lowet, C. M. Langton, J. Dequeker and G. Van der Perre, "A comparison of time-domain and frequency-domain approaches to ultrasonic velocity measurement in trabecular bone," Phys. Med. Biol. **41**, 2421-2435 (1996)

45. G. W. Petley, T. K. Hames, C. Cooper, C. M. Langton and M. I. D Cawley, " A comparison of single photon absorptiometry and broadband ultrasonic attenuation: past. present and future," in *Ultrasonic Studies of Bone*, IOP Short Meetings Series **No. 6**, (Bristol: IOPP 1987)

46. T. J. Plona, "Observation of a second bulk compressional wave in a porous medium at ultrasound frequency," Appl. Phys. Lett. **36**, 259-261 (1980)

47. H. F. Pollard, " Sound waves in solids," (Pion , London, 1977)

48. P. N. Rasolofosaon, "Importance of interface hydraulic condition on the generation of second bulk compressional wave in porous media," Appl. Phys. Lett. **52**, 780-782 (1988)

49. P. N. Rasolofosaon, "Plane acoustic waves in linear viscoelastic porous media: Energy, particle displacement, and physical interpretation," J. Acoust. Soc. Am. **89**, 1532-1550 (1991)

50. S. Rathee, "Quantfication of trabecular bone density using single and dual energy x-ray computed tomography," M.Sc thesis, University of Alberta, 1988

51. S. I. Rokhlin, W. Huang and Y. C. Chu, "Ultrasonic scattering and velocity method for characterization of fiber-matrix interphases," Ultrasonics, **33** No.5,351-364 (1995)

52. D. J. Sachse and Y. Pao, "On the determination of phase and group velocities of dispersive waves in solid," J. Appl. Phys. **49** 4320-4327 (1978)

53. L. J. Serpe and J. Rho, " Broadband ultrasound attenuation value dependence on bone width in vitro," Phys. Med. Biol. **41**, 197-202 (1996)

54. D. J. Sides, K. Attenborough and K. A. Mulholland, "Application of a generalized acoustic propagation theory to fiberous absorbents," J. Sound and Viberations **19**, 49-64 (1971)

55. D. A. Smith, C. J. Hosie and A. D. Deacon, "Broadband ultrasonic attenuation of os calcis: Comparision with CT measurement of the radius," in *Ultrasonic Studies of Bone*, IOP Short Meetings Series **No.6**, (Bristol: IOPP 1987)

56. R. Strelitzki, A. J. Clarke and J. A. Evans, "The measurement of the velocity of ultrasound in fixed trabecular bone using broadband pulses and single-frequency tone bursts," Phys. Med. Biol. **41**, 743-753 (1996)

57. J. Szilard, "Ultrasonic testing: Non-conventional testing techniques," (John Wiley & Sons, New York, 1982)

58. M. B. Tavakoli and J. A. Evans, "Dependence of the velocity and attenuation of ultrasound in bone on the mineral content," Phys. Med. Biol. **36**, 1529-1537 (1991)

59. M. B. Tavakoli and J. A. Evans, "The effect of bone structure on ultrasonic attenuation and velocity," Ultrasonics, vol 29, 127-142 (1993)

60. H. Thesiman, and F. Pfander, " Uber diedurchlassigkeit des knochens fur ultraschall," Strahlentherapie, 80, 607-610 (1949)

61. J. L. Williams, "Ultrasonic wave propagation in cancellous and cortical bone: Prediction of some experimental results by Biot's theory," J. Acoust. Soc. Am. **91**, 1106-1112 (1992)

62. R. C. Weast, "Handbook of Chemistry and Physics", The Chemical Rubber Co.,Cleveland, Ohio, (1969)

63. A. J. Yates, P. D. Ross, E. Lydick, R. S. Epstein, "Radiographic absorptiometry in the diagnosis of osteoporosis," Am. J. Med. **98** 2A 41S-47S, (1995)

64. H. S. Yoon and L. Katz, "Ultrasonic wave propagation in human cortical bone-II. measurement of elastic properties and microhardness," J. Biomech. **9**, 459-464, (1976)

65. M. Zhu, T. S. Keller, E. Moeljanto and D. M. Spengler, "Multiplaner variations in the structural characteristics of cancellous bone," Bone **15**, 251-259 (1994)